RADIOMETRIC CALIBRATION, VALIDATION AND CORRECTION OF MULTISPECTRAL PHOTOGRAMMETRIC IMAGERY

by

Lauri Markelin

Doctoral dissertation for the degree of Doctor of Science in Technology to be presented with due permission of the School of Engineering for public examination and debate in Auditorium M1 at the Aalto University School of Engineering (Espoo, Finland) on the 20th of September 2013 at 12 noon.

Supervisor
Professor Henrik Haggrén
Department of Real Estate, Planning and Geoinformatics, Aalto University School of Engineering, Espoo, Finland

Instructor
D.Sc.(Tech.) Eija Honkavaara
Department of Remote Sensing and Photogrammetry, Finnish Geodetic Institute, Masala, Finland

Preliminary examiners
Dr. Emmanuel Baltsavias
Institute of Geodesy and Photogrammetry, Swiss Federal Institute of Technology, Zürich, Switzerland

Ph.D. Miina Rautiainen
Department of Forest Sciences, University of Helsinki, Helsinki, Finland

Opponents
Assistant Professor Markus Gerke
Faculty of Geo-Information Science and Earth Observation, University of Twente, Enschede, The Netherlands

Dr. Nicolas Paparoditis
Laboratoire MATIS, Institut Géographique National, Paris, France

Abstract

Vast amounts of remote sensing data are acquire daily all over the globe from satellites, from manned or unmanned airborne platforms, and from the ground. Airborne photogrammetry provides a flexible method for acquiring high-resolution imagery in a timely manner over large areas. Aerial images are increasingly being used in a more automatic and quantitative way for applications such as land cover classification and environmental monitoring.

Apart from the high geometric quality of photogrammetric sensors, also their radiometric properties are important. Different objects reflect solar irradiance according to their individual spectral and directional properties, and radiometric analysis can be used to identify such objects and changes in them. The perquisite for quantitative radiometry is the absolute radiometric calibration of the sensor, which links the recorded digital numbers to physical units. The major benefit of a radiometrically calibrated sensor is the possibility to radiometrically correct images form atmospheric effects to surface reflectance. Radiometric correction becomes a necessity, when imagery from different dates and sensors are used for quantitative image analysis.

The objectives of this study were, first, to develop a vicarious method for the radiometric calibration and validation (Cal/Val) of a photogrammetric sensor in a test field. Second, three radiometric correction methods suitable for reflectance image product generation from photogrammetric images were evaluated. Finally, the influence of the solar elevation angle in the radiometric performance of multispectral photogrammetry was evaluated.

The Cal/Val method developed in this study utilizes field measured nadir reflectance factors of the reference targets to match the reflectance factors measured at a laboratory in an exact imaging geometry to the current weather conditions. When evaluating the radiometric correction methods, a reflectance accuracy level of 5 % was achievable with all of the evaluated methods when using well-defined isotropic reference targets. For other targets, reflectance accuracies of between 5 and 20 % were possible. The results showed that a low solar elevation of 25° did not cause the general performance of the photogrammetric processes and 3D point cloud generation to deteriorate.

The radiometric Cal/Val method presented in this study presents a step towards developing traceable processes for photogrammetric sensors. The results also confirmed the high radiometric quality of photogrammetric sensors and proved the suitability of the photogrammetric imagery for radiometric correction. This makes possible the rigorous radiometric processing of photogrammetric images and improves the quality and accuracy of automatic image interpretation and classification tasks.

Tiivistelmä

A? **Aalto-yliopisto**
Insinööritieteiden
korkeakoulu

Tiivistelmä

Kaukokartoitusdataa kerätään päivittäin suuria määriä ympäri maailmaa satelliiteista, miehitetyistä ja miehittämättömistä lentokoneista sekä maasta käsin. Fotogrammetrinen ilmakuvaus on erinomainen tapa kerätä tarkkoja kuvia haluttuna ajankohtana suuriltakin alueilta. Ilmakuvia käytetään yhä enemmän automaattisissa ja kvantitatiivisissa sovelluksissa kuten maan pinnan luokittelussa ja ympäristön seurannassa.

Laadukkaiden geometristen ominaisuuksien lisäksi olennaista fotogrammetrisissa sensoreissa on niiden radiometriset ominaisuudet. Koska kohteet heijastavat auringon säteilyä yksilöllisesti aallonpituudesta ja havaintogeometriasta riippuen, voidaan radiometrisiä ominaisuuksia hyödyntää kohteiden tunnistamisessa ja muutosten seurannassa. Kvantitatiivisen radiometrian perusvaatimus on radiometrialtaan absoluuttisesti kalibroitu sensori. Radiometrisen kalibroinnin avulla sensorin tallentamat sävyarvot voidaan muuntaa fysikaalisiksi suureiksi. Kalibroidun sensorin kuvilla näkyvät ilmakehän aiheuttamat häiriöt voidaan korjata ja kuvat muuntaa vastaamaan maanpinnan heijastusta radiometrisillä korjausmenetelmillä. Radiometrinen korjaus on välttämätöntä, kun halutaan käyttää eri ajankohtina ja eri sensoreilla kerättyjä kuva-aineistoja kvantitatiivisessa analyysissa.

Tämän työn tarkoituksena oli ensinnäkin kehittää menetelmä fotogrammetristen sensorien epäsuoraan radiometriseen kalibrointiin ja arviointiin (Cal/Val) testikentällä. Toiseksi tutkittiin kolmen eri radiometrisen korjausmenetelmän soveltuvuutta fotogrammetrisille ilmakuville. Kolmanneksi tutkittiin auringon korkeuskulman vaikutusta ilmakuvien radiometriaan ja siten fotogrammetristen prosessien suorituskykyyn.

Kehitetty radiometrinen Cal/Val menetelmä hyödyntää laboratoriossa tarkassa havaintogeometriassa tehtyjä heijastusmittauksia, jotka muunnetaan vastaamaan kuvausaikaisia sääolosuhteita maastossa tehtyjen referenssikohteiden nadiiriheijastusmittauksilla. Työssä tutkituilla radiometrisen korjauksen menetelmillä pystyttiin saavuttamaan 5 % heijastustarkkuus, kun käytettiin tarkkoja referenssikohteita. Muita kohteita käyttäen oli mahdollista saavuttaa 5-20 % heijastustarkkuus. Tulokset osoittivat myös, että 25° auringonkulma ei vaikuttanut fotogrammetristen prosessien suorituskykyyn eikä kolmiulotteisten pistepilvien luomiseen.

Tässä työssä esitetty radiometrinen Cal/Val menetelmä on askel kohti fotogrammetrisen sensorien jäljitettävää kuvienkäsittelyketjua. Tulokset vahvistivat sensorien hyvät radiometriset ominaisuudet sekä todistivat niiden kuvien soveltuvan radiometriseen korjaukseen. Tämä mahdollistaa ilmakuvien radiometrian kvantitatiivisen käsittelyn sekä lisää automaattisten kuvantulkintamenetelmien tarkkuutta.

Preface

This thesis has been prepared at the Finnish Geodetic Institute (FGI) in the department of Remote Sensing and Photogrammetry. During this work, a number of people have supported me in one way or another. First, I gratefully acknowledge my instructor Dr. Eija Honkavaara, who patiently and skillfully guided me through this work. Second, I would like to thank Dr. Jouni Peltoniemi for many instructive discussions and help in all the spectroscopy related issues, Dr. Juha Suomalainen and Mr. Teemu Hakala for the help in reference measurements, Dr. Ulrich Beisl and Dr. Ilkka Korpela for their valuable comments and excellent co-operation during many campaigns related to this thesis, and Prof. Juha Hyyppä, Prof. Risto Kuittinen and Prof. Jarkko Koskinen for providing an excellent working environment at the FGI. Third, all my co-authors in the publications are highly appreciated for their help. I would also like to thank my supervisor Professor Henrik Haggrén for introducing me the art of remote sensing and photogrammetry, and valuable advice during my studies. Dr. Emmanuel Baltsavias and Dr. Miina Rautiainen reviewed this manuscript. I am grateful for their thorough review and constructive suggestions for improvements.

Furthermore, I would like to thank Ministry of Agriculture and Forestry for the financial support, Aerial Image Centre of National Land Survey of Finland for the co-operation and European Spatial Data Research Network EuroSDR for providing an international framework for a research project.

Finally, I would like to thank all my friends in GST, OJy and TeTe for free time (sport) activities, my parents and relatives for their support and my wife Saara and children Hilla and Heikki for making me happy.

Kirkkonummi, 9th August, 2013

Lauri Markelin

List of publications

This thesis consists of an overview and of the following scientific publications, which are referred to in the text by their Roman numerals.

I   **Markelin, L.**, Honkavaara, E., Peltoniemi, J., Ahokas, E., Kuittinen, R., Hyyppä, J., Suomalainen, J., Kukko, A., 2008. Radiometric calibration and characterization of a large-format digital photogrammetric sensors in a test field. *Photogrammetric Engineering and Remote Sensing*, 74(12): 1487-1500. https://eserv.asprs.org/PERS/2008journal/dec/2008_dec_1487-1500.pdf

II **Markelin, L.**, Honkavaara, E., Hakala, T., Suomalainen, J., Peltoniemi, J., 2010a. Radiometric stability assessment of an airborne photogrammetric sensor in a test field. *ISPRS Journal of Photogrammetry and Remote Sensing*, 65(4): 409-421. doi:10.1016/j.isprsjprs.2010.05.003

III Honkavaara, E., **Markelin, L.**, Rosnell, T., Nurminen, K., 2012. Influence of solar elevation in radiometric and geometric performance of multispectral photogrammetry. *ISPRS Journal of Photogrammetry and Remote Sensing*, 67(1): 13-26. doi:10.1016/j.isprsjprs.2011.10.001

IV **Markelin, L.**, Honkavaara, E., Beisl, U., Korpela, I., 2010b. Validation of the radiometric processing chain of the Leica ADS40 airborne photogrammetric sensor. *International Archives of Photogrammetry, Remote Sensing and Spatial Information Sciences*, 38(part 7A): 145-150. http://www.isprs.org/proceedings/XXXVIII/part7/a/pdf/145_XXXVIII-part7A.pdf

V   **Markelin, L.**, Honkavaara, E., Schläpfer, D., Bovet, S., Korpela, I., 2012. Assessment of radiometric correction methods for ADS40 imagery. *Photogrammetrie – Fernerkundung - Geoinformation (PFG),* 2012(3): 0251-0266. doi:10.1127/1432-8364/2012/0115

I, II, III and **V** are PEER reviewed journal articles; **IV** is a PEER reviewed conference article.

In all publications, previously unreported results have been presented.

The articles are reprinted with the kind permission of the publishers.

Author's contribution

In publication **I**, the author and Honkavaara did most of the research. The author developed the details of the method, carried out the image processing and all image measurements, participated in the analysis of results and writing, provided the tables and graphics and took part in the field reflectance measurements. Honkavaara did large part of the literature research, designed the method on a general level, supervised the calculations and analysis, and wrote large parts of the text in the article. Peltoniemi supervised the goniometry, and Peltoniemi, Suomalainen, Kukko and the author carried out the field reflectance measurements. Ahokas participated in the method development in the beginning of the project. Ahokas, Hyyppä, and Kuittinen were advisors in the study.

In publication **II**, author and Honkavaara did most of the research. The author developed the details of the method, carried out the image processing and all image measurements, participated in the analysis of results and writing, provided the tables and graphics and took part in the field reflectance measurements. Honkavaara designed the method in general level, supervised all the calculations and data-analysis and took part in the writing of the article. Hakala, Suomalainen and the author carried out the field reflectance measurements and data processing. Peltoniemi supervised the reflectance data processing and analysis.

In publication **III**, the author generated the radiance and reflectance images, performed the vicarious calibration, processed reference reflectance data, performed the general radiometric analysis of the imagery and participated in the writing of the article chapters related to image radiometry. Honkavaara was the main author of the article, did most of the data analysis, writing and supervised the work. Rosnell and Nurminen did the geometric data processing, point cloud generation and participated in the writing.

In publication **IV**, the author did most of the research. Honkavaara designed the analysis methods on a general level, supervised the calculations and the analysis of the results, and assisted in the writing. Beisl assisted in the image processing, data analysis and writing. Korpela organized the Hyytiälä airborne campaign and assisted with the field reference measurements and writing.

In publication **V**, the author did most of the research. Honkavaara designed the analysis methods on a general level, supervised the calculations and the analysis of the results, and assisted in the writing. Schläpfer assisted in ATCOR-4 processing and provided the ATCOR-4 ReSe-dataset. Bovet provided the XPro Swisstopo dataset. Korpela Organized the Hyytiälä airborne campaign and provided the image measurements of the reference targets.

List of Abbreviations

3D	3 Dimensional
6S	Second Simulation of a Satellite Signal in the Solar Spectrum vector code
ACORN	Atmospheric CORrection Now (software)
AERONET	AErosol RObotic NETwork
ADS	Airborne Digital Sensor
AOT	Aerosol Optical Thickness
ATCOR	Atmospheric/Topographic CORrection (software)
BRDF	Bidirectional Reflectance Distribution Function
BRF	Bidirectional Reflectance Factor
CIR	Color infrared
DEM	Digital Elevation Model
DGPF	Deutsche Gesellschaft für Photogrammetrie, Fernerkundung und Geoinformation (German Society of Photogrammetry, Remote Sensing and Geoinformation)
DMC	Digital Mapping Camera
DN	Digital Number
DOS	Dark Object Subtraction
DSM	Digital Surface Model
EuroSDR	European Spatial Data Research Organization
FGI	Finnish Geodetic Institute
FIGIFIGO	FInnish Geodetic Institute FIeld GOniospectrometer
FKS	Fotogrammetrian ja Kaukokartoituksen Seura (The Finnish Society of Photogrammetry and Remote Sensing)
FLAASH	Fast Line-of-Sight Atmospheric Analysis of Spectral Hypercubes (software)
FMC	Forward Motion Compensation
FOV	Field of View
GSD	Ground Sampling Distance
HDRF	Hemispherical-Directional Reflectance Factor
MODTRAN	MODerate resolution atmospheric TRANsmission (software)
MS	Multispectral
NAIP	National Agriculture Imagery Program
NDVI	Normalized Difference Vegetation Index
NIR	Near-infrared
NIST	National Institute of Standards and Technology
PAN	Panchromatic, "black-and-white image"
RadCaTS	Radiometric Calibration Test Site
SI	Le Système international d'unités, The International System of Units
SMEAR	Station for Measuring Ecosystem-Atmosphere Relations
TDI	Time-Delayed Integration
USGS	United States Geological Survey

Contents

1. Introduction

1.1 Background and motivation

At the most general level, remote sensing can be defined as observing a target without touching it. A more detailed definition of remote sensing has been provided by Lillesand et al. (2007):

> Remote sensing is the science and art of obtaining information about an object, area, or phenomenon through the analysis of data acquired by a device that is not in contact with the object, area, or phenomenon under investigation.

Vast amounts of remote sensing data are acquired daily all over the globe from satellites, from manned or unmanned airborne platforms, and from the ground. The users of this data are not restricted only to remote sensing experts; rather anyone with an Internet connection has free access to global databases such as Google Earth (http://earth.google.com), Microsoft Bing (http://maps.bing.com/), and NASA World Wind (http://goworldwind.org/), as well as other international or national services, such as the open topographic datasets of the National Land Survey of Finland (Figure 1; NLS, 2013).
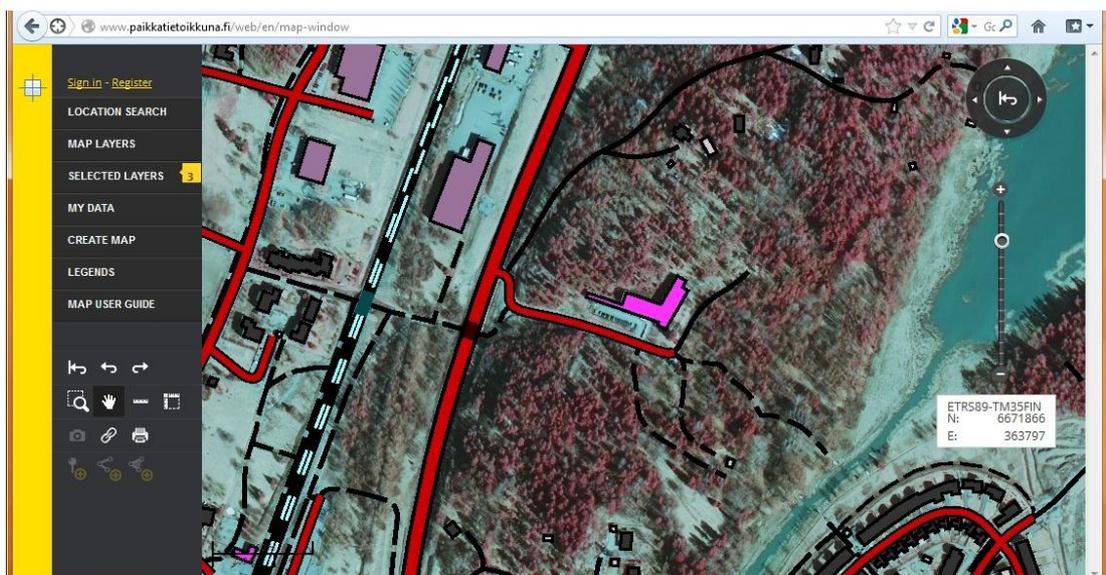

Figure 1. Screenshot from the NLS Paikkatietoikkuna, which is an open and free geographic information service. Figure shows the surroundings of the FGI main building at Masala, Finland. Map layers open are color infrared ortophoto, buildings and transport network.

Many remote sensing systems are based on passive methods. With passive methods, the sensor is dependent upon an external light source, typically the sun. Various digital cameras are typical examples of passive sensors. Remote Sensing makes it possible to measure electromagnetic radiation at a wide range of wavelengths, from ultraviolet, visible, and infrared to microwave radiation with various spectral resolutions, that is, the sizes of the wavelength interval and number of channels from multispectral to hyperspectral (Schott, 2007). Typical platforms for collecting remote sensing data are space and airborne systems. The advantages of space borne remote sensing include global and repetitive coverage, data collection over otherwise inaccessible areas, spectral resolution, and affordability. This data is used in various disciplines, such as agriculture, forestry, hydrology, geology, cartography, meteorology, education, intelligence, and the military (Schowengerdt, 2007).

An important area of remote sensing is photogrammetry, which is defined as the art, science and technology of obtaining reliable information about physical objects and environment through the process of recording, measuring and interpreting photographic images and patterns of electromagnetic radiant energy and other phenomena (Alspaugh, 2004). Photogrammetry is as old as modern photography and can be dated to the mid-nineteenth century. Airborne photogrammetry is a fundamental technique for providing reliable, geometrically accurate, high-resolution geospatial information (Read and Graham, 2002; Alspaugh, 2004). The advantages of airborne photogrammetry include high spatial resolution, stereoscopic data, efficient data collection even on a national level, operational flexibility, that is, the choice of a flying height of between 500 m and 9000 m, the possibility to collect data in a timely manner without long intervals between acquisitions, even under cloud cover, the possibility for high image overlaps, and the possibility for 3D point cloud generation (Paine and Kiser, 2003; Ryan and Pagnutti, 2009; Leberl et al., 2010).

Photogrammetric images are traditionally used to collect geometric information, that is, the locations, shapes, and dimensions of an object in tasks like topographic map generation and updating, the 3D mapping of buildings, and the creation of digital terrain models (DTMs) (Zebedin et al., 2006; Spreckels et al., 2010; Holland et al., 2012), and the data collection from images has been manual or semi-automatic (Paine and Kiser, 2003). Traditionally, the main focus in the quality evaluation of photogrammetric sensors has been on their geometric properties (Honkavaara et al., 2006d; Passini and Jacobsen, 2007; Jacobsen et al., 2010), and, at least from the manufacturer's point of view, the geometry of the new digital sensors is under full control (Cramer, 2011).

Apart from their geometry, the essential property of remote sensing sensors and their images is radiometry. Radiometry is defined as measurement of

electromagnetic radiation (Schott, 2007). Since different objects, such as vegetation and buildings, reflect solar irradiance according to their individual spectral and directional properties, radiometric analysis can be used to identify such objects, their biophysical parameters and changes in them. Previously, the quantitative manipulation of radiation measured with film-based, analog photogrammetric sensors was extremely difficult, but the emergence of digital photogrammetric sensors at the beginning of the 2000s has removed this limitation and improved the radiometric quality of the data significantly (Sandau, 2010; Cramer, 2011). The improvements in radiometry include lower noise levels, linearity, better resolution, and a larger dynamic range (Sandau, 2010). These properties, together with the precise geometric and radiometric calibration of the sensor and its overall metric and radiometric stability, are comprehensively taken into account in digital, large-format photogrammetric sensors (Cramer, 2011).

A perquisite for quantitative radiometry is the absolute radiometric calibration of the sensor, which links the recorded digital numbers (DNs) to the physical units (radiance) that can be traced to international standards (Ryan and Pagnutti, 2009). The radiometric calibration of space borne sensors has been operational for a long time (Dinguirard and Slater, 1999), but only recently manufacturers of the photogrammetric sensors have started to develop laboratory radiometric calibration facilities (Beisl, 2006; Ryan and Pagnutti, 2009). The radiometric calibration of space borne sensors is often based on reference test sites (LANDNET, 2013). The test field–based radiometric calibration method is also possible suited for airborne sensors, especially for radiometric calibration and validation of these sensor systems and their imagery in operational conditions.

Despite of the recent advances in radiometric properties of photogrammetric sensors, the radiometric quality of these sensors and its expected benefits in photogrammetric processes has not been studied in detail yet. And if some analyses are performed, the results are not always published in peer reviewed journals. A questionnaire in the context of **European Spatial Data Research organization's** (EuroSDR) **project "**radiometric aspects of photogrammetric images**" (Honkavaara** et al., 2009b), directed to various interest groups, addressed several problems which hinder the quantitative utilization of image radiometry, make the radiometric processing complicated and laborious, and decrease the quality of output products. These problems included the lack of documentation, lack of information of the quality of the radiometric laboratory calibration, concern about the traceability of the radiometry and lack of validated and reliable image products and processing methods.

The major benefit of radiometrically calibrated aerial sensors is that they make the rigorous radiometric correction of image products from atmospheric effects to surface reflectance possible. These reflectance images or their derivatives (such as

vegetation indices) can be then used for example to estimate different biophysical parameters of vegetation such as leaf chlorophyll concentration (Main et al., 2011). When imagery from different dates and sensors are used for change detection and interpretation, accurate radiometric correction becomes a necessity. Schowengerdt (2007) stated:

> It is clear that remote sensing data must be corrected for atmospheric, topographic, and solar effects if they are to be compared to a library of spectral reflectance curves. Furthermore, relative atmospheric correction is needed if data signatures from one image date are to be compared to those from another date.

Different empirical and rigorous atmospheric correction methods are commonly used with satellite images (Mahiny and Turner, 2007), but there is a need for research on radiometric correction methods suitable for images collected with airborne multispectral photogrammetric sensors (Honkavaara et al. 2009b). In general, the rigorous radiometric processing of aerial images makes possible the use of physical models, such as radiative transfer codes, and lays a more solid foundation for the quantitative analysis of the data. The essential aspect in the comprehensive radiometric analysis of the data is that the directional reflectance properties of the objects are taken into account (Schaepman-Strub et al., 2006).

Aerial images are increasingly being used in a more automatic and quantitative way for purposes such as land use and land cover classification (Le Bris and Boldo, 2008; Waser et al., 2010; Laliberte et al., 2012), tree species classification (Waser et al., 2010; Heikkinen et al., 2011; Korpela et al., 2011), and environmental monitoring, like benthic habitat mapping (Green et al., 2011), forest health monitoring (Wulder et al., 2012), and vegetation index calculations (Martínez et al., 2012). Also, large aerial image databases are being collected, which can be used in various applications. One example is the US National Agriculture Imagery Program (NAIP), which is being used, for example, for disaster preparedness, planning activities, change detection, and measurements (NAIP, 2013). Despite the diverse uses of the photogrammetric images in these various image interpretation tasks, rigorous radiometric processing of the imagery is still rare. Either the imagery is used as is, without any rigorous radiometric calibration or correction, or the radiometric processing procedure is only partial and/or undocumented. Because of these shortcomings in the radiometric processing chain, many of the presented results in the current literature using photogrammetric images can be considered only case studies that cannot easily be generalized or compared to other studies or datasets.

One of the great innovations with digital aerial imagery is the automatic creation of 3D point clouds and digital surface models (DSMs) that utilize the high overlaps of the images (Haala, 2009; Hirschmüller, 2011; Höhle, 2011). An essential aspect of successful point cloud generation is the radiometric quality of the images. When the

imagery has a high dynamic range, it is possible for the algorithms to find more common and reliable points from multiple images. This makes more automated and accurate 3D object reconstruction with textures, multispectral image classification, and efficient data collection for DSM creation possible, compared to other methods (Leberl et al., 2010).

Finland is located in the far north of the northern hemisphere (60N-70N) where the summer is short, the sun does not rise too high above the horizon, and clear days can be rare. The current national regulation on collecting aerial images for mapping stipulates that the solar elevation during the campaign has to be 33° above the horizon (FKS, 1995). Due to the expected high-quality radiometric properties of digital photogrammetric sensors, users of these sensors would like to collect images with lower solar angles, and in this way extend the time windows of the imaging campaigns. So far, the effect of lower solar elevation angles to the quality of the reflectance image products and to photogrammetric processes such as point cloud generation has not been studied in detail.

In recent years, the need for knowledge on the radiometric aspects of photogrammetry has inspired several international projects concentrating, in particular, either on radiometry, such as the EuroSDR "Radiometric Aspects of Digital Photogrammetric Images" (Honkavaara et al., 2009a, 2013) and the Aerial Digital Camera Radiometry Guideline (Ryan et al., 2013), or where radiometry is one part of the project, such as EuroSDR's European Digital Airborne Camera Certification (EuroDAC²) (Cramer, 2008; EuroDAC², 2011), the German Society of Photogrammetry, Remote Sensing and Geoinformation (DGPF) Test on Digital Airborne Camera Evaluation (Cramer, 2010; Schönermark, 2010), and the United States Geological Survey (USGS) Plan for the Quality Assurance of Digital Aerial Imagery (Stensaas and Lee, 2008; USGS, 2013).

1.2   Hypothesis

It is expected that in the future, due to the high-quality radiometric properties of photogrammetric sensors, photogrammetric imagery will be utilized more automatically and quantitatively. The hypothesis of this thesis was that it is possible to perform accurate radiometric correction for imagery collected with the large-format photogrammetric sensors in order to derive reflectance image products suitable for quantitative analysis.

1.3   Objectives of the thesis

Based on the hypothesis, the following objectives were established for the thesis:

- To develop a method for the radiometric calibration and validation of photogrammetric sensors in a test field.

- To evaluate radiometric correction methods suitable for reflectance image product generation using photogrammetric imagery.

- To evaluate the influence of the solar elevation angle on radiometrically corrected reflectance image products and in point cloud creation.

In this thesis, based on the general radiometric performance analysis and vicarious calibration, the sensor can be declared to have a good radiometric quality provided that it can be radiometrically calibrated, that is, that the sensor has a linear response and is radiometrically stable, the sensor also has a high dynamic range and high sensitivity. The objective of the radiometric correction was to correct atmospheric effects from the images, and its output is the reflectance image product. The digital number (DN) values of the reflectance image product are bottom of atmosphere (directional) reflectance values, and the measurement setup is hemispherical-directional by its nature. For well-defined objects and in clear weather conditions the DN values of the reflectance image product are practically hemispherical directional reflectance factors (HDRF, see Section 2.1.3).

1.4 Structure and contribution of the thesis

This thesis consists of a summary and five original publications. Following the introductory section, section 2 presents the essential definitions and terminology of radiometric quantities and a literature review describing previous research on the topics of the study. The materials used are presented in section 3 and the methods are presented in section 4. Section 5 summarizes the results achieved based on the method development and radiometric analysis of the imagery. The quality of the results, their theoretical and practical implications, and the need for further research are discussed in section 6. Finally, the thesis is summarized in section 7.

Regarding the objectives of the thesis, the contribution of the original publications and this summary can be summarized as follows:

In general, the thesis presents a rigorous methodology for performing radiometric calibration, validation and correction of photogrammetric imagery in operational conditions using a test field. Based on the results presented, in the future the radiometrically corrected multispectral photogrammetric imagery can be used in various quantitative image interpretation tasks traditionally performed only for space and airborne borne multi- and hyperspectral non-photogrammetric imagery.

In publications **I**, **II**, **III,** and **IV,** a method for the radiometric calibration and validation of photogrammetric sensors in a test field was developed. The method includes an evaluation of sensor linearity, dynamic range / saturation, sensitivity (**I**), sensor radiometric stability (**II**), the vicarious calibration of the sensor (**I**, **II**, **III**, **IV**), and a quality evaluation of the sensor laboratory radiometric calibration, which was done by comparing it to the vicarious calibration (**IV**). The radiometric quality

of all three leading commercially available large-format photogrammetric sensors (Microsoft UltraCamD, Intergraph DMC, Leica Geosystems ADS40) was evaluated in **I**. Publication **I** was the first published study known to the author that evaluated the radiometric properties of the 1st generation photogrammetric sensors, and publication **II** was the first published study known to the author that evaluated the radiometric stability of a photogrammetric sensor while also taking into account different sensor exposure settings. To the **best of author's knowledge, the method** presented in this thesis is the first study related to airborne photogrammetric sensors that takes into account the anisotropic BRDF properties of reference targets.

Publication **III** investigated both theoretically and empirically the impacts of solar elevation on modern photogrammetric processes and presented an empirical line–based method for generating reflectance image products using frame sensor imagery. Images collected in the morning and at noon were transformed into reflectance image products, and the quality of the imagery was studied both in direct light and in shadows using various natural and artificial targets. The purpose of the reflectance factor measurements from images was to compare relative differences between morning and noon data and shadowed and sun illuminated areas, not to perform quantitative analysis of the object reflectance properties. This was the first study known to the author that thoroughly evaluated on the influence of solar elevation on radiometrically corrected reflectance image products and in point cloud creation from photogrammetric images. The motivation for the study was to provide new national recommendations for solar elevation thresholds in photogrammetric mapping.

In publications **IV** and **V**, two radiative transfer-based radiometric correction methods (Leica XPro and ATCOR-4) for generating reflectance image products from photogrammetric pushbroom imagery were evaluated. The imagery was collected using the 2nd generation Leica ADS40 SH52 sensor. **V** was the first study known to the author that presented a quantitative comparison of the two radiometric correction methods for reflectance image product generation and a thorough accuracy evaluation of the these images. The accuracy evaluation was based on the bidirectional reflectance factors (BRF) of the reference targets in an exact imaging geometry.

Publications **II**, **IV,** and **V** were also part of the EuroSDR**'s** "Radiometric Aspects of Digital Photogrammetric Images" project and the project results have been published in Honkavaara et al. 2009a, 2009b, 2011b, and 2013. Some supplementary results related to **V** are presented in appendix 7 in the final report of the project (Honkavaara et al., 2013).

2. Review

2.1 Radiometric quantities and terminology

2.1.1 Flux, irradiance and radiance

The rate of flow of energy Q passing or propagating in electromagnetic radiation is **called the radiant flux Φ** = dQ/dt [watts, W]. The rate at which the radiant flux is delivered to a surface is then called irradiance **E = dΦ/dA [Wm^{-2}]**, where dA [m^{-2}] is the area element of the surface of interest. The radiant flux per unit area away from **the surface is described by radiant exitance M = dΦ/dA [Wm^{-2}]**. The simplest term to describe the directional information about the flux is the radiant intensity I = **I(θ,φ) = dΦ/dΩ [Wsr^{-1}], where dΩ = dA/r^2 [steradian, sr] is the element of solid angle and θ and φ are generic orientation angles.** To characterize both the spatial and directional information of the radiant flux, term radiance (L [Wm^{-2}sr^{-1}]) is used. It is defined as follows:

$$L = L(x, y, \theta, \varphi) = \frac{d^2\Phi}{dA \cos\theta \, d\Omega} = \frac{dE}{d\Omega \cos\theta} = \frac{dI}{dA \cos\theta}$$
$$= \frac{dM}{d\Omega \cos\theta}$$

(1)

where x and y define the location in the plane of interest, and θ and φ are angles that define the direction of interest relative to the normal to the plane. The radiant exitance and intensity are generally source terms and irradiance is generally associated with receivers or detectors, but radiance can be used to characterize the flux from or onto a surface, as well as flux through any arbitrary surface in space. Radiometric measurements are performed by measuring the flux through a planar surface e.g. a detector, and radiance is a quantity that is independent of the orientation or size of the radiated surface as long as all the flux is captured. When taken into account the fact that the flux is spectrally variable, all the previous radiometric terms also vary with wavelength. In the following we will use the wavelength dependent term spectral radiance L_λ [Wm^{-2}sr^{-1}nm^{-1}] and, for the sake of clarity, call it simply radiance L. Finally, when the spectral response of the sensor is also taken into account, we get the effective spectral radiance $L_{\lambda\text{eff}}$ [Wm^{-2}sr^{-1}nm^{-1}]. The more detailed definitions of all the presented terms can be found from Schott (2007) and Schowengerdt (2007).

2.1.2 Solar energy paths in airborne imaging

Radiometry has to do with measuring the electromagnetic radiation reaching the sensor (at-sensor radiance) (Beisl, 2001; Schott, 2007). A digital imaging sensor measures incoming radiance and stores the result of the measurement as a digital number (DN). The two crucial steps in the imaging process are the radiance transfer from the object to the sensor and translating the radiance entering the sensor into DNs. The principle behind an imaging event for a passive imaging sensor with the most significant solar energy paths reaching the sensor is illustrated in Figure 2.
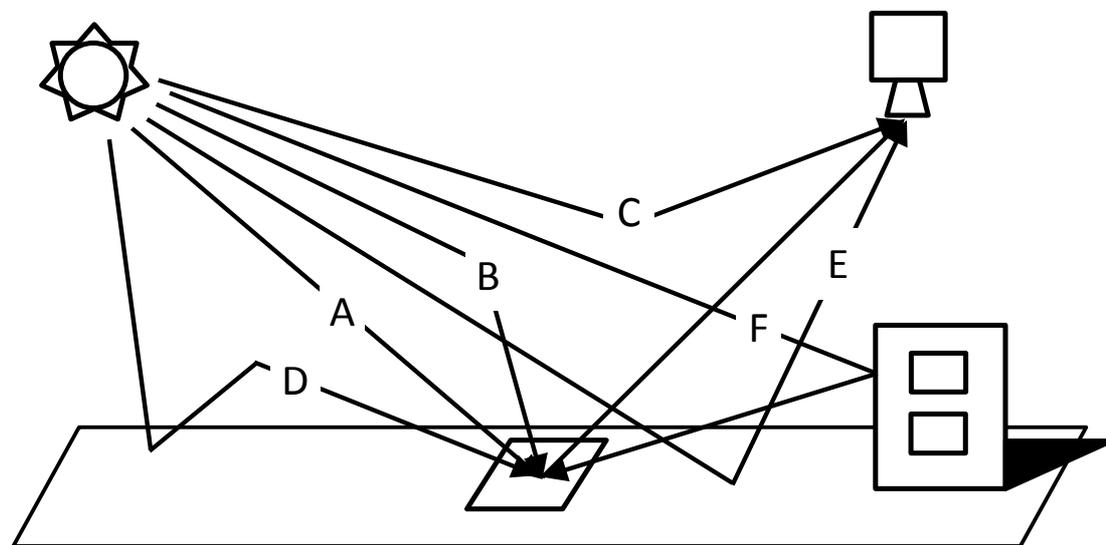
Figure 2. Radiation components reaching the sensor in the solar reflective spectral region (400 nm – 2500 nm). See text below for abbreviations.

The irradiance at flat, well defined object (rectangle at the bottom center) is composed mainly of direct solar radiation (A), skylight (or diffuse irradiance or diffuse solar radiation) (B), multiple scattering (D), and radiation reflected from adjacent objects (F). The radiance entering the sensor also receives contributions from the radiance reflected directly from the object (A), from adjacent objects (E), and from the path-scattered radiance (or upwelled radiance) (C) (Beisl, 2001; Schott, 2007; Schowengerdt, 2007). The at-sensor radiance can be expressed as follows:

$$L_{at\_sensor} = L_A + L_B + L_E + L_D + L_F + L_C \qquad (2)$$

It is also possible, that a photon could be bouncing multiple times in the atmosphere and in between all the possible combinations of atmosphere, target and adjacent objects before reaching the sensor, but these components are ignored in the Figure 2 for the sake of clarity. In general, the relative number of these multiply bounced photons becomes important only as the atmosphere becomes relatively thick and multiple scattering becomes important. Under good weather conditions, the second-order components, D, E, and F may be neglected for flat targets. In practice, in most empirical approaches, type F photons are lumped up with type B photons and type D with type C photons. The more thorough analysis of all the radiation components

and their relative magnitudes can be found in von Schönermark et al. (2004) and Schott (2007). For highly 3-dimensional structures such as forest canopies and rugged terrain, the component F makes a significant contribution (Richter and Schläpfer, 2013). Finally, the photons may also be scattering within the vegetation canopies (often called volume scattering).

2.1.3 Reflectance quantities

The ratio of the radiant exitance M to the irradiance E results in the so-called reflectance ρ, and its values are in the interval [0, 1]. The reflectance factor R is the ratio of the reflected flux of a sample surface compared to the flux reflected into the same geometry and wavelength range by an ideal (lossless) and diffuse (Lambertian) standard surface (in practice, often a Spectralon® panel), irradiated under the same conditions. Reflectance factors can reach values beyond 1. Both ρ and R are dependent on the angular distribution of all incoming and reflected radiance observed by the sensor, and wavelength of the radiation. Conceptual quantities of reflectance include the assumption of infinitesimal elements of solid angle and do not include measurable amounts of radiant flux (Nicodemus et al. 1977). All measurable quantities of reflectance are performed in the conical or hemispherical domain of geometrical considerations. (Schaepman-Strub et al., 2006)

Taking into account all possible combinations of directional, conical and hemispherical options for incoming and reflected radiance leads to nine different quantities (Nicodemus et al., 1977; Schaepman-Strub et al., 2006). The most central one is the bidirectional reflectance distribution function (BRDF), which models the dependence of the object reflectance as a function of illumination and observation geometries. Figure 3 illustrates the imaging geometry and the angles related to BRDF-model. The BRDF describes the intrinsic reflectance properties of a surface and thus facilitates the derivation of conical and hemispherical quantities. The BRDF can be expressed as follows:

$$BRDF_\lambda = f_r(\theta_i, \varphi_i, \theta_r, \varphi_r, \lambda) = \frac{dL_r(\theta_i, \varphi_i, \theta_r, \varphi_r, \lambda)}{dE_i(\theta_i, \varphi_i, \lambda)} \ [sr^{-1}] \tag{3}$$

where r referrers to reflected and i to incident component and θ and φ are the respective zenith and azimuth angles. Following the definition of reflectance factor, the bidirectional reflectance factor (BRF) is given by BRF = $d\Phi_r/d\Phi^{id}_r$ =πf_r [unitless], where id refers to ideal (Lambertian) surface. The concept hemispherical-directional reflectance factor (HDRF) is similar to BRF but includes irradiance from the entire hemisphere. This makes the quantity dependent on the atmospheric conditions and the reflectance of the surrounding terrain. In the strictest definition of HDRF by Nicodemus et al. (1977) the hemispherical irradiance must be completely diffuse, but Schaepman-Strub et al. (2006) loosened the definition to allow non-isotropic illumination field; even including the directional irradiance component of the sun

being part of this HDRF. Finally, the term bihemispherical reflectance factor (BHR), often called albedo, were the both reflected and incident components are hemispherical, has to be mentioned.
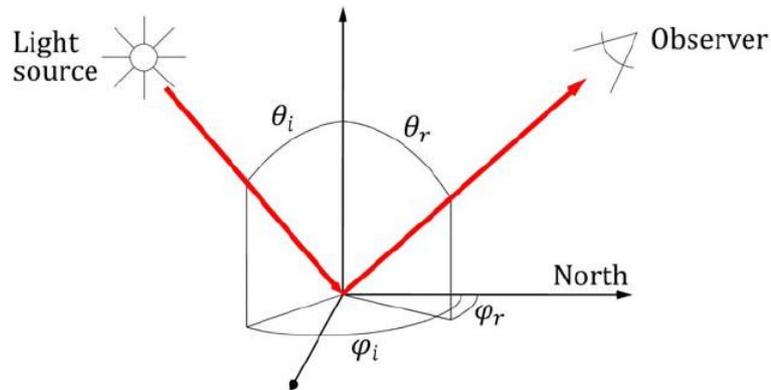
Figure 3. Measurement geometry: θ_i and φ_i are the incident (solar) zenith and azimuth angles respectively, and θ_r and φ_r are the corresponding emergent (observer) angles.

Even though the goniometric reflectance measurements (measurements where both the illumination and/or viewing angles may be varied) performed in laboratory strictly speaking results to biconical reflectance factors (conical-conical reflectance factor) CCRF, in this thesis, for the sake of clarity, these measurements are referred as BRDF-retrieval and its results to BRF. Also, when referring to field measurements with a spectrometer, the correct term would be hemispherical-conical reflectance factors (HCRF), but in this thesis we will call them reflectance factors. When using both the laboratory and field reflectance factor measurements, one has to be careful to compare correctly derived quantities.

Finally, in order to investigate the spectral behavior of the anisotropy, we can define the anisotropy factor (ANIF) as the ratio of the reflectance factor R to the nadir reflectance factor R_o, ANIF = R/R_0 (Beisl, 2001). The anisotropic and spectrally dependent performance of objects could be used to assist the quantitative image analysis, for example, for improving species classification, even though it may disturb the visual applications, the generation of seamless orthophoto mosaics, or classical remote sensing methods utilizing normalized data (Beisl, 2001; Lillesand et al., 2007).

2.2   Radiometric aspects in airborne imaging

From a physical point of view, the most common measurement setup of satellite, airborne and field instruments corresponds to hemispherical-conical configuration by its nature, where the incoming irradiance has both the direct and diffuse components. With high spatial resolution instruments with a small instantaneous field of view (IFOV), the conical field of view practically equals to directional geometry. Based on this assumption, the atmospherically corrected reflectance products from space- and airborne instruments, that in general are bottom of atmosphere (directional) reflectance, are often being referred as HDRF. In this

23

thesis, we will call them reflectance image products because in the strict sense they are not true HDRF and the resulted reflectance values for example from vegetation canopies and from shadowed areas are not well defined.

The DNs of an atmospherically corrected image products are still dependent on the imaging geometry. The term BRDF correction is defined as the process of eliminating the influence of the object reflectance anisotropy, i.e. the reflectance factor of image pixel is corrected for the anisotropic effects to be equivalent as the reflectance factor would have been measured from the nadir direction (Richter and Schläpfer, 2013). In a strict sense the evaluation of the BRDF correction would require the knowledge of the BRDF properties of all objects under concideration. In practice, most BRDF correction algorithms implemented in different software programs either correct only for the brightness gradient related to the large variation of the sensor viewing angle, and/or take into account the large brightness variations due to mountainous terrain (Richter and Schläpfer, 2013). These methods may be based on physical, empirical or semi-empirical surface type dependent or more general BRDF-models or databases (Beisl, 2001; Schott, 2007).

A challenge in modeling the atmospheric composition during airborne imaging campaign, when using radiative transfer codes compared to satellite sensors is that the flying altitude can vary between 500 m and 9000 m. To simplify the radiative transfer modeling, the sensor can be flown above the atmospheric boundary layer (typically from 0 to 2 km). The radiative transfer above this layer is relatively constant and can be modeled more easily than for lower altitudes, which require additional measures to define the boundary conditions for radiative transfer modeling (Ryan and Pagnutti, 2009). An example of radiation components at flying height of 1500 m for an object with an approximate reflectance factor of 0.26 is presented in Figure 4. The ground-reflected part (green line) is composed of reflected direct solar radiation (yellow line) and skylight. It can be seen that the effect of skylight (difference between yellow and green line) and path-scattered radiance (dark blue line) decreases towards longer wavelengths.

The radiation entering the sensor is controlled by the size of the sensor aperture and by the exposure time. During the exposure, the sensor is subject to both forward and angular movements, which can be compensated for by using stabilizing sensor mounts and forward motion compensation (FMC). The at-sensor radiance that goes through the sensor optics, the spectral filters, is converted into an analog signal, amplified in electronics, and finally sampled and quantized as DNs using an appropriate integration time, sampling area (pixel size), and number of quantization levels (pixel depth). This whole process can be described with a simplified sensor model for a pixel p in a certain channel (Schowengerdt, 2007):

$$DN_p = K * L_p + offset \qquad (4)$$

where DN is the recorded digital number, L_p is the channel- and space-integrated at-sensor radiance, and K and the offset are the channel-specific conversion parameters. We therefore have a linear relationship between the recorded DN and at-sensor radiance.
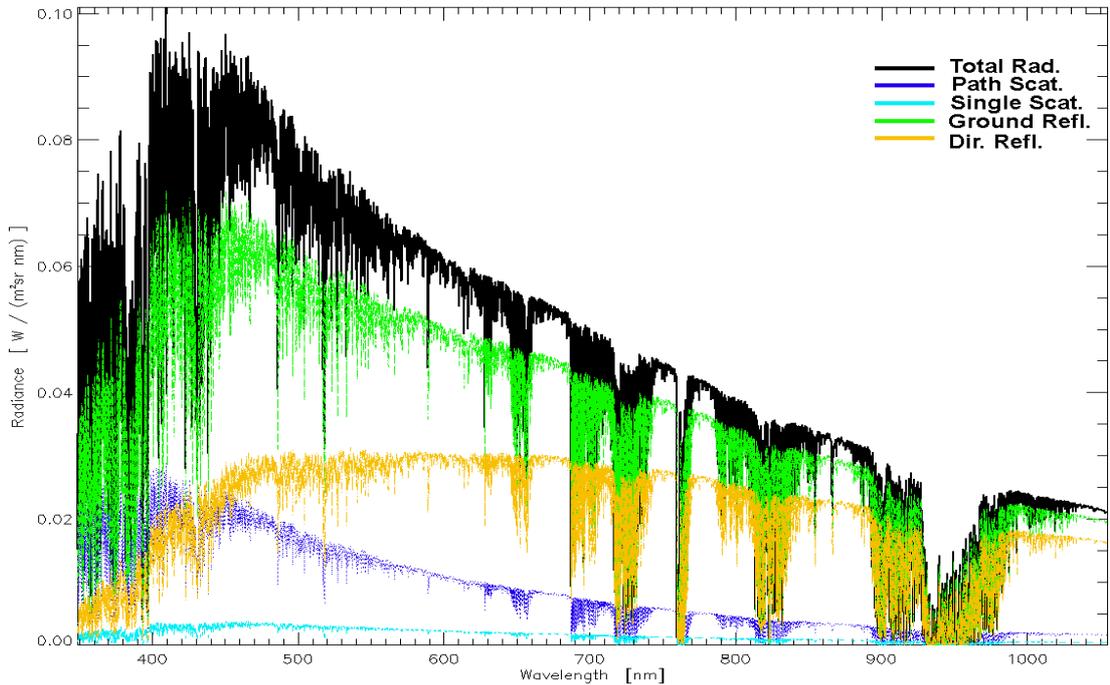
Figure 4. At-sensor radiance components at 1500 m flying height for a reference target with an approximate reflectance factor of 0.26. Total Rad = total radiance seen by the sensor, Path Scat. = total path-scattered radiance, Single Scat. = single scattered path radiance, Ground Refl. = total ground reflected radiance, Dir. Refl. = direct ground reflected radiance. Total Rad. = Ground Refl. + Path Scat. Ground Refl. = Dir. Refl. + skylight. Image is created with MODTRAN4 radiative transfer code.

Photogrammetric image collection is typically performed using a block structure with multiple parallel flight lines, and images are recorded with high overlaps both in the forward and side directions (Honkavaara, 2008b). In order to maximize the usability of photogrammetric imagery in radiometric analysis, several aspects have to be taken into account already when planning the campaign. The essential parameters that need to be decided upon are the flying height, the direction of the flight lines related to the direction of the sun, the forward and side overlap of the images, the time of the campaign, and the sensor parameters, such as the exposure time and the aperture size (Honkavaara et al., 2009b).

Photogrammetric height extraction is based on stereoscopy. The 3D coordinates are determined as the intersection of image rays from multiple images based on the collinear geometrical relationship between the object coordinate and the image point (Kraus, 1993). In photogrammetric applications, signal based matching methods are often used, and this method is also used in publication **III**. A high performance level is reached with high-quality photogrammetric images, utilizing multiple image overlaps and special matching strategies (Haala, 2009; Leberl et al., 2010; Höhle, 2011). In the signal based matching, the fundamental task is to determine correspondence between overlapping image patches. The precision is

dependent on the geometric and radiometric properties of the signals being matched and on the suitability of the geometric and radiometric modeling of the matching method for the task (Förstner, 1995). From the several aspects related to the accuracy of the intersected points, only the matching accuracy is directly related to the image radiometry and solar elevation, other factors are related to the geometric issues. The main radiometric parameter is the dynamic range of the sensor, so that the matching algorithm is able to find common points in various illumination conditions both in direct illumination and in shadows (Höhle, 2011).

2.3 Radiometric calibration

Radiometric calibration determines the radiometric response of an imaging sensor (Dinguirard and Slater, 1999; Lillesand et al., 2007; Schowengerdt, 2007). The main tasks include determining the relative and absolute radiometric calibration, spectral calibration, and possible colorimetric model. The relative radiometric calibration normalizes the output of the sensor so that a uniform response is obtained in the entire image area when the sensor receives a uniform radiance field, and is typically performed in laboratory (Beisl, 2006; Hefele, 2006). A typical remote sensing industry goal for relative radiometry is to have a less than 1 % variation between pixels (LDCM, 2003). With spectral calibration, the sensor response for the spectral irradiance as a function of the wavelength is determined (Schowengerdt, 2007). In most cases, the spectral calibration can only be performed in laboratory. The colorimetric calibration determines the relationship between the sensor and standard color spaces (Martínez et al., 2007). Understanding the sensor absolute and relative radiometric accuracy and uncertainty is a fundamental requirement for data analysis and decision-making based on the results derived from multiple platforms and sensors (Ryan and Pagnutti, 2009).

The absolute radiometric calibration determines for each channel the models and parameters that are needed to transform the DNs into the units of radiance. Typically, a linear model with gain and offset parameters is appropriate for CCD sensors (Schowengerdt, 2007):

$$L = cal_{gain} * DN + cal_{offset} \tag{5}$$

The cal_{gain} and cal_{offset} parameters are unique for each sensor channel, and, depending on the sensor, also for each aperture setting (Ryan and Pagnutti, 2009). A typical remote sensing industry specification for absolute radiometric calibration is a difference less than 5 % from the international standards, with a performance goal of less than 2 % (LDCM, 2003).

Well-known radiometric calibration approaches include laboratory, on-board, test field (vicarious), and self-calibration (on-the-fly) approaches (Cramer, 2005). Different equipment and methods are used for each approach, and they provide

different parameters and levels of accuracy (Honkavaara et al., 2009b). Laboratory calibration determines the sensor calibration in an indoor facility using, most typically, integrating spheres or hemispheres as light sources (Dinguirard and Slater, 1999; Beisl, 2006). On-board calibration determines the sensor calibration in flight conditions using various on-board calibrators or natural light sources (sun, moon). Vicarious methods determine the calibration of the whole system in flight conditions utilizing reference targets present at the scene to accurately determine the radiance entering the system. Self-calibration has to do with determining or improving the system calibration using the actual mapping data and is commonly used with geometry (Fraser, 1997). A European Union- funded project called the European Metrology for Earth observation and Climate program (MetEOC) is aiming to improve the accuracy and traceability of the pre-flight, on-board, and vicarious calibration methods for satellite sensors by factors of 2 to 10 by the end of 2014 (MetEOC, 2013).

In the ideal case, a laboratory calibration would be the only radiometric calibration method needed. The other methods are needed to validate the calibration in operational conditions, to evaluate the stability of the calibration, and to update the parameters of the calibration (Honkavaara et al., 2009b). The advantage of airborne sensors compared to space borne sensors is the possibility to return the sensor to the laboratory for a maintenance calibration.

2.3.1 Vicarious calibration

Vicarious calibration methods are well suited for space- and airborne sensor systems to validate and update the radiometric calibration in operational conditions and to monitor possible temporal effects such as drift, possibly as part of the imaging campaign (Ryan and Pagnutti, 2009). Vicarious methods require either accurate information on the atmospheric conditions and reference target reflectance factor (reflectance-based method) or a simultaneous determination of the at-sensor radiance by a calibrated radiometer (radiance-based method) (Slater et al., 1996; Biggar et al., 2003). With the radiance-based method, an absolutely calibrated radiometer is installed on an aircraft and flown over the reference site at an altitude of 3 km. Most of the atmospheric aerosols and water vapor are below this altitude, so the radiances that are measured are close to the at-satellite values (Slater et al., 1996). It is the most direct and potentially the most accurate vicarious calibration method. The typical reference targets include test fields, deserts, and dry playa lakes for the space borne systems and test fields, artificial painted, concrete, or gravel targets for the airborne systems (Dinguirard and Slater, 1999; Moran et al., 2001; Biggar et al., 2003; Honkavaara, 2008b).

For airborne sensors, a feasible vicarious calibration approach is the reflectance-based method. With this method, the at-sensor radiance is predicted by measuring the reflectance factor of a ground reference target, modeling the atmosphere using a

radiative transfer code and measured atmospheric properties, and then propagating the ground target radiance through the modeled atmosphere (Dinguirard and Slater, 1999; Pagnutti et al., 2002; Biggar et al., 2003). Finally, the calibration is performed using Equation (5). Two radiative transfer codes widely used in the remote sensing community are MODTRAN (Berk et al., 2006) and 6S (Vermote et al., 1997; Kotchenova et al., 2006). The main restriction with the reflectance-based method has to do with successfully executing the radiative transfer code to model the state of the atmosphere. It requires knowledge about the atmospheric transmission, the vertical column profiles of water vapor, pressure, temperature, the total column ozone, and aerosol asymmetry as well as the size distribution. Also, assumptions must be made about several atmospheric parameters, including the atmospheric point spread function and vertical column trace gases. It has been shown that some of these assumptions are not always valid for typical conditions in Finland (Mielonen et al., 2008). Collecting and processing data to develop knowledge about the atmosphere can be labor-intensive and complex, necessitating additional verification steps to ensure accurate vicarious radiometric calibrations (Ryan et al., 2007). The reflectance-based vicarious calibration method was used in all five publications of this thesis.

2.4   Photogrammetric sensors

The technical realizations, the geometric, radiometric, and spectral properties, and the image formats of airborne imaging sensors vary (Petrie and Walker, 2007). Large-format photogrammetric sensors are metric cameras with an image size comparable to analog 23 x 23 cm film, which was the old industry standard for aerial sensors. Other sensor types include small- and medium-format sensors (Grenzdörffer, 2010).

Currently, there are three main manufacturers of large-format photogrammetric sensors: Microsoft Vexcel, Intergraph, and Leica Geosystems. Intergraph and Leica have both been part of the Hexagon group since July 2010. The large-format photogrammetric sensors produced by these companies are the Microsoft UltraCam series (Gruber et al., 2011, Wiechert and Gruber, 2011), the Intergraph DMC series (Neumann, 2011b) and the Leica ADS series (Wagner, 2011). The basic properties of the latest generation of sensors from these series are presented in Table 1, and the imaging principles of these sensors are shown in Figure 5. Compared to the 1st and 2nd generation sensors evaluated in this study, the current sensors have for example larger image sizes, better frame rates, better radiometric sensitivities, better dynamic range and more advanced post-processing software. The Leica ADS sensors have from the beginning been designed to suit for quantitative remote sensing applications, while Microsoft UltraCam and Intergraph DMC sensors are originally designed more towards traditional topographic mapping.

28

Figure 5. From left: Imaging principle of Leica ADS80 SH92 pushbroom sensor with backward and nadir looking red (R), green (G), blue (B), near infrared (NIR) and panchromatic (PAN) lines and forward looking PAN line (from Wagner, 2011); Intergraph DMC-II with single optics for PAN, R, G, B and NIR channels (from Neumann, 2011a); Microsoft UltraCam Eagle with four optics for PAN image (MC, C1, C2, C3), single optics for R, G, B and NIR channels, and its PAN array orientation of nine CCD-frames behind the four optics (from Gruber et al., 2011).

Table 1. Properties of photogrammetric sensors. R = red, G = green, B = blue, NIR = near infrared, PAN = panchromatic, MS = multispectral, f = focal length, AD = analog-to-digital conversion, FOV = Field of view, CT = cross track, AT = along track, FMC = forward motion compensation, stag. = staggered, TDI = time-delayed integration.

		ADS80 SH92	DMC II$_{250}$	UltraCam Eagle
Type		Pushbroom, single head, two 4-band beamsplitters, 2 single Pan, 1 pair of Pan stag., 2x(R, G, B, NIR) lines	Multi head, 1 PAN frame, separate R, G, B NIR frames, separate optics for all channels	Multi head, 9 PAN frames with 4 optics; separate R, G, B, NIR frames with separate optics
Array size	**PAN**	2 x 12000 stag.	17216 x 14656	6670 x 4360
[pixels]	**MS**	12000	6846 x 6096	6670 x 4360
Image size	**PAN**	2 x 12000 stag.	17216 x 14656	20010 x 13080
[pixels]	**MS**	12000	6846 x 6096	6670 x 4360
pixel size [µm]	**PAN/MS**	6.5 / 6.5	5.6 / 7.2	5.2 / 5.2
Ratio	**PAN/MS**	1:1 (1:2 stag.)	1:3.2	1:3
f [mm]	**PAN/MS**	65 / 65	112 / 45	80 / 27
Dynamic range	**[bit]**	12 (16 AD)	14	12> (14 AD)
FOV	**CT/AT**	64 / 0 & 16	46.6 / 40.2	66 / 46
Frame rate	**[Hz]**	1000 (line rate)	0.59	0.56
FMC		-	TDI	TDI
	PAN	465-676	380-730	400-700
	Blue	420-492	390-503	400-580
Channels [nm]	**Green**	533-587	482-592	490-660
	Red	604-664	530-704	595-710
	NIR	833-920	695-921	690-970
Radiometric calibration		Absolute	Absolute	Relative

The dynamic range in Table 1 refers to the bit depth of a sensor that is to how many different DN values the radiance seen by the sensor can be recorded. The dynamic range (or radiometric resolution) can be expressed as base 2 exponents 2^x, where x is a positive real number, referred to as a bit. The typical maximum dynamic ranges for digital images based on the file format are as follows: 8 bits: 2^8 = 256, 12 bits: 2^{12} =

4096, and 16 bits: 2^{16} = 65536 (Schowengerdt, 2007). Another definition for the dynamic range of a digital sensor is the ratio of the maximum and minimum output signals that the sensor can record without saturation (Graham and Koh, 2004). The latter definition is used further in this thesis (Section 4.1), since it relates the dynamic range of the sensor to the minimum and maximum object reflectance that the sensor can record. In many photogrammetric applications, the images are down-scaled to 8 bits per channel, but the full native bit depth of the sensor (Table 1, dynamic range) should be used for quantitative radiometric applications.

Other, not so widely used, large-format photogrammetric sensors include VisionMap A3 (Pechatnikov et al., 2009), Optech CH-15000 (formerly known as DiMAC) (Optech, 2013), IGI Quatro DigiCAM (Minten, 2009; IGI, 2013), IGN CAMv2 (Souchon et al., 2010) and Jenoptik JAS150s sensors (Georgi et al., 2005). The geometric performance of the digital, large-format photogrammetric sensors has been studied thoroughly (Passini and Jacobsen, 2007; Honkavaara, 2008b; Jacobsen et al., 2010), and their suitability for efficient 3D point cloud and DSM generation has also been validated (Hirschmüller, 2011; Höhle, 2011; Haala and Rothermel, 2012).

Leica Geosystems ADS

The requirements of quantitative remote sensing and classical mapping applications were taken into account when constructing the Leica ADS, including radiometric and spectral laboratory calibrations. The ADS provides wide-band panchromatic imagery as well as narrow-band multispectral channels, which do not overlap and which have been optimized for both visual and remote sensing applications (Sandau et al., 2000). The radiometric laboratory calibration involves determining the dark signal non-uniformity (DSNU), the photo response non-uniformity (PRNU), and the absolute radiometric calibration factors with an integrating sphere (Beisl, 2006). All of the radiometric calibrations are performed using NIST traceable light sources. For post-processing the ADS imagery, Leica provides software program, called Leica XPro; the basic output is a radiometrically calibrated, at-sensor radiance image. In addition, XPro provides several options for producing radiometrically corrected surface radiance and reflectance image products, with or without BRDF- correction (Beisl et al., 2008). The radiometric quality of the first-generation ADS40 sensor was evaluated in publication **I,** and the second-generation ADS40-SH52 sensor in publication **IV**; the quality of the reflectance image products generated using the Leica XPro software was evaluated in publications **IV** and **V**.

Intergraph DMC

The radiometric laboratory calibration of the DMC involves both the relative and absolute calibration. The sensitivity differences between the individual elements of a CCD array, defect pixels, light falloff, linearity, and dark signal are determined for

each aperture, temperature, and TDI setting using an integrating sphere (Diener et al., 2000; Hefele, 2006; Ryan and Pagnutti, 2009). All radiometric calibrations are performed using NIST-traceable light sources. The absolute radiometric calibration parameters are calculated separately for each aperture, and the expected radiometric accuracy is approximately 3 % in the laboratory (Ryan and Pagnutti, 2009). For post-processing the DMC imagery, Intergraph provides a software program called PPS, which produces photometrically color balanced output. The radiometric quality of the first-generation DMC sensor was evaluated in publications **I**, **II** and **III**, and its imagery was converted into a reflectance factors in publication **III** using a modified empirical line−based method.

Microsoft UltraCam

The laboratory calibration of the UltraCam includes the relative calibration of pixel non-uniformities, light falloff correction, and a colorimetric calibration. During the post-processing phase, the shutter release feedback and a dynamic aperture model are taken into account (Schneider and Gruber, 2008). There is no information available concerning the absolute radiometric calibration of the UltraCam in the laboratory. For the end-to-end photogrammetric processing workflow of UltraCam imagery, Microsoft offers UltraMap software, which in radiometric terms provides model-based radiometric correction to compensate for or remove hotspots, atmospheric effects, and haze, as well as project-based color balancing (UltraMap, 2013). The radiometric quality of the first-generation UltraCam sensor the UltraCamD was evaluated in publication **I**.

2.4.1   Radiometric evaluations of photogrammetric sensors

Until recent years, only a few scientific studies on the radiometric performance of photogrammetric sensors have been presented. In the following, essential studies found from the literature are presented, and their results related to the ones obtained in this thesis are discussed in the Results and Discussion sections (5 and 6).

 The Institut Cartogràfic de Catalunya (ICC) in Spain has presented a colorimetric calibration for the DMC sensor (Martínez et al., 2007), a vicarious method for radiometrically calibrating the DMC by acquiring simultaneous hyperspectral CASI imagery (Martínez and Arbiol, 2008; Martínez et al., 2010), and an NDVI (Normalized Difference Vegetation Index) product based on atmospherically corrected reflectance image products from the DMC (Martínez et al., 2012). Korpela et al. (2011) and Heikkinen et al. (2011) used the same at-sensor radiance and reflectance image products created using the Leica XPro software as in publications **IV** and **V** for tree species classification. Korpela et al. (2011) analyzed the variations caused by directional reflectance anisotropy and the within-species variation in tree reflectance factor properties at the level of a single tree. Heikkinen et al. (2011) used

a support vector machine (SVM) algorithm for the tree species classification and compared the results obtained using the at-sensor radiance imagery and reflectance image products. Studies of the ICC, by Korpela et al. (2011) and Heikkinen et al. (2011) are related to the EuroSDR's "Radiometric Aspects of Digital Photogrammetric Images" project (Honkavaara et al., 2013).

Within the scope of the DGPF's "Evaluation of digital photogrammetric aerial cameras systems" project (Cramer, 2010), a trial for the vicarious radiometric calibration of the several large-format photogrammetric sensors was performed on a test field but without success due to unfavorable weather conditions and problems with the ground truth measurements (Schönermark, 2010). As part of the same project, Hanusch and Baltsavias (2009) conducted histogram analysis, the detection of artifacts, sensor linearity, vignetting, and noise analysis for the DMC, ADS40, and UltraCamX sensors. Waser et al. (2010) evaluated the potential of digital sensors for land cover and tree species classification and used the images without any atmospheric corrections. Imagery from this project was also used by Beisl and Adiguezel (2010) to validate the atmospheric correction and accuracy of the reflectance image products from ADS40 imagery created using the Leica XPro software.

In other studies, Rosso et al. (2008) evaluated and compared the ADS40, ADS40-SH52, UltraCamD, and DMC sensors in terms of their applicability to biotype mapping in northern Germany. Haest et al. (2009) performed a vicarious reflectance-based radiometric calibration for the UltraCamD imagery using reference measurements performed four years after the image acquisition. Alvarez et al. (2010) performed a radiometric characterization and evaluation of the UltraCamX and UltraCamXp sensors and a partial empirical line–type radiometric correction for the images in order to evaluate the usability of the images in National Plan of Aerial Orthophotography (PNOA) in Spain. Green et al. (2011) performed quantitative and qualitative comparisons of the suitability of the ADS40-SH52, DMC, and UltraCamD sensors for a benthic habitat and propeller scar mapping. Hernández-López et al. (2012) performed a vicarious radiometric calibration for the ADS40 sensor and compared the results to the laboratory calibration of the sensor. The comparisons were performed for reflectance image products based on both calibrations. Passini et al. (2012) evaluated the radiometric quality of the DMC-II and UltraCam Eagle sensors using edge analysis. They could not detect any loss of information in pan-sharpened color images. The effect of pan-sharpening to the radiometric quality of frame sensor images is not evaluated in this thesis.

2.5   Radiometric correction

The different processing operations performed to the image DNs can be divided to two groups: restoration and enhancement (Lillesand et al. 2007). The idea of

restoration operations is to restore the image from all kinds of distortions and artifacts to present the correct information of the recorded object. The idea of image enhancement is to optimize the image DNs for specific purposes and these operations may lose some of the original information content of the image. The radiometric correction processes evaluated in this thesis belong to the image restoration group, and the topic of various image enhancement operations is beyond the scope of this thesis.

A typical need in different image applications is the removal of the time- and scene-dependent effects from the imagery; this is often called image normalization (Mahiny and Turner, 2007). The variability between images is normally a result of differences in the atmospheric properties, imaging and illumination geometry, exposure settings, and sensor stability. The choice between different image normalization methods depends on the application: For visual applications, relative and/or subjective user dependent normalization can give satisfactory results, but for quantitative applications the objective is to obtain either reflectance factors or to correct relative magnitudes of the radiance/reflectance between the channels, images, and different dates (Honkavaara et al., 2009b).

In this study, the objective of radiometric correction is defined as the generation of reflectance image products. Normally, the starting point for reflectance image product generation is a radiometrically calibrated sensor. Also, the term atmospheric correction is commonly used for the process of converting image DNs into reflectance factors. Radiometric correction includes the removal of the path-scattered radiance and the normalization of the solar irradiance. These two steps are often performed simultaneously in radiometric correction software. Starting from the original recorded raw DNs, they are first converted to at-sensor radiance with linear transformation (see Equation (5)), and in the second step, these radiances are converted via often nonlinear transformation to reflectance factors. Song et al. (2001) have shown that for satellite images, atmospheric correction affects the results of the ratio transformations calculated using images such as the NDVI, and that image classification is the image analysis procedure least affected by atmospheric correction.

Converting the DN of a pixel into a reflectance factor using atmospheric models is a well-known procedure with satellite images (Richter, 1990; Chavez, 1996; Schowengerdt, 2007; Immizer et al., 2012). Such methods have also been established for airborne imaging spectroscopy (Richter, 1996; Martínez et al., 2010). However, radiometric correction methods are rare when using aerial photogrammetric images due to the special features of photogrammetric data acquisition, such as the wide field of view, varying flying heights, the frame image format, and varying sensor exposure settings (Read and Graham, 2002; Ryan and Pagnutti, 2009; Beisl, 2012). Also the relatively wide multispectral channels of

photogrammetric sensors and the lack of channels in the shortwave infrared region (1-3 µm) require adaptation of the traditionally used atmospheric correction algorithms (Richter, 2008).

Image mosaics combined from multiple aerial images are often created using photogrammetric software packages, in which the creation of the mosaic is based on the statistical adjustment and local feathering of image borders, and combines the atmospheric and BRDF corrections in a single step (Honkavaara et al. 2009b). This is often called dodging. One problem with these methods is that the physical connection between the radiance seen by the sensor and the final DN on the image mosaic is lost.

2.5.1 Empirical methods

The lack of atmospheric information and other information required for the radiative transfer-based correction models and the large size of the data, that is, the large computational workload, are central reasons for using empirical radiometric correction methods (Collings et al., 2011).

Earlier studies have presented empirical methods for performing relative radiometric corrections on aerial images. Tuominen and Pekkarinen (2004) presented a local radiometric correction method for reducing the BRDF effects on aerial images by utilizing the satellite imagery from the same area. Because of the narrower field of view and the larger GSD compared to the aerial imagery, the BRDF effects are lower in the satellite imagery. Packalen et al. (2009) presented a relative correction for aerial images by utilizing the overlapping areas of neighboring images as a substitute for radiometric correction.

The well-known empirical method for producing reflectance image products is the empirical line-based method (Smith and Milton, 1999; Clark et al., 2011). With this method, a line is fitted between the reference target image DNs and the target reflectance factor acquired either from field measurements or from spectral database. The method requires at least two ground reference targets, and the calculations are done separately for each sensor channel. Then, the linear parameters are used to convert the whole image into a reflectance image product. The same parameters can be used for all images in the image block. The basic assumption when using the empirical line-based method is that the atmospheric conditions are homogenous and stable throughout the whole campaign area. With this method, the sensor can be radiometrically calibrated, or, if not, then the method combines the linear conversions from the raw DNs to at-sensor radiance and from at-sensor radiance to reflectance factor into a single linear transformation (Haest et al., 2009). Haest et al. (2009) and Clark et al. (2011) used the empirical line-based method for data where the reference reflectance factor measurements were taken at a different time than the original imagery, which lacked atmospheric data.

A recent method for creating homogenous image mosaics from frame sensor imagery is the so-called radiometric aerotriangulation method (Wu, 2006; Chandelier and Martinoty, 2009; Collings et al., 2011; Hernández-Lopéz et al., 2011; Honkavaara et al., 2012). With this method, the idea is to correct both the within- and between-scene differences by using the so-called radiometric tie points from overlapping images and to leave the true differences between the objects unchanged. These methods may include empirical (Kennedy et al., 1997) or semi-empirical models (Roujean et al., 1992; Wanner et al., 1995) for BRDF correction, which are solved based on the imagery only. It is possible to use the empirical line method principle to convert the whole image mosaic into a reflectance factors or to perform mosaicing and reflectance conversion as a simultaneous process (Collings et al., 2011; Honkavaara et al., 2012).

2.5.2 Radiative transfer-based methods

With radiative transfer-based radiometric correction methods, the interaction between the radiance and the atmosphere is modeled using radiative transfer codes such as MODTRAN and 6S. The inversion of the radiative transfer code retrieves the directional reflectance factor from the radiometrically calibrated imagery.

In a simplified case, when the multiple scattering radiance components are neglected, the key formula for radiometric correction is the model used for surface reflectance factor:

$$\rho = \frac{\pi \left(\left(cal_{offset} + cal_{gain} * DN \right) - L_0 \right)}{T_{down} T_{up} S \cos \theta_i} \tag{6}$$

where ρ is the surface reflectance factor, cal_{gain} and cal_{offset} are the sensor calibration parameters, DN is the recorded target digital number, L_0 is the path-scattered radiance, T_{down} is the total downward transmittance from the top of the atmosphere (TOA) to the ground, T_{up} is the total upward transmittance from the ground to the sensor, S is the mean extraterrestrial solar irradiance, and θ_i is the solar zenith angle (Schowengerdt, 2007; Beisl et al., 2008; Richter and Schläpfer, 2013).

The main atmospheric parameters needed with a high degree of accuracy in Equation (6) are the aerosol type, the horizontal visibility or optical thickness, and the water vapor, because these influence the values of the path-scattered radiance, transmittance, and extraterrestrial solar irradiance (Richter and Schläpfer, 2013). There are two basic approaches for acquiring these parameters: Either to estimate the atmospheric parameters based on the imagery itself (Chavez, 1996; Schowengerdt, 2007; Beisl et al., 2008) or to use in-situ atmospheric measurements. Also, if the main atmospheric parameters and the reflectance factor of two reference targets are known, the quantities L_0, T_{up}, T_{down}, S, and ρ can be solved. So, a vicarious in-flight radiometric calibration of the sensor can be performed (Richter and Schläpfer, 2013).

Class of simple data-driven radiometric correction methods in the visible region are the so-called Dark Object Subtraction (DOS) methods (Chavez, 1996), in which the path-scattered radiance, L_0, is estimated based on the dark objects found in the image (deep clear lakes, shadows).

For airborne photogrammetric pushbroom imagery, two examples of commercially available software programs that provide the possibility for radiometric correction are Leica XPro (Beisl et al., 2008) and ATCOR-4 (Richter and Schläpfer, 2013). All of the corrections in XPro rely entirely upon a priori sensor calibration information and the atmospheric information derived from the dark pixels (and bright pixel statistics for BRDF correction) in the image data. An integral part of all ATCOR versions is a large database containing the radiative transfer calculations which are based on the MODTRAN®5 code. Just recently, a new add-on for ATCOR-4, called ATCOR-ADS, was presented to provide a more straightforward and efficient work flow for the rather sophisticated user interface of the original ATCOR (Schläpfer et al., 2012). Two other atmospheric correction software programs based on the MODTRAN radiative transfer code are ACORN (ImSpec, 2013) and FLAASH (Adler-Golden et al., 2008). ACORN is available as stand-alone software program and works for hyper- and multispectral space borne and airborne pushbroom imagery. FLAASH is an atmospheric correction module for ENVI image analysis remote sensing software designed for satellite and airborne hyperspectral sensors. The ability to use ACORN and FLAASH software with multispectral photogrammetric pushbroom sensors has not been studied yet.

For airborne photogrammetric frame sensor imagery, there are only a few radiometric correction software solutions and their performance has not been documented in scientific publications. One is Image Calibrator atmospheric correction software (Image Calibrator, 2013) and another solution is currently being developed by Leica Geosystems (Beisl, 2012).

MODTRAN®5 includes a new option for generating atmospheric correction data. This spectral data provides the information required to convert radiances from down-looking, solar-region, hyperspectral imagers into surface reflectance factors (Berk et al., 2006). The usability of this option for photogrammetric sensors needs further studies.

Even though the programs mentioned in this section try to correct the atmospheric effects from the imagery as accurately as possible, they still have restrictions, simplifications in their physical interactions, and underlying assumptions that limit their usability and accuracy. For example multiple scattering components are often either ignored or modeled only with limited accuracy. The successful execution of these programs requires an experienced user, accurate knowledge of the atmospheric parameters (derived either from the imagery or measured in-situ), and possibly an iterative execution of the codes (Ryan et al., 2007).

3. Materials

3.1 Imagery

The imagery used in this thesis was collected over the **Finnish Geodetic Institute's** (FGI) Metsähovi photogrammetric image quality test field (**I**, **II**. The test field was formerly known as Sjökulla) and over the Hyytiälä forestry test site (**III**, **IV**, **V**). The Metsähovi test field is located in southern Finland, in Kirkkonummi (60°15'N, 24°23'E). It was established in 1994, modernized in 2008 and it is designed for calibration and validation (Cal/Val) of various airborne sensors. The test field includes signals for geometric calibration and an image quality test field for radiometric and spatial resolution calibration (Figure 6, Figure 7). The details of the Metsähovi test field have been described in Kuittinen et al. (1994, 1996), Ahokas et al. (2000), and Honkavaara et al. (2008). The Hyytiälä forestry test site is located in southern Finland, in Juupajoki (61°51'N, 24°17'E), and it is maintained by the **University of Helsinki's** Faculty of Agriculture and Forestry. Hyytiälä is an active field center for multidisciplinary research on forests, peatlands and the atmosphere (Hyytiälä, 2013).

Table 2 summarizes the imagery used in the thesis. The imagery used in publication **I** was collected in particular for geometric and radiometric calibration and validation of photogrammetric sensors, and results related to these evaluations are reported in the following studies: Becker et al. (2006), Honkavaara et al. (2006a, 2006b, 2006c, 2006d, 2008a, 2008b), Markelin et al. (2006) and Honkavaara and Markelin (2007). The imagery used in publication **II** was originally collected for acceptance testing of the new camera system owned by the National Land Survey of Finland and the results of this test have been reported in Honkavaara et al. (2011a). The imagery used in publication **III** was collected so that it could be used both in radiometric evaluations and tree species classification. The imagery used in publications **IV** and **V** was collected both for radiometric evaluations and for tree species classification and the first classification results have been published by Heikkinen et al. (2011) and Korpela et al. (2011). The images used in publications **II**, **IV,** and **V** became part of the empirical material for the EuroSDR**'s** "Radiometric aspects of digital photogrammetric images" project. The results of this project can be found in the final report by Honkavaara et al. (2013). The ADS sensor used in

publications **IV** and **V** was the second-generation ADS40 SH52, in contrast to the first-generation ADS40 sensor used in publication **I**.

Table 2. Imagery used in publications. Pub. = Publication, FH = flying height, GSD = ground sampling distance, PAN = panchromatic sensor, MS = multispectral sensor. In **II** all flight lines were flown with different sensor exposure settings.

Pub.	Sensor	Date dd.mm.yyyy	Time [UTC+3]	FH [km]	GSD PAN/MS [cm]	Flight lines
I	DMC	01.09.2005	10:50	0.50	5/22	1
I	DMC	01.09.2005	11:40	0.80	8/38	1
I	ADS40	26.09.2005	13:18	1.50	15/15	1
I	ADS40	26.09.2005	12:30	2.50	25/25	1
I	UltraCam$_D$	01.07.2006	11:30	0.94	8/24	1
I	UltraCam$_D$	05.07.2006	10:45	0.48	4/12	1
II	DMC	01.09.2008	10:19-11:41	0.50	5/24	3
II	DMC	25.09.2008	11:39-12:27	0.50	5/24	6
III	DMC	31.05.2009	8:07	2.00	20/80	1
III	DMC	31.05.2009	8:21	3.00	30/120	1
III	DMC	31.05.2009	8:33	4.00	40/160	1
III	DMC	31.05.2009	11:15	2.00	20/80	1
III	DMC	31.05.2009	11:46	3.00	30/120	1
III	DMC	31.05.2009	11:58	4.00	40/160	1
IV, V	ADS40	23.08.2008	9:56-10:36	1.00	10/10	3 (1 in IV)
IV, V	ADS40	23.08.2008	10:45-11:03	2.00	20/20	2 (1 in IV)
IV, V	ADS40	23.08.2008	11:18-11:35	3.00	30/30	3 (1 in IV)
IV, V	ADS40	23.08.2008	11:43-11:54	4.00	40/40	2 (1 in IV)

3.2 Reference targets

The main radiometric analysis of all the campaigns was based on the well-defined flat reference targets (permanent gravel targets (**II**) and portable reference tarpaulins (tarps) (all publications)). In publications **III**, **IV,** and **V** also additional permanent targets (asphalt, sand, grass, weeds) were used. Finally, in publication **III**, asphalt road, field and trees were used in analyzing the effect of shadows and illumination angle. The properties of all these targets are described in Table 3 and close-up pictures of selected targets are shown in Figure 9. The reflectance properties of the Metsähovi old permanent gravel targets are described in detail in Peltoniemi et al. (2007), whereas the new permanent gravel targets and portable reference tarps are described in detail in Honkavaara et al. (2010).

Figure 6 shows the Metsähovi test field during the DMC and ADS40 campaigns discussed in publication **I, with all eight of the FGI's portable reference tarps** installed (named P05, P10, P20, P25, P30, P45, P50, P70). The tarps are flat, well-defined targets; their colors have been made as isotropic as possible. During the UltraCamD campaign in 2006, only four tarps were used. Figure 7 shows the modernized Metsähovi test field during the 1.9.2008 campaign discussed in

publication **II**. Figure 8 presents the reference target configuration at the Hyytiälä forestry test site during the campaigns discussed in publications **III**, **IV**, and **V**.

Table 3. Description of the reference targets used in the thesis. Pub. = publication where the target was used. Letters after asphalt, grass, gravel, sand and weed targets refers to the abbreviation used in different publications, see Figure 8. For close-up images of selected targets, see Figure 9 and for field nadir reflectance factor spectra, Figure 10.

Target name	Pub.	Description
P20		Portable tarpaulins, sized 5 m by 5 m each, are made of polyester with PVC coating, and painted with the mix of titanium oxide and carbon-black pigments to achieve as isotropic different shades of gray as possible. Tarps can be installed in different combinations from single tarp to all eight tarps forming a grayscale.
P30	**All**	
P50		
P10		
P45	**I**	
P70		
P05	**I,III,IV,V**	
P25	**I,II,III**	
B1		Permanent black (B1, B2a, B2b), gray (G2), red (R1) and white (W2) gravel targets. Size of B1 and R1 are 6 m x 6 m, others 14 m x 15 m. B2a and B2b are made of the same gravel with grain size of 4-12 mm. Grain size of other gravels is 8-16 mm.
B2a		
B2b	**II (no R1)**	
R1		
G2		
W2		
Asphalt (A)		Rather old asphalt road
Grass (B,C)	**III,IV,V**	Grass football field
Gravel (D,F,G)		Gravel road
Sand (C,E)		Beach volley sand
Weeds (H,I)	**IV**	Non-maintained open field
Asphalt		Asphalt road, average of 20 plots of size 1.6 m x 1.6 m
Field	**III**	Average of 7 plots of size 2 m x 2 m
Coniferous trees		Average of 20 trees, window size 1.6 m x 1.6 m each
Deciduous trees		

Figure 6. Metsähovi image quality test field in 2005 with all eight portable reference tarps installed in the form of grayscale (from **I**).

Figure 7. The modernized Metsähovi image quality test field in 2008 during the 1.9.2008 DMC campaign. For abbreviations, see Table 3 (from **II**).

Figure 8. Hyytiälä forestry test site during the DMC campaign of **III** (left) and ADS40 campaign of **IV** and **V** (right, from **IV**). For abbreviations, see Table 3, and for close-up images of targets, see Figure 9.

Figure 9. Close-ups of selected reference targets. From top left: Metsähovi gravels B2a and W2, Hyytiälä asphalt and football field grass. From bottom left: portable tarp P20, Hyytiälä gravel road, Hyytiälä beach volley sand and Hyytiälä weeds. Image colors and scales are not comparable. See Table 3 for description of the targets.

3.3 Reference measurements

During all of the campaigns, the reflectance factor of the reference targets in the nadir observing direction were measured using an ASD Field Spec Pro FR spectroradiometer from the FGI. Each target was measured multiple times at different places, and these measurements were averaged to get the final nadir field reference reflectance factor (ρ_{field_nadir} in Equation (7)). The average measurement accuracy of the field reference was estimated to be better than 5 % for uniform targets and between 5 % and 20 % for the other targets. In publications **III** and **V,** the laboratory BRDF retrieval was used to obtain BRFs for the reference targets (the portable samples of Metsähovi gravels and the portable reference tarps) in exact imaging geometry. The BRDF retrieval was performed using the FIGIFIGO goniospectrometer (Suomalainen et al., 2009). Figure 10 shows an example of the nadir field reflectance factor spectra of the reference targets used in publication **IV**.

During the campaigns discussed in publications **I** and **II,** no in-situ atmospheric measurements were available, so horizontal visibility and temperature information from the Helsinki-Vantaa Airport (34 km NE from the Metsähovi test field) was used for the radiative transfer modeling. The Hyytiälä forest research station is equipped with a state-of-the-art SMEAR-II weather station (Hari and Kulmala, 2005; SMEAR, 2013), which is also part of the NASA AERONET network (Holben et al., 1998). Weather information (horizontal visibility, temperature, AOT, CO_2, H_2O, O_3) from this station was used for the radiative transfer modeling discussed in publications **III**, **IV,** and **V**.
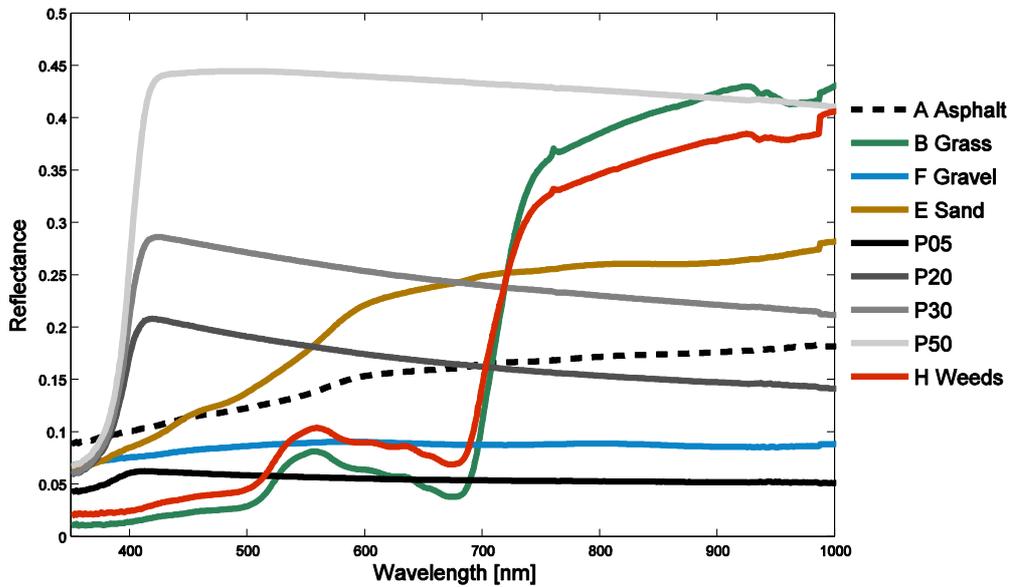
Figure 10. Example of the nadir field reflectance factor spectra of the reference targets used in **IV**. See Table 3 for description of the targets and Figure 9 for close-up images of selected targets.

The weather conditions varied during the campaigns. In many cases, there was only a short time window of opportunity for the campaign and the campaign had to be performed in suboptimal conditions. In **I**, the weather conditions were excellent during the DMC campaign and acceptable for the photogrammetric projects during the ADS40 and UltraCamD campaigns. The weather conditions during the DMC campaigns discussed in **II** were excellent. In **III**, the imaging conditions were excellent, with an average horizontal visibility of 45 km and aerosol optical thickness (AOT) at 500 nm for approximately 0.058 during the morning and 0.075 during midday. During the ADS campaign discussed in **IV** and **V**, the weather conditions were mostly clear, but some clouds were present when capturing the 3 km and 4 km flight lines (Figure 11).

Figure 11. Clouds on 3 km flying height nadir looking ADS line 3A (left) and 4 km flying height 16° backward looking line of 4A (right), CIR images.

4. Methods

4.1 General

Different radiative transfer modeling scenarios used and the radiometric correction options evaluated in this thesis are shown in Figure 12. The airplane equipped with a photogrammetric sensor collects images over the target area.
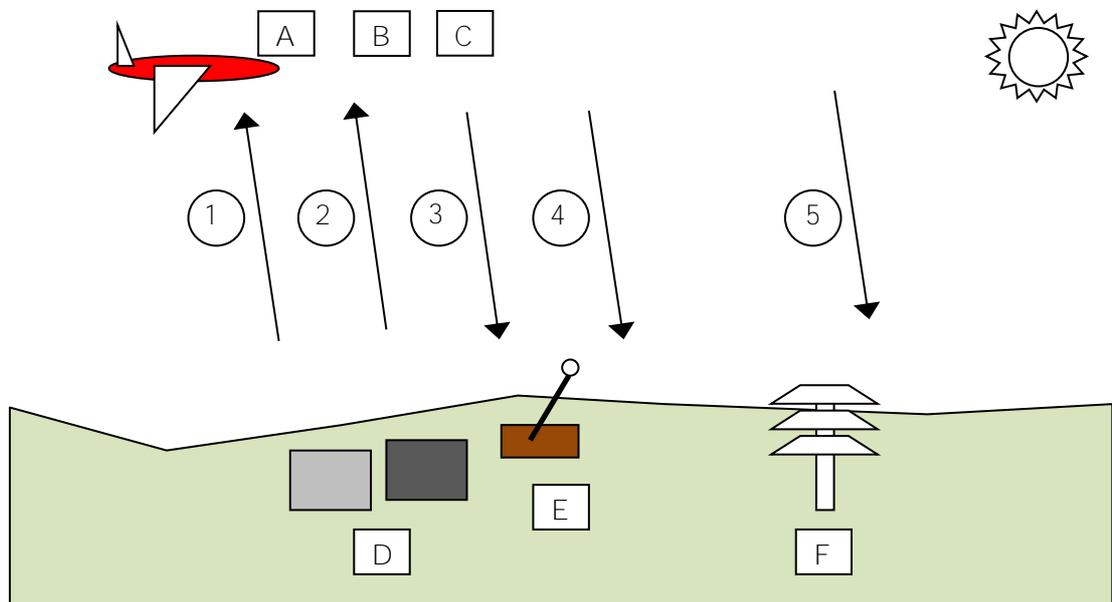
Figure 12. Different components used in radiative transfer modeling and radiometric correction. The sensor radiometric calibration can be either from A = laboratory, B =vicarious calibration using MODTRAN or C = using ATCOR-4. On the ground are reference targets (D), in situ reflectance factor measurements (E), and in situ atmospheric measurements (F). 1: MODTRAN at-sensor radiance; 2: ATCOR-4 vicarious calibration; 3: empirical line, 4: XPro and 5: ATCOR-4 radiometric correction.

The arrows in the Figure 12 indicate the different forward radiative transfer modeling (arrows pointing upwards) and radiometric correction methods (arrows pointing down, inverse modeling) used in the thesis. The different scenarios shown in Figure 12 were used in the original publications as follows. Arrow 1 refers to at-sensor radiance calculations using the MODTRAN-4 radiative transfer code (**I**, **II**, **III**, **IV**) used for sensor evaluation (**I**, **II**) and vicarious calibration (**I**, **II**, **III**, **IV**), arrow 2 refers to the vicarious calibration done using ATCOR-4 software (**V**), arrow 3 refers to reflectance image product generation using the modified empirical line-based method (**III**), arrow 4 refers to radiometric correction using photogrammetric Leica XPro software (**IV**, **V**) and arrow 5 refers to radiometric correction using ATCOR-4 software (**V**). In publication **IV**, the calibrations and at-sensor radiances

based on the sensor laboratory calibration (A) and the vicarious calibration were compared (B).

4.2   Image measurements and general performance analysis

To evaluate the radiometric properties of the sensors and to assess the radiometric quality of the data, various image measurements were taken and a general radiometric performance analysis was conducted.

The basic image statistics in all of the studies was the average DN value of the reference targets measured for each target and the sensor channel from all of the images. Also, the standard deviation and the DN range for each target were measured. These reference target average DNs with at-sensor radiances from the radiative transfer modeling (Section 4.3) were used to evaluate the linearity, dynamic range, and saturation in publications **I** and **II**, to evaluate the sensitivity in publication **I**, and to evaluate the sensor radiometric stability in publication **II**. These image measurements provided the reference target data reflectance factors in publications **III**, **IV,** and **V** (the data in Equation (8) and Table 5). In publication **II**, the reference target DNs were normalized with respect to the exposure time and both the exposure time and the aperture size for compensate the effect of the camera exposure settings. In publications **III**, the image DN (reflectance) measurements from asphalt, field, and forest in both direct sunlight and shadow were used to evaluate the effect of the solar elevation angle on the image radiometry. The purpose of the reflectance factor evaluations in **III** was to compare relative differences between morning and noon data and shadowed and sun illuminated areas, not to perform quantitative analysis of the target reflectance properties.

In publications **I**, **II** and **III,** the image histograms and DN distribution metrics (average, standard deviation, minimum, maximum, 100% and 99% efficiency, i.e. the full width of the histogram and the width of the histogram after 0.5 % of the DNs are left out from both ends) of the whole images were calculated for all of the images, separately for each channel. These statistics were used to evaluate the saturation of the imagery and the dynamic range of the photogrammetric sensors.

The linearity of the sensor response to varying amounts of radiance was evaluated by presenting the measured reference target average DNs as a function of the reference target at-sensor radiance as well as by analyzing the fit of the linear model and calculating the coefficient of determination R^2 (**I**, **II**). The linearity was evaluated using the range between the darkest and brightest reference target DN values that the sensor could record without saturation.

The image saturation (in bright targets, it is the result of overexposure, whereas in dark targets it is the result of underexposure) was evaluated by using the standard deviation statistics of the reference target DNs (**II**), by analyzing the image

histogram statistics (**I**, **II**, **III**) and by finding the non-linearities from the linearity analysis (**I**, **II**).

In the case of field calibration, the dynamic range is related to the width of the object reflectance range that the sensor can record without saturation, and it can be expressed either as a reflectance range or as the width of the DN range of image, which can be converted into bits (Section 2.4). In publications **I**, **II**, and **III**, the dynamic range of the sensor was evaluated by using 100% and 99% efficiency image histogram statistics, and the evaluations were supplemented by analyzing the image saturation results.

The radiometric stability of the sensor was evaluated in publication **II** by making pair-wise comparisons of the absolute radiometric calibration parameters determined from the images collected with different sensor exposure settings. The similarity between the vicarious calibration parameters of the two different sensor settings was assessed by evaluating the similarity of the regressions using the F-test with a 95 % confidence level (Pindyck and Rubinfeld, 1991).

The sensitivity of a sensor indicates how small the object reflectance differences can be while the sensor is still able to record them (Graham and Koh, 2004). In this thesis, sensitivity was related to the differences between the sensor channel responses. The sensor channel sensitivities were analyzed in publication **I** by comparing the DN responses of the various channels to certain at-sensor radiances.

In this thesis, based on the general radiometric performance analysis and vicarious calibration, the sensor can be declared to have good radiometric quality if it can be radiometrically calibrated, that is, if the sensor has a linear response and is radiometrically stable, and the sensor has a high dynamic range and high sensitivity.

4.3   Vicarious calibration

The at-sensor radiances used for vicarious calibration in publications **I**, **II**, **III**, and **IV** were calculated using MODO software (Schläpfer and Nieke, 2005; Schläpfer, 2011), which is a graphical front end to a MODTRAN-4/MODTRAN®-5 radiative transfer code (Berk et al., 1999; Berk et al., 2006). The nadir field reflectance factor of the reference targets, the relevant solar angles, the general atmospheric model (mid-latitude summer) and the atmospheric parameters (horizontal visibility and temperature in **I**, **II** and **III**, and in addition the H_2O, CO_2 and O_3 concentrations in **III** and **IV**) served as input for the calculations. These at-sensor radiances, together with the image DN measurements of the reference targets, were used for the vicarious calibration of the sensor using the linear model (Equation (5)). This calibration gave the linear parameters (gain and offset) for converting the image DNs into at-sensor radiances [$W/(m^2$ sr nm)]. In publication **V**, the vicarious

calibration was performed by using the in-flight radiometric calibration module that was a part of the ATCOR-4 software.

To improve the accuracy of the vicarious calibration, an image-wise method for relative radiometric scaling was developed in publication **II** that tries to compensate for the possible changes in the atmospheric conditions between the different images. The idea was that the differences between two PAN images of the same target would show the changes in illumination integrated over the 350-1000 nm wavelength range, when assuming a stable sensor. In this study, the black gravel (B2b in Figure 7) was used as reference.

4.4 Radiometric correction

In publication **III**, an empirical line-based method, modified to take into account the anisotropy of the object reflectance, was used to generate reflectance image products. The anisotropy of each reference target was taken into account using the following equation to create the reference reflectance factor in an exact imaging geometry:

$$\rho_{ref} = \rho_{lab\_exact} \frac{\rho_{field\_nadir}}{\rho_{lab\_nadir}} \tag{7}$$

where ρ_{field_nadir} is the target nadir reflectance factor measurement during the **imaging campaign,** ρ_{lab_nadir} is the target nadir BRF measured at the laboratory, and ρ_{lab_exact} is the target BRF in the exact imaging geometry of the respective image (illumination and viewing angles) measured in the laboratory. The laboratory BRDF retrieval was done using the FIGIFIGO goniospectrometer (Suomalainen et al., 2009). A linear regression model was then fitted between the reference target image DNs and the ρ_{ref} to generate linear parameters for the DN used for the reflectance conversion. These parameters were calculated separately for each sensor channel.

In publications **IV** and **V**, reflectance image products were created using the Leica XPro photogrammetric software and the ATCOR-4 (in **V** only) software dedicated to physical atmospheric correction. With XPro, there were no user adjustable settings for reflectance image product generation. **The XPro's default settings** were used for the images with the BRDF correction.

The nadir-looking, orthorectified, at-sensor radiance versions of the ADS-imagery that had been created using Leica XPro constituted the starting point for the ATCOR-4 processing. Different image versions were created based on the laboratory calibration of the sensor, the vicarious in-flight calibration of the sensor, the atmospheric parameters derived automatically from the image data, and the atmospheric parameters provided by the user (in-situ measurements).

As part of the EuroSDR radiometry project, three different participants (FGI, Swisstopo (ST), ReSe Applications Schläpfer) carried out the image processing in

publication **V**, which resulted in a total of 12 different reflectance image products. These image products are summarized in Table 4.

Table 4. Image versions used in **V.** XA = XPro radiometric correction, XF = XA with BRDF correction, AL = ATCOR-4 radiometric correction with sensor laboratory calibration and AV with vicarious calibration. Par.: participant, Cal.: origin of the sensor radiometric calibration (lab: laboratory, vic: vicarious calibration); Atm.: origin of the atmospheric parameters used (imag: derived from the imagery, in-situ: in-situ measurements). Other: BRDF = with empirical BRDF-correction, cal.1B = sensor calibration based on image line 1B; shd. = with shadow removal (from **V**).

	XA1	XA2	XF1	XF2	AL1	AL2	AL3	AV1	AV2	AV3	AV4	AV5
Par.	FGI	ST	FGI	ST	FGI	FGI	ReSe	FGI	FGI	FGI	ReSe	ReSe
Cal.	lab	lab	lab	lab	lab	lab	lab	vic.	vic.	vic.	vic.	vic.
Atm.	imag.	imag.	imag.	imag.	in-situ	imag.	imag.	in-situ	imag.	imag.	imag.	imag.
Other			BRDF	BRDF						cal.1B		shd.

4.5 Performance analysis

The main equation for the error, precision, and accuracy analysis used in this thesis was used in the following form:

$$E_\% = 100 * (Data - Reference)/Reference \qquad (8)$$

where $E_\%$ is the relative error/precision/accuracy in percentages, Data is the measurement, and Reference is the reference against which the data is compared. All the combinations of data and reference used in this thesis are described in the Table 5. Also the equation $E = Data - Reference$ was used in publications **IV** and **V** to obtain the reflectance error in reflectance units.

Based on the Equation (8), the root-mean-square error in percentage ($RMSE_\%$) can be obtained as follows:

$$RMSE_\% = \sqrt{\frac{\sum_{k=1..n} E_\%^2}{n}} \qquad (9)$$

where n is the number of measurements used in the evaluation. Equations (8) and (9) were used in publication **II** to evaluate the accuracy of the calibration parameters, in **IV** and **V** to evaluate the reflectance error in percentages, and in **IV** to evaluate the differences between the at-sensor radiance of the ADS40 sensor and the radiative transfer modeling. Equation (7) was used in publication **V** to obtain the reference target BRF in the exact imaging geometry.

In publication **II**, the precision of the calibration was determined based on an analysis of the relative residuals calculated using Equation (8) between the at-sensor radiance from the radiative transfer modeling and the at-sensor radiance derived from the DN and the calibration parameters. The residuals were calculated separately for all of the reference targets. The standard error of unit weight was then calculated from the residuals (Equation (9), but with degrees of freedom in the denominator rather than n). In publications **I** and **II**, the significance of the

vicarious calibration parameters was evaluated using the t-test with a 95 % confidence level (Pindyck and Rubinfeld, 1991).

Table 5. Different evaluations performed in the publications (Pub.) using the Equation (8). ASR = at-sensor radiance, RF = nadir reflectance factor, BRF = bidirectional reflectance factor, RIP = reflectance image product, ASD = nadir field reflectance factor measurements using ASD spectrometer, FIGIFIGO = BRDF retrieval in exact imaging geometry in laboratory using FIGIFIGO, MODTRAN = MODTRAN-based radiative transfer modeling, XPro and ATCOR-4 = radiometric correction based on XPro and ATCOR-4 software.

Targets used	Evaluation	Data	Reference	Pub.
B1, B2a, B2b, G2, W2, P20, P30, P50	Precision and accuracy of the radiometric calibration	ASR from MODTRAN + ASD	ASR from DNs + calibration parameters	**II**
P05, P20, P25, P30, P50	Accuracy of empirical-line radiometric correction method	RIP from DNs + empirical line conversion	BRF from FIGIFIGO + ASD	**III**
P05, P20, P30, P50, Asphalt, Grass, Gravel, Sand, Weeds	ASR difference	ASR from XPro + ADS40 laboratory calibration	ASR from MODTRAN + ASD	**IV**
P05, P20, P30, P50	Difference of the gain radiometric calibration parameter	Gain from DNs + MODTRAN + ASD	Gain from ADS40 laboratory calibration	**IV**
P05, P20, P30, P50, Asphalt, Grass, Gravel, Sand, Weeds	Accuracy of the XPro radiometric correction	RIP from XPro	RF from ASD	**IV**
P05, P20, P30, P50, Asphalt, Grass, Gravel, Sand, Weeds	Internal repeatability of the XPro radiometric correction	RIP from 2km, 3km and 4km + XPro	RIP from 1km + XPro	**IV**
P05, P20, P30, P50	Internal repeatability of the XPro and ATCOR-4 radiometric corrections	RIP from 2km, 3km and 4km + XPro and ATCOR-4	RIP from 1km + XPro / ATCOR-4	**V**
P05, P20, P30, P50	Accuracy of the XPro and ATCOR-4 radiometric corrections	RIP from XPro and ATCOR-4	BRF from FIGIFIGO + ASD	**V**
Asphalt, Grass, Gravel, Sand	Accuracy of the XPro and ATCOR-4 radiometric corrections	RIP from XPro and ATCOR-4	RF from ASD	**V**

5. Results

5.1 Radiometric calibration and validation of the photogrammetric sensors

5.1.1 Method development

The central new result developed in publications **I**, **II**, **III**, and **IV** was the method for the radiometric calibration and validation of photogrammetric sensors in a test field. The general process flow for this method is shown in Figure 13. The main phases of the developed method are described in the following sections, and based on the experiences gained from all of the publications from this thesis, recommendations for the radiometric calibration and validation workflow are given.

```
        ┌─────────────────────────────┐
        │     Campaign planning       │
        └─────────────────────────────┘
                      │
        ┌─────────────────────────────┐
        │  Preparation of the test field │
        └─────────────────────────────┘
            │                     │
  ┌──────────────┐      ┌──────────────────────┐
  │ Image        │      │ In situ measurements:│
  │ collection   │      │ -Reflectance         │
  │              │      │ -Atmosphere          │
  └──────────────┘      └──────────────────────┘
         │                        │
  ┌──────────────┐      ┌──────────────────────┐
  │ Image        │─────▶│ Implementation of    │
  │ orientation  │      │ the laboratory data  │
  └──────────────┘      └──────────────────────┘
         │                        │
  ┌──────────────┐      ┌──────────────────────┐
  │ Image        │      │ At-sensor radiance   │
  │ measurements │      │ simulations          │
  └──────────────┘      └──────────────────────┘
            │                     │
        ┌─────────────────────────────┐
        │ Calibration and validation / analysis │
        └─────────────────────────────┘
```
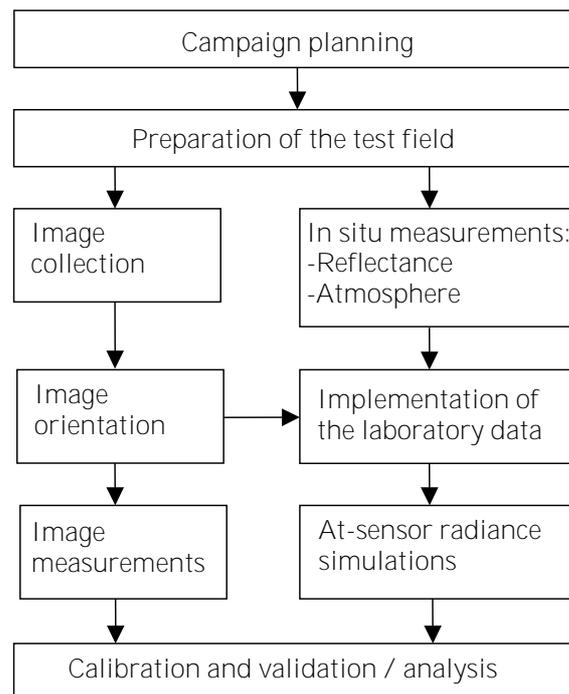
Figure 13. Diagram for the radiometric calibration and validation of the photogrammetric production line in a test field. Compare to Figure 3 in **I**.

The campaign planning includes planning the flight (i.e. flight line patterns, distribution of the reference targets on the image plane, flying heights, sensor parameters, time of day, number of flight days) and the required field work, including the number of reference targets. The requirements for the campaign depend on the goals of the campaign; the goal can be a comprehensive calibration

and validation of the sensor or just a quick vicarious calibration before engaging in other campaigns. The test field can be a permanent photogrammetric image quality test field, like Metsähovi, or any relatively flat area with some permanent natural or manmade reference targets (e.g., gravel, asphalt) or an area with enough space for portable reference targets. With the presented method, two reference targets is the minimum for vicarious calibration, but at least four targets are recommended for performing a more detailed radiometric validation.

After the image collection, the image orientations are solved and the imaging geometry (the viewing and illumination angles) for all of the reference targets visible on the images is calculated. The image measurements include the calculation of the DN distribution metrics for the reference targets and for the whole images. Also, the imaging parameters (the exposure time and aperture size) are collected. The image measurements can be done for the various image versions available during the image processing chain: For the raw images without any processing to evaluate the sensor performance; for intermediate images, to evaluate the effects of processing parameters; and for final images, to evaluate the complete image processing chain and the quality of the end product. For the vicarious calibration and the reflectance image product generation, images with the full native bit depth of the sensor (i.e. no down-scaling to 8 bits per channel), and without any non-linear processing, should be used.

The in-situ field reference measurements during the imaging campaign include the nadir reflectance factor measurements of the reference targets and the atmospheric measurements of the weather conditions (temperature, pressure, AOT and/or horizontal visibility, H_2O, CO_2, O_3). Also, the BRDF retrieval of the reference targets using a goniospectrometer can be performed in the field, if possible. For reference targets with comprehensive laboratory BRDF retrieval, BRF in the exact imaging geometry is retrieved from the laboratory data, and this data is scaled using the nadir field reflectance factor measurements of the same target. The reflectance factors of the reference targets and the in-situ atmospheric measurements are given as inputs for the radiative transfer modeling of the reference target at-sensor radiances. All the reference measurements should be performed in clear weather conditions with accurately calibrated equipment with known uncertainty.

The at-sensor radiance values for each reference target are modeled using a proper radiative transfer code. The reliability and validity of the radiative transfer modeling should be evaluated through a recursive process where the sensitivity of the radiance to each of the input parameters is solved. The at-sensor radiances are finally integrated to match the sensor spectral responses.

Finally, the actual radiometric calibration and validation of the sensor is performed. In the comprehensive format, this phase includes the vicarious calibration of the sensor, that is, the calculation of the absolute radiometric

calibration parameters, the evaluation of the linearity, the dynamic range, the saturation, the channel sensitivities, and the stability of the system. If the sensor being evaluated incorporates radiometric laboratory calibration, then a comparison between the laboratory and vicarious calibration as well as between the at-sensor radiances based on the laboratory calibration and those based on the radiative transfer modeling should be performed. If imagery acquired using the several exposure settings is evaluated, then the DNs can be scaled using the exposure time and/or aperture size. Finally, if the campaign lacks in-situ atmospheric measurements, a relative image-based radiometric scaling can be performed for the imagery to compensate for possible changes in the atmospheric conditions between images. However, because the suggested scaling method is based on the ratio of reference target DNs on a certain channel, it works only if the spectral composition of the illumination does not change, i.e. the changes cannot be wavelength dependent.

5.1.2   Vicarious calibration

The vicarious radiometric calibration of the photogrammetric sensor DMC was performed in publications **I** and **II**, and the vicarious calibration of the ADS40 in publications **I**, **IV** and **V** respectively. In many cases, the offset parameter was detected as being statistically insignificant for the DMC when using a t-test. One possible reason for this is the problem of detecting statistical significance of value close to zero with rather few reference targets. However, the full two-parameter linear model was used in publication **II**, because the full model decreased systematic residuals and provided better accuracy. In contrast to the existing literature (Beisl, 2006; Hernández-Lopéz et al., 2012), in publications **I** and **IV**, a full linear model with both parameters (gain and offset) was detected as being necessary for the radiometric calibration of the ADS40 sensor. A possible reason for this is the insufficient modeling of the atmosphere. In publication **V**, the in-flight radiometric calibration of the ADS40 sensor was performed with two and four reference targets using the vicarious calibration tool provided by the ATCOR-4 software. When using this tool with more than one reference target, both gain and offset parameters are automatically calculated. ATCOR-4 does not provide estimation of the statistical significance of these calibration parameters. The radiometric calibration parameters used in **V** are given in appendix 7 of Honkavaara et al. (2013).

In publication **II**, the absolute calibration parameters for all nine different sensor exposure settings used with the DMC sensor were calculated. When the DNs were normalized with respect to the aperture size (f-stop) and exposure time, the absolute calibration parameters for all of the settings were close to one another in percentages. In particular, the gain parameters became almost identical for each color channel. This indicates that the normalization of the DNs managed to remove the differences between the different exposure settings quite well. This differs from

the results presented by Martínez and Arbiol (2008) and Ryan and Pagnutti (2009), who suggested that the radiometric calibration parameters should be calculated separately for each aperture size (f-stop) of the DMC-sensor. If aperture-specific parameters are available, they should be used, otherwise one can use the presented normalization method.

The precision of the calibration was determined in publication **II** based an analysis of the relative residuals between the at-sensor radiances from radiative transfer calculations and those calculated from the DNs and calibration parameters. As an example, Figure 14 shows the residuals of all of the reference targets for the red channel. The individual residuals were mostly less than 5 %, but especially in the case of the NIR channel, larger values appeared.
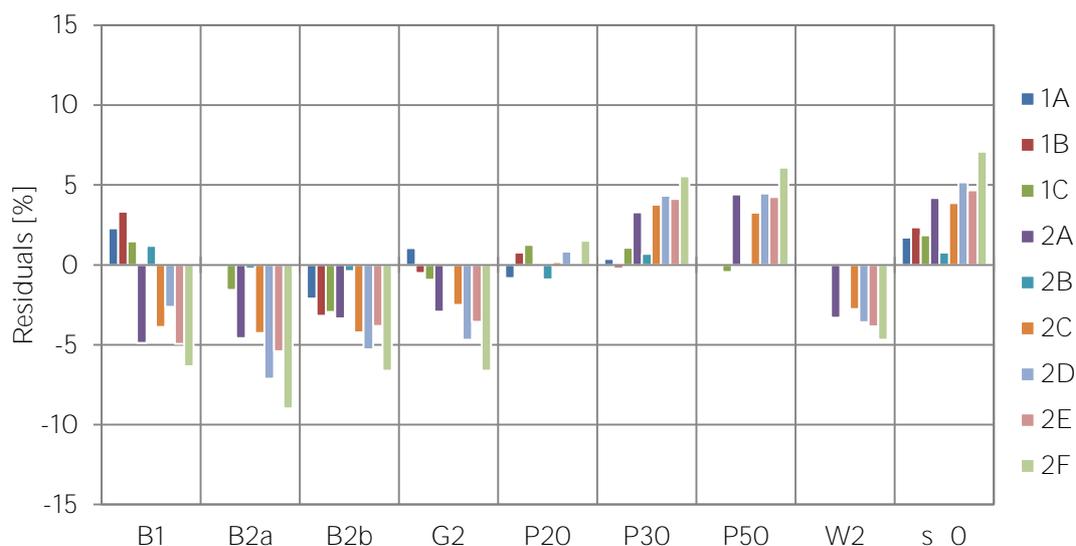

Figure 14. Calibration residuals (% in radiance) per reference target for the red channel, all nine sensor exposure settings, 1A-1C: first day, 2A-2F: second day. s_O is the standard error of unit weight. Compare to Figure 6 in **II**. Details of the reference targets on x-axis are described in Table 3.

Ryan and Pagnutti (2009) stated that the accuracy of the DMC radiometric calibration can be expected to be approximately 3 % in the laboratory, which is below the industry standard of 5 % (LDCM, 2003). In this thesis, the vicarious calibration of the DMC reached an accuracy of below 5 % at best, and the good radiometric quality and stability of the sensor was confirmed. Also in this thesis, the same accuracy level of the vicarious calibration was achieved when using the ADS, at least for some datasets.

In publication **IV**, the reference target at-sensor radiances measured from the ADS40 imagery that was related to the laboratory calibration parameters were compared to the at-sensor radiances calculated using the radiative transfer modeling. The radiative transfer modeling always provided higher at-sensor radiance values than the XPro software. Figure 15 shows the radiance differences between the laboratory calibration and the radiative transfer modeling for the reference targets on the 2 km flying height image. The radiometric calibration parameters acquired using the vicarious calibration of the ADS40 sensor were

compared to the laboratory calibration by comparing the differences in the gain parameters. As could be expected from the systematic difference between the ADS40 radiances and the simulated at-sensor radiances, there was a substantial difference between the vicarious calibration and laboratory calibration. All the differences between the modeled and image measured radiances are likely to be due to the systematic errors in MODTRAN radiative transfer modeling parameters used in **IV** and/or sensor laboratory calibration.
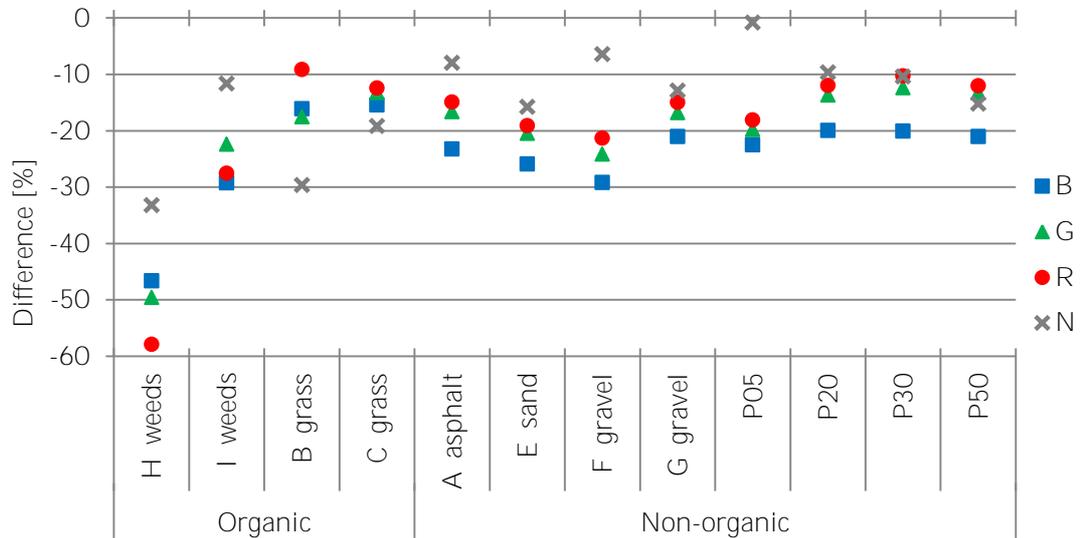

Figure 15. Relative difference between the at-sensor radiances based on laboratory calibration of the ADS40 sensor and the radiances from radiative transfer modeling. 2 km flying height image 2A. B = blue, G = green, R = red, N = NIR channel. For the details of the targets on x-axis, see Table 3, Figure 8 and Figure 9.

5.1.3   Sensor evaluation

Based on the general performance analysis and vicarious calibration (Section 5.1.2), all of the evaluated sensors were detected to have a good radiometric quality. Still, some problems with radiometric properties were detected. The main reasons for the problems with the saturation, sensitivity and dynamic range of the imagery had to do with the over- or underexposure of the sensors. To fully utilize the radiometric potential of the sensor, the sensor exposure and aperture settings have to be chosen carefully to avoid over- and underexposure. Hanusch and Baltsavias (2009) obtained similar results to those presented in this thesis for the histogram analysis, sensor linearity and dynamic range evaluation of the DMC, ADS40, and UltraCamX sensors and confirmed the channel sensitivity differences of the sensors found in publication **I**. The linearity of the UltraCamD sensor was also supported at the study by Haest et al. (2009). Rosso et al. (2008) concluded that one of the fundamental aspects related to the sensor properties to take into account when using photogrammetric imagery in biotype mapping is The DN range of each channel i.e. the dynamic range. The results of the general performance analysis are analyzed in more detail in the following sections.

Linearity

The linearity of the ADS40 and UltraCamD sensors was evaluated in publication **I**. The R^2 values of the linear regression were between 0.94 and 0.99 for the ADS40 sensor, and better than 0.99 for the UltraCamD sensor. The linearity of the DMC sensor was evaluated in publications **I** and **II**. The DMC sensor showed linear behavior on all channels; the R^2 values of the linear regression were better than 0.99 for all of the channels. These results indicated that the linearity of all of the evaluated sensors was good, that is, the R^2 values were close to 1. Figure 16 shows an example of the DMC NIR channel linearity for nine different exposure settings used in **II**.
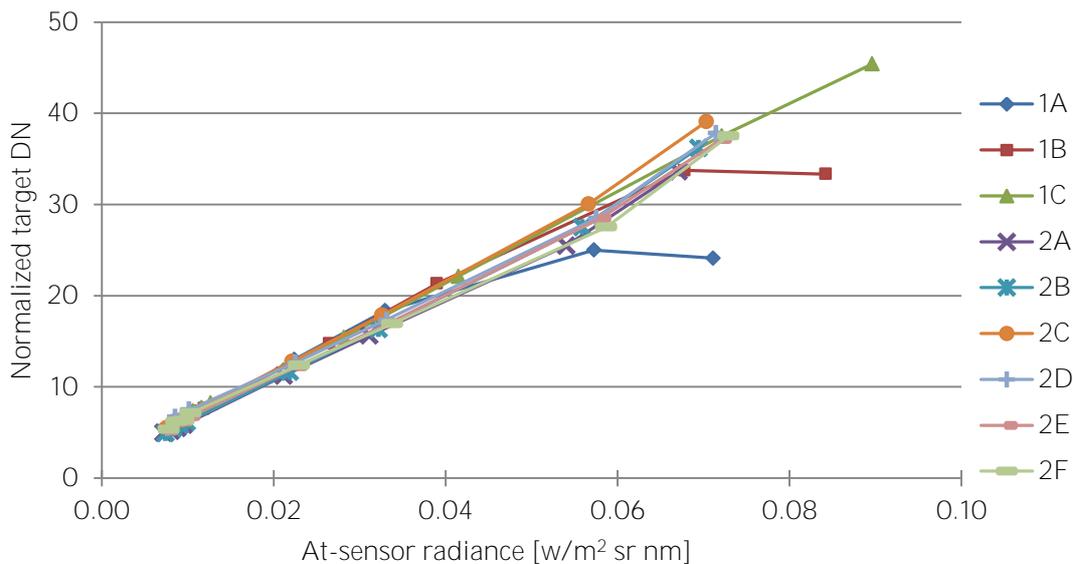

Figure 16. Reference target DNs normalized with aperture size and exposure time as a function of simulated at-sensor radiances. All nine sensor exposure settings (1A-1C: first day, 2A-2F: second day), NIR channel. The tick marks are the used reference targets (see Table 3 and Figure 7) Compare to Figure 4 in **II**.

Dynamic range / saturation

The dynamic range and the sensitivity to saturation of the ADS40 and UltraCamD photogrammetric sensors were evaluated in publication **I**. In the case of the ADS40, the dynamic range of images was 10 bits for the red and green channels, 9 bits for the blue channel, close to 11 bits for the NIR channel, and almost 13 bits for the PAN channel. The results for the PAN channel indicated that the dynamic range of the sensor was more than 12 bits, as expected, but due to the sensitivity properties of the sensor and other mission conditions, this range could not be reached for the multispectral channels. The UltraCamD analysis indicated a dynamic range of up to 12.7 bits. The UltraCamD PAN and red channels saturated at the reflectance level of the brightest reference target (P70, with an average nadir reflectance factor of 0.65) due to overexposure at the 800 m flying height.

The dynamic range and the sensitivity to saturation of the DMC sensor was evaluated in publications **I**, **II** and **III**. In **I** and **II**, the histogram analysis of the whole images showed that the dynamic range was practically a full 12 bits at each

54

channel. As the amount of radiance entering the sensor decreased in relation to the exposure settings used in **II**, the average DN values, the standard deviations, and the 99% width of the histogram decreased, which was an expected performance. The most serious problem with the imagery had to do with the saturation that occurred with many exposure settings due to overexposure. In the worst cases, the P30 reference target (average nadir reflectance factor 0.26) was saturated, whereas at other settings, the W2 reference target (average nadir reflectance factor 0.51) was not saturated. The saturation did not always appear as the highest possible DN (4095), especially on the green and NIR channels. No saturation was detected on the DMC images used in publication **III**. On the individual channels, the 99% efficiency of the image histograms varied from 348 (blue channel, flying height 2 km, morning) to 2015 (NIR channel, flying height 2 km, morning). These results showed that for some flight lines, the sensor exposure settings could have been selected differently to provide a wider dynamic range.

Sensitivity

The radiometric sensitivity of the sensors was evaluated in publications **I** and **II**. For the DMC, the sensitivity of the PAN, red and blue channels appeared to be similar, whereas the green and NIR-channels appeared to be clearly more sensitive than the other three channels. In the case of the ADS40 sensor, the sensitivity of the multispectral channels was clearly lower than the sensitivity of the panchromatic channels. The reason for this was the short integration time used because of the low flying height and high aircraft speed. For the UltraCamD sensor, the sensitivity of the red and NIR channels appeared to be fairly similar, while the green channel was slightly less sensitive. The sensitivity of all of the evaluated sensors for detecting small radiometric differences in light was superior compared to the analog film images. In publication **II,** the blue and green channels of the DMC were found to be most sensitive to overexposure; whereas the panchromatic channel was least sensitive to overexposure.

Stability

The radiometric stability of the DMC photogrammetric sensor was evaluated in publication **II**. The results indicated relatively good stability. After scaling the DNs both with the aperture size and exposure time, and performing the relative radiometric scaling based on the PAN channel, all of the comparisons (same f-stop and same day; different f-stop and same day; different f-stop and different day, with the f-stop determining the aperture size) between the images with different exposure settings provided similar estimates of stability; the RMSEs were better than 5 % in most of the evaluations. The largest RMSEs appeared on NIR channel on comparisons with different f-stop. Figure 17 shows a comparison between one setting (2C) from the second day and all settings (1A-1C) from the first day.
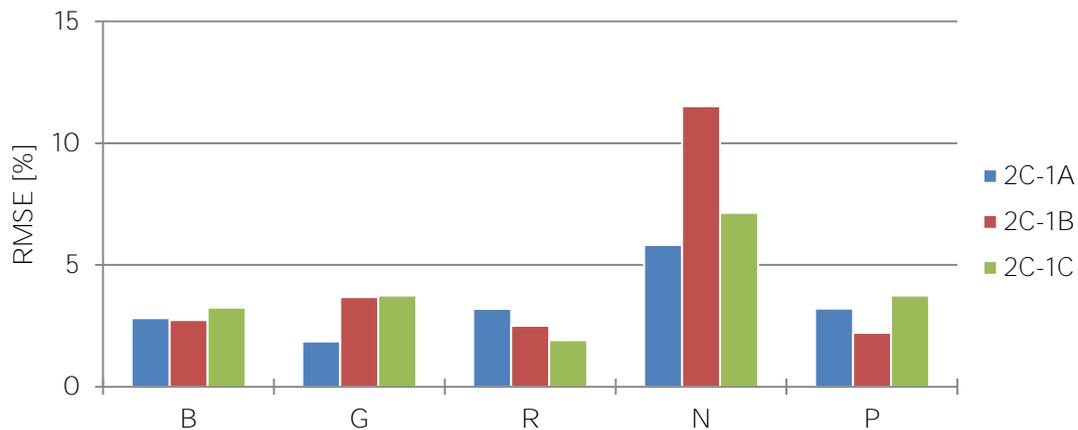
Figure 17. RMSE statistics (%) for stability comparisons between sensor setting 2C from day two and all settings from the day one (1A-1C), normalized and PAN-scaled data. B =blue, G = green, R = red, N = NIR and P = panchromatic channel. Compare to figure 9 in **II**.

5.2 Radiometric correction

5.2.1 Empirical line-based method

An empirical line-based method was modified to take into account the anisotropy of the object reflectance and used in publication **III** to carry out the radiometric correction needed to generate reflectance image products. This procedure provided channel averaged reflectance factor with an estimated accuracy of better than 5 % in areas that had similar illumination conditions as the reference targets; in other areas (especially in shadowed areas), the values were not reflectance factors. Figure 18 shows the standard deviation (in %) for the linear regression calculated from the relative difference between the reference BRFs in exact imaging geometry and the reflectance factors obtained using empirical line conversion parameters. The images with the reference targets located at the center of the image were used for all of the flight lines. The same targets (tarps P05, P20, P25, P30 and P50) were used both for the modeling and as reference.
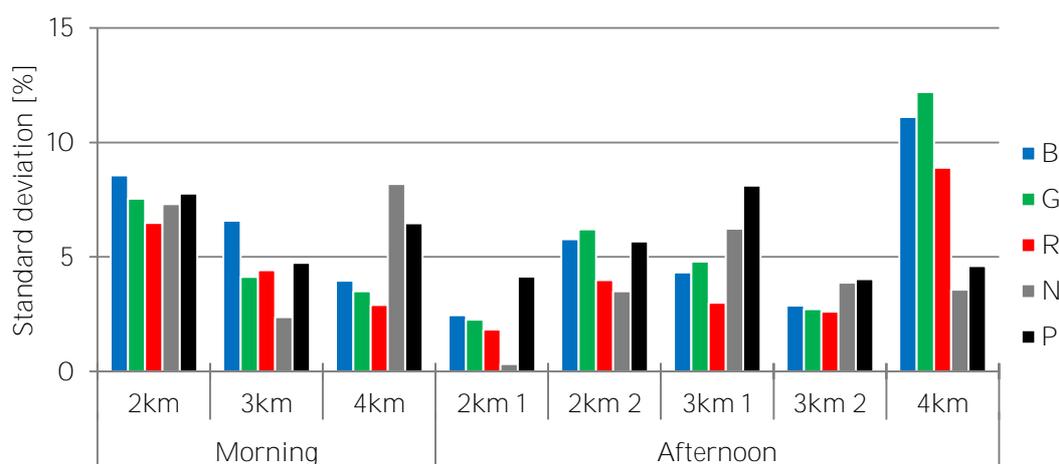

Figure 18. Standard deviation of the linear regression (in %) between the reference BRFs and reflectance factors from the radiometrically corrected images. One image from each flying height (2km, 3km, 4km) and flight line where the targets were visible (in the afternoon, two lines for km and 3km flying heights). B = blue, G = green, R = red, N = NIR and P = panchromatic channel.

The relative differences between the sun illuminated and shadowed area reflectance factors were studied using field and asphalt road targets, and the relative differences between the morning and noon reflectance factors were studied using field, asphalt and forest targets. In the shadowed areas, the average road reflectance varied on all channels between 0 and 0.03, and on sun-illuminated roads between 0.14 and 0.21. The reflectance factor spectra of field in the morning both in direct sunlight and in shadow, and at noontime in direct sunlight measured from flying height images of 2, 3, and 4 km are shown in Figure 19, left. For the sunny fields, the reflectance factor minimums and maximums varied from between 0.02 and 0.07 for the blue channel to between 0.20 and 0.30 for the NIR channel. For the shadowed fields, the reflectance factor variation was dramatically reduced, showing minima and maxima reflectance values of 0.00-0.02 in all of the channels, and the spectral signatures were uniform and completely different from the signatures in the sun-illuminates areas. For forests, the minimum reflectance factor was on the level of 0 in the morning and at noontime, and the maximum reflectance factor values were 0.13-0.29 for the morning and 0.09-0.20 at noontime. The probable reasons for higher reflectance factor variation in the morning are the changing view-illumination geometry related to the flying direction and larger amount of shadows in the morning. Deciduous trees showed much higher values in the NIR channel compared to coniferous trees, but the general behavior was similar.
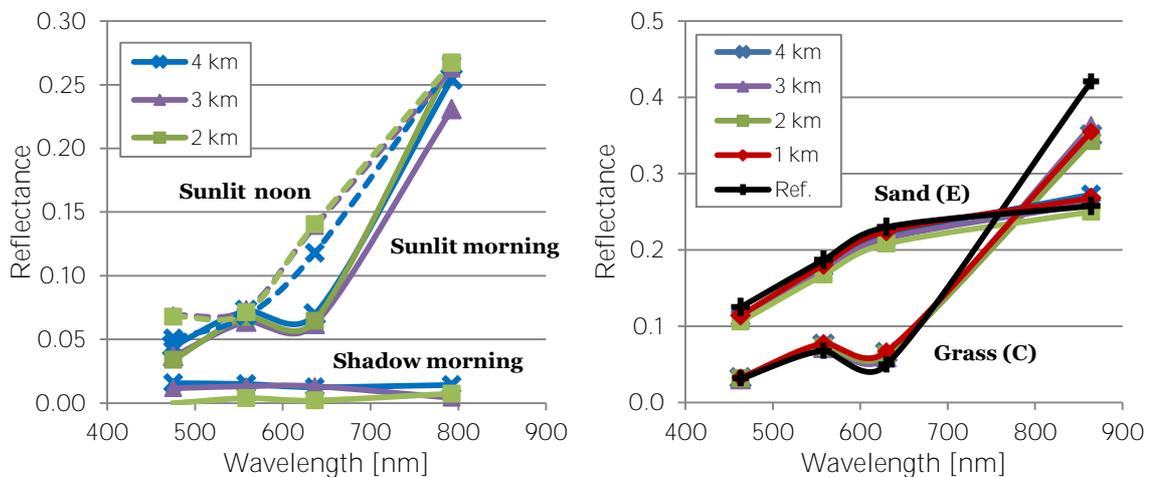

Figure 19. Left: reflectance factor of field in the morning in sunlit (solid line) and in shadow (dotted line) and in the noon in sunlit (dashed line) measured from the DMC images. Right: reflectance factors of sand and grass measured from AV2 versions from ADS40 imagery, all flying heights, nadir looking lines, and field nadir reference reflectance factor. The markers in the figures are the center wavelengths of the DMC and ADS40 sensor channels.

5.2.2 Radiative transfer-based methods

In publications **IV** and **V**, the accuracy of the reflectance image products created using the Leica XPro photogrammetric software and the ATCOR-4 software (only in **V**) dedicated to physical atmospheric correction was evaluated. A total of 12 different radiometrically corrected reflectance image products that had been collected with the ADS40 sensor were processed for the analysis. Samples of the

reflectance factor spectra for sand and grass measured using ATCOR-4 corrected AV2 versions (cf. Table 4), all four flying heights, and the nadir field reference reflectance factor are shown in Figure 19, right.

Both evaluated software programs provided high reflectance accuracy, even without accurate in-situ measured atmospheric parameters, that is, both methods were able to estimate the necessary parameters automatically from the image data itself. The XPro produced stable results on all channels and at all flying heights when using the laboratory calibration of the sensor. With the ATCOR-4, the vicarious radiometric in-flight calibration of the sensor improved the reflectance accuracies of all of the processed images compared to the image versions obtained using the sensor laboratory calibration.

In general, the results varied depending on the target, sensor channel, the method used for the radiometric calibration of the sensor, the flying height, and the weather conditions. With tarps, a reflectance accuracy of better than 5 % was achievable when using all of the evaluated methods, at least on some channels (Figure 20). With non-organic targets (asphalt, gravel, sand), both the XPro and the ATCOR-4 provided a reflectance accuracy of the level of 5 % at best, and $RMSE_{refl\%}$ between 5 and 10 % for all flying heights, with some exceptions. These accuracies are supported by the findings of Beisl and Adiguezel (2010). In the DGPF project, they found that the Leica XPro reflectance image product generation workflow made it possible to produce images with relative reflectance differences of less than 10 %, even for dark objects.
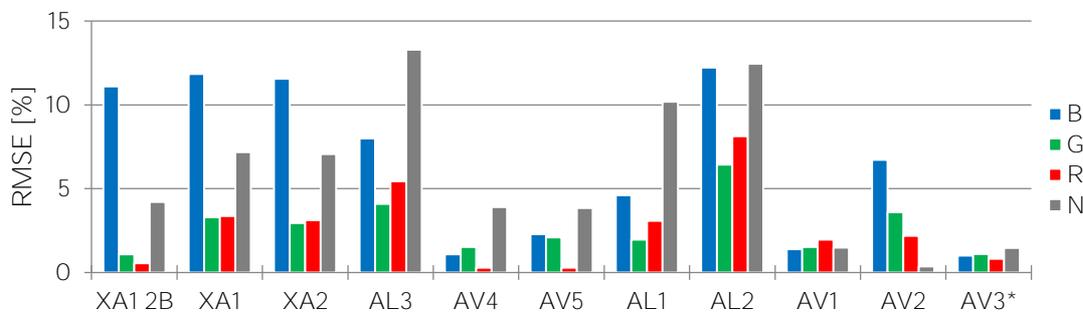

Figure 20. $RMSE_{refl\%}$ results for the bright tarps (nadir looking image line 2A, except for XA1 2B backward looking line). XA = XPro radiometric correction, AL = ATCOR-4 radiometric correction with sensor laboratory calibration and AV with vicarious calibration. B = blue, G = green, R = red, N = NIR channel. * denotes that the results for AV3 are not independent (modified from **V**).

The internal repeatability of the methods was evaluated by comparing the 2, 3, and 4 km flying height data to the 1 km flying height data. Both the Leica XPro and the ATCOR-4 provided a reflectance difference of 5 % or less for the 2 km flying height and a difference of between 5 and 20 % for the other flying heights. With both the Leica XPro and the ATCOR-4, a dependency of the reflectance errors (in reflectance units) on the magnitude of the reflectance factor was detected for most of the methods, color channels and flying heights. After scaling the reflectance errors to the relative errors, the dependency of the reflectance error on the magnitude of

reflectance remained when using the Leica XPro, but it mostly disappeared when using the ATCOR-4. For a broadband multispectral sensor like the ADS40, the rather simple approach of the Leica XPro for atmospheric correction yielded results that were comparable to those obtained when using the ATCOR-4. However, if ground reference data were available, the results could be improved by using of the ATCOR-4.

5.3   Influence of solar elevation

The influence of solar elevation on the radiometric performance of multispectral photogrammetry in point cloud creation was studied in publication **III**. The relative quality evaluations of images collected from several flying heights and converted to reflectance image products were performed both in sun-illuminated and in shadowed areas in forests, on roads, in fields, and with reference targets.

The histogram analysis of the whole images showed that the flying height did not greatly influence the histograms. Moreover, the histograms from the morning and noontime flights were similar. The results indicated that the exposure settings of the camera had been tuned successfully to produce similar reference target DNs at different times, even though, in reality, the level of solar irradiance in the morning was roughly 60 % of what it was at noontime. The small differences in the shapes of, in particular, the NIR histograms between the morning and noontime may be due to a larger amount of shadows in the morning imagery.

For sunlit fields, the spectral signature was typical for that of vegetated surfaces. The largest differences between the morning and noontime reflectance factor values were in the red channel (Figure 19, left). One possible reason for this could be the stronger adjacency effect from the neighboring forests close to the field during the noon time. Shadowed and sun-illuminated reflectance factor data for the asphalt surfaces showed quite similar behavior compared to the field data. For forests, a rather large variation appeared in the reflectance factor measurement from different flying heights, and the reflectance factor range in forests was higher in the morning data than it was in the noontime data. Probable reasons for these variations in forest reflectance factors are the different imaging geometry between morning and noon data (different flying directions related to sun) and the larger amount of shadows in the morning data.

With the 3D point cloud generation, the differences in the point densities for the same areas in the morning and at noontime were less than 3 % for the data collected from 2 and 3 km flying heights and less than 8 % for the data collected from a flying height of 4 km. These general results showed that the terrain extraction based on image matching was, in general, successful and that the lower solar elevation did not deteriorate the general performance of the multispectral photogrammetric processes.

6. Discussion

Based on the objectives of this thesis (Section 1.3), a quantitative method for the radiometric calibration and validation of photogrammetric sensors in a test field was developed. Second, three radiometric correction methods for photogrammetric imagery were evaluated and the accuracy of the reflectance image products was studied, and finally, the influence of the solar elevation angle on the quality of reflectance image products and on photogrammetric process of point cloud generation was evaluated. The results demonstrated the high radiometric quality of the photogrammetric sensors and confirmed the hypothesis (Section 1.2) that the photogrammetric imagery can be radiometrically corrected to provide accurate reflectance image products suitable for quantitative analysis. The theoretical and practical implication of the results, as well as their reliability and validity, and, finally, topics of the future research are discussed in the following sections.

6.1   Theoretical implications

The research results of this thesis showed that images collected with photogrammetric sensors are suitable for rigorous radiometric processing. Many studies have highlighted the importance of rigorous radiometric processing of images in all phases of the image processing chain (Stensaas and Lee, 2008; Schönermark, 2010; Cramer, 2011).

  The gain in using imagery collected with absolutely calibrated sensor is that it makes the rigorous radiometric correction of imagery to surface reflectance factors possible (Schowengerdt, 2007). Song et al. (2001) have shown that atmospheric correction has major effect on ratio transforms (such as vegetation indices) calculated using images. Waser et al. (2010) found out that photogrammetric sensors have very high potential to produce meaningful results in land cover and tree species classification. To overcome problems related to varying atmospheric conditions due to different image acquisition dates they suggested further studies in radiometric correction. The research results of this thesis have shown that the radiometric properties of photogrammetric sensors are high quality, and that images collected with these sensors are suitable for quantitative radiometric correction. This means that images collected with airborne multispectral photogrammetric sensors

can in the future more accurately and reliably be used in various quantitative applications including vegetation health monitoring through vegetation indices, time series analysis and change detection, and these images and products derived from them can be quantitatively compared and combined with other datasets collected with airborne and space borne sensors. Green et al. (2011) concluded that the imagery of the ADS40-SH52, DMC, and UltraCamD sensors was of a radiometrically high quality and suitable for benthic habitat and propeller scar mapping. Also various case-specific parameters of classification algorithms could be generalized if they are used with a standardized reflectance image products (Heikkinen et al., 2011). Compared to satellite imagery, airborne datasets provide higher spatial resolution and operational flexibility, which will provide new high-quality datasets for these applications. It is also fundamental to know and understand the radiometric quality of the sensor and accuracy of the derived reflectance image product, if one wants to study for example climate and climate change. It is impossible to distinguish the effects due to varying atmospheric conditions or individual sensor performance from those due to long term environmental factors without accounting for the atmosphere and tying the data to standard point of reference (Ryan and Pagnutti, 2009).

Prior to this thesis, publications in peer reviewed journals presenting rigorous methods for radiometric calibration, validation and correction of multispectral photogrammetric sensors and their imagery have been rare. The radiometric calibration and validation method presented in this thesis was the first study to quantitatively evaluate the radiometric quality of photogrammetric sensors using reference BRF in an exact imaging geometry and in real imaging conditions in a test field, and also solving the radiometric calibration of the sensor. A vicarious calibration method that takes into account the exact imaging geometry of the reference target has previously been presented only for space borne sensors (Ryan et al., 2007). Also, the accuracy evaluation of radiometrically corrected reflectance image products was the first study presented for photogrammetric imagery.

The reflectance image products generated in this thesis with the Leica XPro software were used for tree species classification by Korpela et al. (2011) and Heikkinen et al. (2011). Their results suggested that the stereo view capability of the ADS40 sensor was able to improve the tree species classification performance, and that the reflectance factor estimation with normalization of anisotropic reflectance behavior led to similar classification performance as with the at-sensor radiance data, but it can in some cases improve the generalization properties of the training data as well. Essential radiometric factors affecting to the classification result using multi-angular aerial image data were the accuracy of the radiometric calibration and correction and the optimal test set-up together with consideration of the flight line directions in relation with the sun.

6.2   Practical implications

The main practical implications of this thesis include the confirmation of high radiometric quality of photogrammetric sensors and also revealing some problems in the processing chains, providing practical methods for performing radiometric calibration and validation of photogrammetric sensors efficiently in operational conditions, evaluating the usability of three different radiometric correction methods suitable for photogrammetric imagery, and providing recommendations for quantitative radiometric processing and performing photogrammetric campaigns with varying solar elevation angles.

The radiometric evaluations of the 1st generation photogrammetric sensors performed in this thesis revealed some serious problems, such as low and varying channel sensitivities, insufficient calibration and insufficient processing chains without proper documentation. These campaigns were performed in co-operation with the sensor manufacturers and now many of these problems have been corrected in the next generation sensors. As with this thesis, Hanusch and Baltsavias (2009) emphasized the importance of evaluating the radiometry based on unprocessed imagery and stressed that the sensor manufacturers should provide more details about their sensors.

The reflectance factor accuracy level of 5 % at best achieved in this thesis is a strong indicator that the reflectance image products generated with the Leica XPro and collected with the ADS sensor, are well suited for quantitative image interpretation. The reflectance image product generation workflow when using the Leica XPro software required minimal user interaction, and in this thesis, it proved to be efficient even with large amounts of imagery, which is an essential requirement for practical applications. The research results of this thesis showed that the laboratory calibration of the ADS sensor can be improved by vicarious calibration. This finding is supported by Hernández-Lopéz et al. (2012). The advances of vicarious calibration compared to the laboratory calibration are the possibility to verify the calibration in operational conditions and to monitor possible temporal effects such as drift (Ryan and Pagnutti, 2009).

Within the scope of the DGPF project, Schönermark (2010) noted that the in-flight calibration module of the ATCOR-4 software requires highly isotropic reference targets in order to work correctly and suggested using of natural surfaces. The **FGI's** portable reference tarps that were used in this thesis have proved to be well suited for vicarious calibration, and they also worked well with ATCOR-4 software. The requirements for the reference targets designed for calibration and validation purposes are temporal stability, spatial uniformity, and homogeneity, that is to say the isotropic properties, as Schönermark (2010) has also stressed. Partly based on the experiences gathered during the process of completing this thesis, and within the context of the EuroSDR radiometry project, the developers of the ATCOR-4 software

62

created an add-on module called the ATCOR-ADS. This add-on module provides a more efficient procedure for reflectance image product generation from ADS imagery collected in mountainous terrain (Schläpfer et al., 2012).

When images are combined to larger mosaics, the traditionally used statistical dodging methods destroy the physical connection between the radiance seen by the sensor and the final DN on the image mosaic. If the image mosaics will be used in quantitative image interpretation tasks such as time series analysis or vegetation monitoring, the mosaics should be based on radiometrically calibrated at-sensor radiance images or radiometrically corrected reflectance image products, the images should undergo physically-based BRDF-correction and, in the case of frame images, it is suggested to use a radiometric aerotriangulation-based method for mosaicking.

Alvarez et al. (2010) concluded that partial empirical line-type method for generating reflectance image products from frame sensor imagery can be satisfactory, but that the radiometric correction parameters should be solved individually for each image. This can be the case if the desired end product is a seamless orthomosaic. In this thesis, a single set of radiometric correction parameters was used for the whole image block when generating reflectance image products from frame sensor imagery using the modified empirical line-based method. Images corrected with this method are suitable for analysis when the BRDF-dependent properties of objects are used to assist the image interpretation.

In this thesis, it was found that the in-situ atmospheric measurements were not necessary when using the radiative transfer-based radiometric correction methods. This means that both evaluated methods were able to estimate the needed atmospheric parameters automatically from the image data itself. This is a great advance for operational reflectance image product generation when arranging in-situ reference measurements can be difficult.

The motivation behind a study on the influence of solar elevation in photogrammetric processes was to provide new national recommendations for solar elevation thresholds in photogrammetric mapping, which is a relevant issue all over the world. With the evaluated data, the object was measurable at a solar elevation of 25°, even in shadows. The verified, high dynamic range of modern photOgrammetric sensors makes it possible to reduce the effect of shadows in image measurements. Also, the results showed that in sun-illuminated areas, there was no deterioration of performance in point cloud generation with decreasing solar elevation. The analysis also showed that it is important to consider radiometric aspects in the context of point cloud generation because the radiometric quality of the image has a direct influence on the matching accuracy and thereby to the quality of a point cloud. These results will be used as a basis for new national recommendations for photogrammetric campaigns.

6.3   Reliability and validity

The research presented in this thesis has been conducted using only large-format, multispectral photogrammetric sensors, and these sensors represented the first and second generation of these sensors; the radiometric properties of the currently available sensors are much more advanced (better frame rates, better radiometric sensitivities, better dynamic range and more advanced post-processing software) (Cramer, 2011; Gruber et al., 2011; Neumann, 2011b; Wagner, 2011). The radiometric evaluation results for the sensors presented here are only indicative because the methodology used in the study become more highly developed during the course of the research and the test-setups used were not always optimal. However, the comprehensive method for radiometric calibration and validation of the sensors in a test field presented in this thesis can be considered valid. The method can also be applied to medium and small-format sensors and even to hyperspectral and high-spatial resolution satellite sensors. Hyperspectral sensors can be more sensitive to small atmospheric changes because of narrower channels, so more extended in-situ atmospheric measurements may be needed for radiative transfer modeling.

During the image processing performed in this thesis, all the original raw data, intermediate and final images were available for analysis. Photogrammetric image **end users, who do not collect the images by themselves, don't always hav**e access to the original raw image DNs and because of this, they are dependent on the image processing of the image supplier. This means that the whole image processing chain has to be well documented and the document must be delivered to the customer together with the imagery, so that the end users can perform reliable and accurate radiometric calibration, validation and/or correction.

Obtaining accurate radiometric information about the sensor and performing absolute vicarious radiometric calibrations sets strict requirements for the test site and reference measurements. The method presented here for radiometric calibration and validation is based on a photogrammetric image quality test field, high-quality portable reference targets and in-situ field reflectance factor measurements. Radiometric test fields and portable reference targets are rare, and it can be difficult to arrange the field campaign during operational imaging flights. However, permanent test sites equipped with proper, ideally autonomous field instrumentation would make it easier to arrange the radiometric test campaigns. The method presented here is best suited for a comprehensive acceptance inspection of a photogrammetric sensor or a yearly check of **a sensor's** radiometric quality. But in particular the vicarious calibration method can also be streamlined for more frequent, even campaign-based uses. However, the test field calibration is only a supplementary calibration method; the most accurate pixel-wise and spectral calibration must be performed in laboratory.

With the vicarious calibration, the statistical importance of the linear offset parameter was difficult to obtain. Its value is expected to be close to zero, and detecting its statistically significant non-zero value would require a large number of reference targets in the linear regression model, which were not always available for the purposes of this thesis. Also, the accuracy of the radiative transfer modeling of the at-sensor radiance affects the calculations for the offset parameter.

One of the main shortcomings of this thesis was the unknown accuracy and sensitivity of the performed radiative transfer modeling. In many phases, the default settings of the MODTRAN were used, and even though extensive atmospheric measurements were available and used with the Hyytiälä datasets, their accuracy and effect on the modeling result was unknown. Because of this, the accuracies of absolute radiometric calibrations can only be considered indicative. A more rigorous method for radiative transfer modeling would be to recursively analyze the accuracy and sensitivity of the modeling as a way of adjusting the optimal parameters (Ryan et al., 2007).

The importance of the accuracy of the in-situ atmospheric parameters were minor for the radiative transfer–based radiometric correction methods compared to the vicarious calibration because the evaluated correction methods were able to estimate the needed atmospheric parameters automatically from the image data itself. One reason for this may be because multispectral sensors with broad spectral channels are not very sensitive to small changes in the aerosol and molecule concentrations. It is also possible that the in-situ data was not optimally utilized in the radiative transfer modeling to obtain any notable gain from them.

The evaluated radiative transfer-based radiometric correction methods are well suited for multispectral pushbroom line sensors, but they still need to be adapted for frame sensors. The modified empirical line–based radiometric correction method presented in this thesis is applicable for small-, medium-, and large-format frame sensors, but the limitation of the method is that it does not correct the images for BRDF effects and it requires stable atmospheric conditions when the images are being acquired. If the goal of the radiometric correction of the frame imagery is a seamless nadir reflectance factor orthomosaic, then radiometric aerotriangulation–based methods are recommended (Collings et al., 2011; Hernández-Lopéz et al., 2011; Honkavaara et al., 2012).

The most thorough analysis of the reflectance accuracy was evaluated using well-defined, isotropic, flat reference targets (portable tarps, gravels). Their anisotropic factors were detected as being less than 10 % for observer zenith angles of ±10° and between 10 and 30 % for angles of ±30° (Honkavaara et al., 2010). The results obtained with these targets can considered reliable and representative of the evaluated methods. Only some indicative results were presented with anisotropic targets and 3D structures such as grass, fields, and forests. Also, when analyzing the

reflectance data it must to be remembered that the radiometric correction is valid only for objects directly illuminated by the sun. Rough surfaces, mountainous terrain, and especially shadows would require knowledge of the BRDF and terrain model and calculations for the locally varying, diffuse irradiance component.

Nevertheless, some analysis was performed for targets in shadows. The spectral signatures and image dynamics were reduced in the shadows. For the 3D point cloud generation, it was demonstrated that the random errors in height measurements were higher in areas shadowed by trees than in areas of direct solar illumination, and that, in particular, the probability of measuring the correct terrain surface with deep shadows decreased. Problems caused by shadows are to be expected, especially if the images from different strips are matched together. The results also demonstrated that the shadow correction method used in the ATCOR-4 software version 5.1 was not applicable for high–resolution, multispectral sensors because it interpreted many dark targets in direct illumination as being shadows. The reason for this is that originally the ATCOR-4 software has been developed for 5-10 m resolution hyperspectral imagery. New cast shadow correction algorithms suitable for high-spatial resolution multispectral photogrammetric imagery are already under development (Schläpfer et al., 2012).

The results presented in this thesis demonstrated that, with the ATCOR-4 software, the vicarious radiometric in-flight calibration of the sensor improved the reflectance accuracies of all of the processed images compared to the image versions obtained via the laboratory calibration of the ADS40 sensor. It remains unclear whether this was due to sensor instability, the inaccuracy of the laboratory calibration, or some other reason. On the other hand, the rationale for performing the vicarious calibration is to compensate for the other uncertainties in radiometric correction and to adapt the image to the current atmospheric conditions. Also, it remains unclear whether the variations in the reflectance image products between the different flying heights were due to inaccurate atmospheric and BRDF modeling, sensor instability, or some other reason.

It is difficult to obtain an accurate reference reflectance factors for vicarious calibration and radiometric correction. One shortcoming of this thesis was that the accuracy of the field and laboratory reflectance factor measurements was not perfectly known and not utilized in the analysis. Based on the multiple measurements of the field targets, the accuracy of the field reference measurements was estimated to be better than 5 % for uniform targets. This uncertainty includes the accuracy of the spectrometer and variations in the target. The same level of accuracy was estimated for the laboratory BRDF retrieved BRFs (Honkavaara et al., 2010).

The weather conditions during some of the imaging campaigns used in this thesis were not perfect. The vicarious calibration of the sensor should always be performed

in clear weather, but it is also important to evaluate the radiometric performance of the sensors in suboptimal conditions. During the ADS Hyytiälä campaign, the visibility was good, but some small clouds changed the diffuse illumination. These conditions were typical for Finland, thus the results were representative in Finland. To be better suited for tree species classification, the direction of the flight lines in relation to the direction of the sun should be prepared better, that is, they should be towards or perpendicular to the sun (Korpela et al., 2011).

The influence of the solar angle in photogrammetric processes was evaluated using empirical data collected with solar elevation angles of 25° and 48° and over an area consisting mainly forests and fields. It remains unclear how well the results can be generalized for lower solar angles or urban areas.

6.4 Future research

The study has raised several topics for further research and development. Basically, these are related to improving and expanding the developed methods, the reliability and accuracy of the methods, and the improvements that the new, radiometrically corrected datasets will offer for different automatic image interpretation and classification tasks.

In the previous chapter, it was noted that arranging a campaign for radiometric calibration and validation can be difficult for many reasons. Because the image quality test fields are rare and rather laborious to maintain, a national or regional network of test fields should be established. These test fields could be used by sensor manufacturers, national mapping agencies, photogrammetric companies and research institutes. One possible solution to ease the needed field work during the campaigns could be a test field with permanent reference targets close to the airport, with an autonomous sensor web monitoring the reference targets and weather conditions either all the time or on demand. The automatic nadir reflectance factor measurements at the exact time of the over flight could be combined with the BRDF information from the reference target stored in a database (such as the SPECCHIO online spectral database: http://www.specchio.ch/). This would make it possible to conduct radiometric calibration flights over the reference targets at any time with accurate in-situ reference data and without any field work during the campaign. One solution for the autonomous test site for earth-observing sensors is the Radiometric Calibration Test Site (RadCaTS) concept developed by a remote sensing group at the University of Arizona (Czapla-Myers et al., 2010); another autonomous sensor web is being developed as part of the European Union -funded MetEOC program (MetEOC, 2013).

In future studies, the accuracies and uncertainties during all the phases of the presented radiometric calibration and validation method should be evaluated. This includes the accuracy evaluation of the radiative transfer modeling and its sensitivity

to changes in different parameters. The MODO frontend to the MODTRAN radiative transfer code makes it possible to run a sensitivity series by varying the value of one parameter at a time. With this kind of evaluation, the most crucial atmospheric parameters could be detected and measured in-situ during forthcoming campaigns. Also, the use of the radiative transfer modeling should be developed in a more automatic direction. An essential part of this comprehensive accuracy evaluation has been the accuracy of the reference reflectance factor. In future studies related to the MetEOC project, the accuracy of the FIGIFIGO BRDF retrieval will be evaluated and the traceability chain to SI units will be established.

The usability of photogrammetric imagery collected in low solar illumination below 25° over various ground cover types, including urban areas, should be studied further. Ryan et al. (2012) have suggested extending the envelope of airborne photogrammetric imaging even from pre-sunrise to post-sunset operations.

A future research topic for software developers and camera manufactures will be to device a radiative transfer–based radiometric correction method that is suitable for frame sensors. Since researchers have already demonstrated that some of the assumptions made in the radiative transfer models are not always valid for typical conditions in Finland (Mielonen et al., 2008), new models and options should be developed for these conditions. Also the shadow correction algorithms implemented in the radiative transfer–based radiometric correction software programs need to be improved to be suitable for high-spatial resolution imagery.

Aerial images are already being widely used in various image interpretation and classification tasks (Zebedin et al., 2006; Le Bris and Boldo, 2008; Waser et al., 2010; Green et al., 2011; Laliberte et al., 2012; Wulder et al., 2012). Further studies are needed to verify the applicability and expected gain from using radiometrically corrected image products compared to uncorrected images in these tasks. It is also important to develop methods that are not so sensitive to changes in the solar illumination geometry and shadows. This is due to fact that automatic interpretation of data will also be necessary in the future in shadowed conditions in order to improve the productivity and cost-efficiency of the photogrammetric mapping and to enable the efficient use of photogrammetric technology in a wide variety of application areas, such as in disaster mapping. The challenges with shadows could be compensated by using, for example, automatic shadow correction methods (Dare, 2005; Schläpfer et al., 2012).

7. Summary

In this thesis there were three main objectives. First, a quantitative method for the radiometric calibration and validation of photogrammetric sensors in a test field was developed. Second, three radiometric correction methods for photogrammetric imagery were evaluated and the accuracy of the reflectance image products was studied. And finally, the influence of the solar elevation angle in photogrammetric processes was evaluated. Based on the results of these evaluations, the hypothesis set out in this thesis was confirmed, that is, that the multispectral photogrammetric imagery can be radiometrically corrected to yield accurate reflectance image products suitable for quantitative analysis.

The photogrammetric campaigns and radiometric evaluations performed during the preparation of this thesis have taught many things. It is important to properly plan the radiometric campaigns, and demanding to perform comprehensive field reference measurements. The objective of the campaign should determine the needed preparations, target area and required weather conditions. Unfortunately the campaigns cannot always be performed in perfect conditions, but it is also important to evaluate the performance of the systems in suboptimal conditions. Permanent test fields with autonomous reference measurements would ease the organizing of radiometric campaigns significantly. Finally, it is also important to understand and evaluate the accuracies and uncertainties related to each component of the radiometric image processing chain, including the sensors, radiative transfer modeling, processing software and reference measurements.

The essential requirement of quantitative radiometry is the absolute radiometric calibration of the sensor. It makes it possible to radiometrically correct image products form atmospheric effects to surface reflectance factors. This is a necessary step when comparing imagery from different dates, weather conditions and sensors as part of various image interpretation and change detection tasks such as vegetation health monitoring through vegetation indices. The radiometric calibration and validation method developed in this thesis was the first method that quantitatively analyzed the radiometric performance of photogrammetric sensors and performed the vicarious reflectance-based radiometric calibration of the sensor. This method utilizes nadir field reflectance factor measurements obtained during

the campaign and comprehensive BRDF retrieved BRFs from the same reference targets in an exact imaging geometry that were acquired from the laboratory. The field reflectance factor is used to adapt these BRF values to match the atmospheric conditions of a campaign.

The radiometric correction potential of converting photogrammetric imagery into reflectance image products was evaluated using three different methods. One was a modified empirical line-based method suitable for both frame and line sensors and the other two were radiative transfer-based methods for pushbroom line sensors. With well-defined isotropic reference targets, a reflectance accuracy of better than 5 % was achievable with the methods using vicarious calibration and an accuracy level of 5 % was possible with a sensor laboratory calibration, even without in-situ atmospheric measurements. For the other targets, such as asphalt, sand and grass, reflectance accuracies of between 5 and 20 % were possible. These results confirmed the suitability of the photogrammetric imagery for radiometric correction. This means that the imagery collected with the photogrammetric sensors has a great deal of potential in many quantitative image interpretation and change detection tasks. The results achieved in this thesis were the first known to the author that presented quantitative evaluation of these radiometric correction methods suitable for multispectral photogrammetric images. Based on the results presented in this thesis, it is recommended to use radiometrically calibrated at-sensor radiance images as the basis for all other photogrammetric processes. For quantitative image interpretation applications, one should use radiometrically corrected reflectance image products.

The influence of the solar elevation on the radiometric performance of the photogrammetric processes was studied with imagery collected at several different flying heights in the morning (solar elevation 25°) and at noontime (48°). The quality evaluations were performed both in sun-illuminated and shadowed areas in forests, roads, and fields and using reference targets. The results indicated that the sensor settings were possible to select properly for producing similar reference target DNs at different times of the day. The results also showed that the 3D point cloud and DSM extraction was, in general, successful, and that the lower solar elevation did not deteriorate the general performance of the photogrammetric processes. These results will make it possible to lower the minimum solar angle restriction for photogrammetric campaigns in national recommendations.

The high radiometric quality of modern photogrammetric sensors and their imagery has been verified in this thesis. The radiometric calibration and validation method presented here is a step towards providing SI-traceable processes for photogrammetric sensors. This makes the rigorous radiometric processing of photogrammetric images possible and improves the quality and accuracy of automatic image interpretation and classification tasks. Finally, it can be expected that the future of radiometrically quantitative photogrammetry is bright.

References

Adler-Golden, S.M., Mathew, M.W., Berk, A., Fox, M.J., Lee, J., Ratkowski, A.J., 2008. Improvements in aerosol retrieval for atmospheric correction. *Proceedings of the Geoscience and Remote Sensing symposium IGARSS*, 7-11 July 2008, Boston, Massachusetts, USA, pp. 130-133.

Ahokas, E., Kuittinen, R., Jaakkola, J. 2000. A system to control the spatial quality of analogue and digital aerial images. *International Archives of Photogrammetry and Remote Sensing*, 33(1B): 45-52.

Alspaugh, D., 2004. A brief history of photogrammetry. In: McGlone, J.C. (ed.) Manual of Photogrammetry, Fifth Edition. *American Society for Photogrammetry and Remote Sensing*, USA, pp. 1-12. ISBN 1-57083-071-1

Alvarez, F., Catanzarite, T., Rodriguez-Perez, J.R., Nafria, D., 2010. Radiometric calibration and evaluation of UltraCamX and XP using portable reflectance targets and spectrometer data. Application to extract thematic data from imagery gathered by the national plan of aerial orthophotography (PNOA). *Proceedings of the Calibration and Orientation workshop Workshop EuroCOW*, 10-12 February 2010, Castelldefels, Spain, 6p.

Becker, S., Haala, N., Honkavaara, E., Markelin, L., 2006. Image restoration for resolution improvement of digital aerial images: a comparison of large format digital cameras. *International Archives of Photogrammetry, Remote Sensing and Spatial Information Sciences*, 36(1A): 5-10.

Beisl, U., 2001. Correction of bidirectional effects in imaging spectrometer data. *Remote Sensing series 37*, Remote Sensing Laboratories, Department of Geography, University of Zurich, 2001, 188p.

Beisl, U., 2006. Absolute spectroradiometric calibration of the ADS40 Sensor. *International Archives of the Photogrammetry, Remote Sensing and Spatial Information Sciences*, 36(1A): 14-18.

Beisl, U., Telaar, J., Schönermark, M., 2008. Atmospheric correction, reflectance calibration and BRDF correction for ADS40 image data. I*nternational Archives of the Photogrammetry, Remote Sensing and Spatial Information Sciences*, 38(7B): 7-12.

Beisl, U., Adiguezel, M., 2010. Validation of the reflectance calibration of the ADS40 airborne sensor using ground reflectance measurements. *International Archives of the Photogrammetry, Remote Sensing and Spatial Information Sciences*, 38(7B): 80-85.

Beisl, U., 2012. Reflectance calibration scheme for airborne frame camera images. *International Archives of the Photogrammetry, Remote Sensing and Spatial Information Sciences*, 39(7B): 1-5.

Berk, A., Anderson, G.P., Bernstein, L.S., Acharya, P.K., Dothe, H., Matthew, M.W., Adler-Golden, S.M., Chetwynd, J.H. Jr., Richtsmeier, S.C., Pukall, B., Allred, C.L., Jeong, L.S., Hoke, M.L., 1999. MODTRAN4 radiative transfer modeling for atmospheric correction. *Proceedings of the SPIE Annual Meeting*, 19 July 1999, Denver, Colorado, USA, vol. 3756, pp. 348-353.

Berk, A., Anderson, G.P., Acharya, P.K., Bernstein, L.S., Muratov, L., Lee, J., Fox, M., Adler-Golden, S.M., Chetwynd, J.H., Hoke, M.L., Lockwood, R.B., Gardner, J.A., Cooley, T.W., Borel, C.C., Lewis, P.E., Shettle, E.P., 2006. MODTRAN™5: 2006 Update. *Proceedings SPIE. 6233, Algorithms and Technologies for Multispectral, Hyperspectral, and Ultraspectral Imagery XII* 62331F, 5 May 2006, Orlando, Florida, USA, 8p.

Biggar, S.F., Thome, K.J., Wisniewski, W., 2003. Vicarious radiometric calibration of EO sensors by reference to high reflectance ground targets. *IEEE Transactions on Geoscience and Remote Sensing,* 41(6): 1174–1179.

Chandelier, R., Martinoty, G., 2009. Radiometric aerial triangulation for the equalization of digital aerial images and orthoimages. *Photogrammetric Engineering & Remote Sensing,* 75(2): 193-200.

Chavez, R., 1996. Image-based atmospheric corrections - revisited and improved. *Photogrammetric Engineering & Remote Sensing,* 62(9): 1025-1036.

Clark, B., Suomalainen, J., Pellikka, P., 2011. An historical empirical line method for the retrieval of surface reflectance factor from multi-temporal SPOT HRV, HRVIR and HRG multispectral satellite imagery. *International Journal of Applied Earth Observation and Geoinformation,* 13(2011): 292-307.

Collings, S., Cacetta, P., Campbell, N., Wu, X. 2011. Empirical models for radiometric calibration of digital aerial frame mosaics. *IEEE Transactions on Geoscience and Remote Sensing,* 49(7): 2573-2588.

Cramer, M., 2005. 10 Years ifp Test Site Vaihingen/Enz: An Independent Performance Study. *Photogrammetric Week 2005*, (Fritsch, D., Ed.), Wichmann Verlag, Heidelberg, Germany, pp. 79-92.

Cramer, M., 2008. The EuroSDR approach on digital airborne camera calibration and certification. *International Archives of the Photogrammetry, Remote Sensing and Spatial Information Sciences*, 38(4B): 1753-1758.

Cramer, M., 2010. The DGPF-Test on Digital Camera Evaluation – Overview and Test Design. *Photogrammetrie – Fernerkundung - Geoinformation (PFG)*, 2010 (2): 73-82.

Cramer, M., 2011. Geometry perfect – radiometry unknown? *Photogrammetric Week 2011*, (Fritsch, D., Ed.), Wichmann Verlag, Heidelberg, Germany,pp. 65-77.

Czapla-Myers, J.S., Thome, K.J., Leisso, N.P., 2010. Radiometric calibration of earth-observing sensors using an automated test site at Railroad Valley, Nevada. *Canadian Journal of Remote Sensing*, 36(5): 474-487.

Dare, P.M., 2005. Shadow analysis in high resolution satellite imagery of urban areas. *Photogrammetric Engineering & Remote Sensing,* 71(2): 169-177.

Dinguirard, M.; Slater, P.N., 1999 Calibration of space-multispectral imaging sensors: A review. *Remote Sensing of Environment*, 68(3): 194-205.

Diener, S., Kiefner, M., Dörstel, C., 2000. Radiometric normalisation and colour composite generation of the DMC. *International Archives of Photogrammetry and Remote Sensing and Spatial Information Sciences*, 33 (1B): 82-88.

EuroDAC², 2011. EuroSDR initiative Digital Airborne Camera Calibration (EuroDAC²) Digital Camera Calibration & Validation. http://www.ifp.uni-stuttgart.de/eurosdr/EuroDAC/index.en.html (accessed 10 June, 2013)

FKS, 1995. Suositukset Suomessa tehtävälle mittaus- ja kartoitusilmakuvaukselle (in Finnish, Recommendations for aerial photogrammetry for mapping in Finland). Publications of The Finnish Society of Photogrammetry and Remote Sensing 1/1995. http://foto.hut.fi/seura/julkaisut/erillisjulkaisu1_1995/teksti.html (accessed 10 June, 2013)

Fraser, C.S., 1997. Digital camera self-calibration. *ISPRS Journal of Photogrammetry and Remote Sensing*, 52(4): 149-159.

Förstner, W., 1995. Matching Strategies for Point Transfer. *Photogrammetric Week 1995*, (Fritch, D., Hobbie, D., Eds.), Wichmann Verlag, Heidelberg, Germany, pp. 173-183.

Georgi, C., Stognienko, R., Knuth, S., Albe, G., 2005. JAS: The next generation digital aerial scanner. *Photogrammetric Week 2005*, (Fritsch, D., Ed.), Wichmann Verlag, Heidelberg, Germany, pp. 147-154.

Graham, R. and Koh, A. (Eds.), 2004. Detectors and Sensors. In McGlone, J. C. (ed.). Manual of Photogrammetry, 5th ed. *American Society for Photogrammetry and Remote Sensin*g, USA, pp. 505-580 ISBN 1-57083-071-1

Green, K., Tukman, M., Finkbeiner, M., 2011. Comparison of DMC, UltraCam and ADS40 imagery for benthic habitat and propeller scar mapping. *Photogrammetric Engineering and Remote Sensing*, 77(6): 589-599.

Grenzdörffer, G., 2010. Medium Format Cameras. *Report of EuroSDR projects, Official Publication no. 58*, 270 pages. Frankfurt a.M., Germany, 2010.

Gruber, M., Ponticelli, M., Wiechert, A., 2011. UltraCam, a brand of continuous developments. *Photogrammetric Week 2011*, (Fritsch, D., Ed.), Wichmann Verlag, Heidelberg, Germany, pp. 103-109.

Haala, N., 2009. Comeback of Digital Image Matching. *Photogrammetric Week 2009*, (Fritsch, D., Ed.), Wichmann Verlag, Heidelberg, Germany, pp. 289-301.

Haala, N., Rothermel, M., 2012. Dense multi-stereo matching for high quality digital elevation models. *Photogrammetrie – Fernerkundung - Geoinformation (PFG)*, 2012 (4); 331-343.

Haest, B., Biesemans, J., Horsten, W., Everaerts, J., 2009. Radiometric calibration of digital photogrammetric image data. I*n the proceedings of Annual American Society of Photogrammetry and Remote Sensing Conference*, 9-13 March 2009, Baltimore, Maryland, USA, 12p.

Hanusch, T.H., Baltsavias, E., 2009. Evaluation of digital photogrammetric aerial camera systems - Radiometric Evaluation of DMC, ADS40 and UltracamX. *Annual meeting of DGPF*, 24-26 March 2009, Jena, Germany. http://www.ifp.uni-stuttgart.de/dgpf/PDF/JT09-Radiometrie-HANUSCH&BALTSAVIAS.pdf 11p. (accessed 10 June, 2013)

Hari, P., Kulmala, M., 2005. Station for Measuring Ecosystem-Atmosphere Relations (SMEAR-II). *Boreal Environment Research*, 10(5): 315-322.

Hefele, J., 2006. Calibration experience with the DMC. In the *Proceedings of the EuroSDR Commission I and ISPRS Working Group 1/3 Workshop EuroCOW*, 25-27 January 2006, Castelldefels, Spain, unpaginated CDROM, 6p.

Heikkinen, V., Korpela, I., Tokola, T., Honkavaara, E., Parkkinen, J., 2011. An SVM classification of tree species radiometric signatures based on the Leica ADS40 sensor. *IEEE Transactions on Geoscience and Remote Sensing. IEEE Transactions on Geoscience and Remote Sensing*, 49(11): 4539-4551.

Hernández-López , D., Felipe García, B., González Piqueras, J., Villa Alcázar, G., 2011. An approach to the radiometric aerotriangulation of photogrammetric images. *ISPRS Journal of Photogrammetry and Remote Sensing*, 66(6): 883–893.

Hernández-López , D., Felipe García, B., Sánchez, N., González-Aguilera, D., Gomez-Lahoz, J., 2012. Testing the radiometric performance of digital photogrammetric images: vicarious vs. laboratory calibration of the Leica ADS40, a study in Spain. *Photogrammetrie – Fernerkundung - Geoinformation (PFG),* 2012(5): 0557-0572.

Hirschmüller, H., 2011. Semi-Global Matching – Motivation, Developments and Applications. *Photogrammetric Week 2011*, (Fritsch, D., Ed.), Wichmann Verlag, pp. 173-184.

Holben, B.N., Eck, T.F., Slutsker, I., Tanré, D., Buis, J. P., Setzer, A., Vermote, E., Reagan, J.A., Kaufman, Y.J., Nakajima, T., Lavenu, F., Jankowiak, I., Smirnov, A., 1998. AERONET—A federated instrument network and data archive for aerosol characterization. *Remote Sensing of Environment*, 66(1): 1–16.

Holland, D., Gladstone, C., Sargent, I., Horgan, J., Gardiner, A., Freeman, M., 2012. Automating the photogrammetric workflow in a national mapping agency. *ISPRS Annals of Photogrammetry, Remote Sensing and Spatial Information Sciences*, 1(4): 83-88.

Honkavaara, E., Jaakkola, J., Markelin, L., Peltoniemi, J., Ahokas, E., Becker, S., 2006a. Complete photogrammetric system calibration and evaluation in the Sjökulla test field – case study with DMC. I*n the Proceedings of EuroSDR Commission I and ISPRS Working Group 1/3 Workshop EuroCOW*, 25-27 January 2006, Castelldefels, Spain, unpaginated CD-ROM, 6p.

Honkavaara, E., Ahokas, E., Hyyppä, J., Jaakkola, J., Kaartinen, H., Kuittinen, R., Markelin, L., Nurminen, K., 2006b. Geometric test field calibration of digital photogrammetric sensors. *ISPRS Journal of Photogrammetry and Remote Sensing,* 60(6): 387-399.

Honkavaara, E., Jaakkola, J., Markelin, L., Becker, S., 2006c. Evaluation of resolving power and MTF of DMC. *International Archives of Photogrammetry, Remote Sensing and Spatial Information Sciences*, 36(1A): 17-22.

Honkavaara, E., Jaakkola, J., Markelin, L., Nurminen, K., Ahokas, E., 2006d. Theoretical and empirical evaluation of geometric performance of multi-head large format photogrammetric sensors. *International Archives of Photogrammetry, Remote Sensing and Spatial Information Sciences*, 36(1A): 11-16.

Honkavaara, E., Markelin, L., 2007. Radiometric Performance of Digital Image Data Collection - A Comparison of ADS40/DMC/UltraCam and EmergeDSS, *Photogrammetric Week 2007*, (Fritsch, D., Ed.), Wichmann Verlag, Heidelberg, Germany, pp. 117-129.

Honkavaara, E., Peltoniemi, J. Ahokas, E., Kuittinen, R., Hyyppä, J., Jaakkola, J., Kaartinen, H., Markelin, L., Nurminen, K., Suomalainen, J., 2008a. A permanent test field for digital photogrammetric systems. *Photogrammetric Engineering & Remote Sensing*, 74(1): 95-106.

Honkavaara, E., 2008b. Calibrating digital photogrammetric airborne imaging systems using a test field. Doctoral thesis. *Publications of the Finnish Geodetic Institute*, N:o 140, Kirkkonummi, Finland, 2008. Available from http://urn.fi/URN:ISBN:978-951-711-276-5

Honkavaara, E., Arbiol, R., Markelin, L., Martínez, L., Cramer, M., Korpela, I., Bovet, S., Thom, C., Chandelier, L., Ilves, R., Klonus, S., Reulke, R., Marshall, P., Tabor, M., Schläpfer, D., Veje, N., 2009a. Status report of the EuroSDR project "Radiometric aspects of digital photogrammetric airborne images". *International Archives of the Photogrammetry, Remote Sensing and Spatial Information Sciences*, 38 (1-4-7/W5): 6p.

Honkavaara, E., Arbiol, R., Markelin, L., Martínez, L., Cramer, M., Bovet, S., Chandelier, L., Ilves, R., Klonus, S., Marshall, P., Schläpfer, D., Tabor, M., Thom, C., Veje, N., 2009b. Digital airborne photogrammetry—a new tool for quantitative remote sensing?—a state-of-the-art review on radiometric aspects of digital photogrammetric images. *Remote Sensing* 2009 1(3): 577-605.

Honkavaara, E., Hakala, T., Peltoniemi, J., Suomalainen, J., Ahokas, E., Markelin L., 2010. Analysis of Properties of Reflectance Reference Targets for Permanent Radiometric Test Sites of High Resolution Airborne Imaging Systems. *Remote Sensing*, 2010, 2(8): 1892-1917.

Honkavaara, E., Nurminen, K., Markelin, L., Suomalainen, J., Ilves, R., 2011a. Calibrating and validating multispectral photogrammetric 3D imaging system at a permanent test site – Case study with an Intergraph DMC. *Photogrammetric Record*, 26 (134): 229-249.

Honkavaara, E., Arbiol, R., Markelin, L., Martínez, L., Bovet, S., Bredif, M., Chandelier, L., Heikkinen, V., Korpela, I., Lelegard, L., Pérez, F., Schläpfer, D., Tokola, T., 2011b. The Eu**roSDR project "Radiometric aspects of digital photogrammetric images"** – Results of the empirical phase. *International Archives of Photogrammetry, Remote Sensing and Spatial Information Sciences*, 38(4/W19): 8p.

Honkavaara, E., Hakala, T., Markelin, L., Rosnell, T., Saari, H., Mäkynen, J., 2012. A process for radiometric correction for UAV image blocks. *Photogrammetrie – Fernerkundung - Geoinformation (PFG)*, 2012 (2): 0115-0127.

Honkavaara, E., Markelin, L., Arbiol, R., Martínez, L., 2013. Radiometric aspects of digital photogrammetric images. *EuroSDR official publication No 62.* Gopher, Netherlands, 95p. Available from http://www.eurosdr.net/publications/62.pdf

Hyytiälä, 2013. Hyytiälä Forestry Field Station. http://www.helsinki.fi/hyytiala/english/index.htm (accessed 10 June, 2013)

Höhle, J., 2011. On the potential of new digital aerial cameras for DEM generation. *The Photogrammetric Journal of Finland*, 22(2): 27-36.

Immitzer, M., Atzberger, C., Koukal, T., 2012. Tree species classification with random forest using very high resolution 8-band WorldView-2 Satellite data. *Remote Sensing,* 4(9): 2661-2693.

Jacobsen, K., Cramer, M., Ladstädter, R., Ressl, C., Spreckels, V., 2010. DGPF project: Evaluation of digital photogrammetric camera systems – geometric performance. P*hotogrammetrie – Fernerkundung – Geoinformation (PFG)*, 2010(2): 83-97.

Kennedy, R.E., Cohen, W.B. Takao, G., 1997. Empirical methods to compensate for a view-angle dependent brightness gradient in AVIRIS imagery. *Remote Sensing of Environment*, 62(3): 277–291.

Korpela, I., Heikkinen, V., Honkavaara, E., Rohrbach, F., Tokola, T., 2011. Variation and directional anisotropy of reflectance at the crown scale - Implications for tree species classification in digital aerial images. *Remote Sensing of Environment*, 115 (8): 2062-2074.

Kraus, K., 1993. Photogrammetry, Volume 1: Fundamentals and Standard Processes. Ferdinand Dümmels Verlag, Bonn, Germany, 402 p. ISBN: 3-427-78684-6.

Image Calibrator, 2013. Image Calibrator - Atmospheric Correction Software. http://www.discover-aai.com/ic.htm (accessed 10 June, 2013)

IGI, 2013. IGI Quatro DigiCAM. http://www.igi.eu/quattro-digicam.html (accessed 10 June, 2013)

ImSpec, 2013. ImSpec LCC Advanced imaging and spectroscopy. http://www.imspec.com/ (accessed 10 June, 2013)

Kotchenova, S.Y., Vermote, E.F., Matarrese, R., Klemm, F.J., 2006. Validation of a vector version of the 6S raditative transfer code for atmospheric correction of satellite data. Part I: Path radiance. *Applied Optics,* 45(26): 6762-6774.

Kuittinen R., Ahokas, E., Högholen, A., Laaksonen, J., 1994. Test field for aerial photography. *The Photogrammetric Journal of Finland*, 14(1): 53-62.

Kuittinen R., Ahokas, E., Järvelin, P., 1996. Transportable test-bar targets and microdensitometer measurements: A method to control the quality of aerial imagery, I*nternational Archives of Photogrammetry and Remote Sensing*, 31(1): 99-104.

Laliberte, A.S., Browning, D.M., Rango, A., 2012. A Comparison of three feature selection methods for object-based classification of sub-decimeter resolution UltraCam-L imagery. *International Journal of Applied Earth Observation and Geoinformation*, 15(2012): 70-78.

LANDNET, 2013. LANDNET sites (CEOS reference sites). http://calvalportal.ceos.org/cvp/web/guest/ceos-landnet-sites (accessed 10 June, 2013)

LDCM, 2003. Landsat Data Continuity Mission (LDCM) Implementation Phase, Data Specification. Goddard Space Flight Center, Maryland, USA, January 2003. http://prod.nais.nasa.gov/eps/eps_data/102577-SOL-001-005.pdf 45p. (accessed 10 June, 2013)

Leberl, F., Irschara, A, Pock, T., Meixner, P., Gruber, M., Shcolz, S., Wiechert, A., 2010. Point clouds: lidar versus 3D vision. *Photogrammetric Engineering and Remote Sensing* 76(10): 1123-1134.

Le Bris, A., Boldo, D., 2008. Extraction of land cover themes from aerial ortho-images in mountainous area using external information. *The Photogrammetric Record,* 23(124): 387-404.

Lillesand, T., Kiefer, R.W., Chipman, J., 2007. Remote Sensing and Image Interpretation. John Wiley & Sons, Inc, U.S.A., 6th ed., 804 p. ISBN: 978-0470052457.

Mahiny, A.S., Turner, B.J., 2007. A comparison of four common atmospheric correction methods. *Photogrammetric Engineering & Remote Sensing*, 73(3): 361-368.

Main, R., Cho, M.A., Mathieu, R., **O'Kennedy,** M.M., Ramoelo, A., Koch, S., 2011. An investigation into robust spectral indices for leaf chlorophyll estimation. *ISPRS Journal of Photogrammetry and Remote Sensing,* 66(2011): 751-761.

Markelin, L., Honkavaara, E., Peltoniemi, J., Suomalainen, J., Ahokas, E., 2006. Radiometric evaluation of digital aerial cameras. I*nternational Archives of Photogrammetry, Remote Sensing and Spatial Information Sciences*, 36(1B): 75-80.

Martínez, L., Arbiol, R., Palà, V., Pérez, F., 2007. Digital Metric Camera radiometric and colorimetric calibration with simultaneous CASI imagery to a CIE Standard Observer based colour space. *In the proceedings of the IEEE International Geoscience and Remote Sensing Symposium IGARSS*, July 23-28, 2007, Barcelona, Spain, pp. 4140 – 4143.

Martínez, L., Arbiol, R., 2008. ICC experiences on DMC radiometric calibration. *In the proceedings of the Calibration and Orientation workshop Workshop EuroCOW*, 30 January - 1 February 2008, Castelldefels, Spain, 7p.

Martínez, L., Pérez, F., Arbiol, R., Tardà, A., 2010. Radiometric characterisation of VNIR hyperspectral imaging system for accurate atmospheric correction. *In the proceedings of 2nd Workshop on Hyperspectral Image and Signal Processing: Evolution in Remote Sensing (WHISPERS)*, 14-16 June 2010, Reykjavik, Iceland, 4p.

Martínez, L., Pérez, F., Arbiol, R., Magarios, A., 2012. Development of NDVI WMS geoservice from reflectance DMC imagery at ICC. *In the proceedings of the Calibration and Orientation workshop Workshop EuroCOW*, 8-10 February 2012, Castelldefels, Spain, 5 p.

MetEOC, 2013. Metrology for Earth Observation and Climate. http://www.meteoc.org/ (accessed 10 June, 2013)

Mielonen, T., Kaurila, T., Arola, A., Lihavainen, H., Kompula, M., Lehtinen, K.E.J., 2008. Effect of aerosols on the infrared transmission in Lakiala, Finland. *Atmospheric Environment*, 42(2008): 2603-2610.

Minten, H., 2009. The modular system consept of IGI. Photogrammetric Week 2009, (Fritsch, D., Ed.), Wichmann Verlag, Heidelberg, Germany, pp. 41-47.

Moran, M.S., Ross, B.B., Clarke, T.R., Qi, J., 2001. Deployment and calibration of reference reflectance tarps for use with airborne imaging sensors. *Photogrammetric Engineering & Remote Sensing*, 67(3): 273-286.

NAIP, 2013. NAIP Imagery. http://www.fsa.usda.gov/FSA/apfoapp?area=home&subject=prog&topic=nai i (accessed 10 June, 2013)

Neumann, K.J., 2011a. Z/I DMC II Camera Family. *Presentation at Civil Commercial Imagery Evaluation Workshop JACIE,* March 29-31 2011, Boulder, Colorado, USA. http://calval.cr.usgs.gov/JACIE_files/JACIE11/Presentations/ThurAM/1010 _Neuman_JACIE_11.105.pdf (accessed 20 June, 2013)

Neumann, K.J., 2011b. The Z/I DMC II – "Imaging revolution". *Photogrammetric Week 2011*, (Fritsch, D., Ed.), Wichmann Verlag, Heidelberg, Germany, pp. 97-101.

Nicodemus, F.E., Richmond, J.C., Hsia, J.J., 1977. Geometrical considerations and nomeclature for reflectance. *Washington, DC: National Bureau of Standards, US Deparment of Commerce*, 67p.

NLS, 2013. Datasets free of charge. http://www.maanmittauslaitos.fi/en/opendata (accessed 10 June, 2013)

Optech, 2013. Optech Aerial Digital Cameras. http://www.optech.ca/cameras.htm (accessed 10 June, 2013)

Packalén, P., Suvanto, A., Maltamo, M., 2009. A two stage method to estimate species-specific growing stock. *Photogrammetric Engineering & Remote Sensing*, 72(12): 1451-1460.

Pagnutti, M., Holekamp, K.. Ryan, R., Blonski, S., Sellers, R., Davis, B., Zanoni, V., 2002. Measurement sets and sites commonly used for characterizations. *International Archives of Photogrammetry and Remote Sensing*, 34(1): 6p.

Paine, D.P., Kiser, J.D., 2003. Aerial photography and image interpretation. John Wiley & Sons, New York, U.S.A., 2nd ed., 632 p. ISBN: 0-471-20489-7

Passini, R., Jacobsen, K., 2008. Accuracy analysis of large size digital aerial cameras. *International Archives of the Photogrammetry, Remote Sensing and Spatial Information Sciences*, 38(1B): 507–513.

Passini, R., Jacobsen, K., Day, D., 2012. Accuracy and radiometric study on latest generation large format digital frame cameras. *In the proceedings of the Civil Commercial Imagery Evaluation Workshop JACIE*, 17-19 April, 2012 Fairfax, VA, USA, 12p.

Pechatnikov, M., Shor, E., Raizman, Y., 2009. The new Vision Map A3 airborne camera system. *Photogrammetric Week 2009*, (Fritsch, D., Ed.), Wichmann Verlag, Heidelberg, Germany, pp. 99-109.

Peltoniemi, J., Piironen, J., Näränen, J., Suomalainen, J., Kuittinen, R., Markelin, L., Honkavaara, E., 2007. Bidirectional reflectance spectrometry of gravel at the Sjökulla test field. *ISPRS Journal of Photogrammetry and Remote Sensing*, 62 (2007): 434-446.

Petrie, G.; Walker, S., 2007 Airborne digital imaging technology: a new overview. *The Photogrammetric Record*, 22(119): 203-225.

Pindyck, R.S., Rubinfeld, D.L., 1991. Econometric models and economic forecasts. McGraw-Hill International Editions, New York, USA, 596p.

Read, R.E., Graham, R.W., 2002. Manual of air survey: primary data acquisition. Whittles Publishing, Chaithness, Scotland, UK, 408p.

Richter, R., 1990. A fast atmospheric correction algorithm applied to Landsat TM images. *International Journal of Remote Sensing*, 11 (1): 159-166.

Richter, R., 1996. Atmospheric correction of DAIS hyperspectral image data. *Computers & Geosciences*, 22 (7): 785-793.

Richter, R., 2008. Classification metrics for improved atmospheric correction of multispectral VNIR imagery. *Sensors*, 2008 8(11): 6999-7011.

Richter, R., Schläpfer, D., 2013. Atmospheric / Topographic Correction for Airborne Imagery (ATCOR-4 User Guide, Version 6.2.1, February 2013). *DLR report DLR-IB 565-02/12,* Wessling, Germany, 217p. Latest version is always available from http://www.rese.ch/download

Rosso, P.H., Klonus, S., Ehlers, M., Tschach, E., 2008. Comparative properties of four airborne sensors and their applicability to land surface interpretation. *International Archives of the Photogrammetry, Remote Sensing and Spatial Information Sciences*, 38(1B): 545-550.

Roujean, J.L., Leroy, M., Deshchamps, P.Y., 1992. A bidirectional reflectance model of the Earth's surface for the correction of remote sensor data. *Journal of Geophysical Research*, 97(D18): 455−468.

Ryan, R.E., Holekamp, K., Pagnutti, M., Stanley, T., 2007. A simplified approach to radiometric vicarious calibration. *Poster presented in Joint Agency Commercial Imagery Evaluation Workshop (JACIE),* 20-22 March 2007, Fairfax, Virginia, USA. http://calval.cr.usgs.gov/wordpress/wp-content/uploads/JACIE_files/JACIE07/Files/PRyan.pdf (accessed 10 June, 2013)

Ryan, R.E., Pagnutti, M., 2009. Enhanced Absolute and Relative Radiometric Calibration for Digital Aerial Cameras. *Photogrammetric Week 2009*, (Fritsch, D., Ed.), Wichmann Verlag, Heidelberg, Germany, pp. 81-90.

Ryan, R.E., Pagnutti, M., Holekamp, K., 2012. Extending the operational envelope of aerial optical imaging from pre-sunrise to post-sunset operation. *Presentation given in in Joint Agency Commercial Imagery Evaluation Workshop (JACIE),* 17-19 April 2012, Fairfax, Virginia, USA. http://calval.cr.usgs.gov/wordpress/wp-content/uploads/Ryan_Low_light_JACIE2012.pdf (accessed 10 June, 2013)

Ryan, R.E., Pagnutti, M., Stensaas, G., 2013. Aerial Imaging Quality Assurance. *Presentation given in in Joint Agency Commercial Imagery Evaluation Workshop (JACIE),* 16-18 April 2013, St. Louis, Missouri, USA. https://calval.cr.usgs.gov/wordpress/wp-content/uploads/Ryan_Aerial_Imaging_Quality_JACIE_2013.pdf (accessed 10 June, 2013)

Sandau, R., Braunecker, B., Driescher, H., Eckardt, A., Hilbert, S., Hutton, J., Kirchhofer, W., Lithopoulos, E., Reulke, R., Wicki, S., 2000. Design principles of the LH Systems ADS40 airborne digital sensor. *International Archives of Photogrammetry and Remote Sensing*, 33(1B): 258-265.

Sandau, R., 2010. Digital airborne camera: introduction and technology. Springer, 356p. ISBN: 978-1402088773

Schaepman-Strub, G., Schaepman, M., Painter, T.H., Dangel, S., Martonchik, J.V., 2006. Reflectance quantities in optical remote sensing − definitions and case studies. *Remote Sensing of Environment*, 103(2006): 27-42.

Schläpfer, D., Nieke, J., 2005. Operational simulation of at sensor radiance sensitivity using the MODO/MODTRAN4 environment. In: Zagajewski B., Sobczak M., Wrzesie M., (Eds.), *In the proceedings of the 4th EARSeL Workshop on Imaging Spectroscopy*, 26-29 April 2005, Warsaw, Poland, 8p.

Schläpfer, D., 2011. MODO − MODTRAN®-5 for Remote Sensing Applications User Manual, Version 5. Wil (SG), Switzerland, 96p. Latest version is always available from http://www.rese.ch/download

Schläpfer, D., Richter, R., Kellenberger, T., 2012. Atmospheric and topographic correction of photogrammetric airborne digital scanner data (ATCOR-ADS). *In the proceedings of the EuroSDR Commission I and ISPRS Working Group 1/3 Workshop EuroCOW*, 8-10 February 2012, Barcelona, Spain, 5p.

Schneider, S., Gruber, M., 2008. Radiometric quality of UltraCamX images. *International Archives of the Photogrammetry, Remote Sensing and Spatial Information Sciences*, 38(1B): 539-544.

Schott, J.R., 2007. Remote Sensing: the Image Chain Approach. Oxford University Press, New York, USA, 2nd ed., 688p. ISBN: 978-0195178173

Schowengerdt, R.A., 2007. Remote Sensing – Models and Methods for Image Processing. 3rd ed., Academic Press, USA, 515p. ISBN: 0-12-369407-8

von Schönermark, M., Geiger, B., Röser, H.P. (Eds.), 2004. Reflection properties of vegetation and soil - with a BRDF data base. Wissenschaft und Technik Verlag, Berlin, 352p.

von Schönermark, M., 2010. Status report about the evaluation of the radiometric properties of digital photogrammetric airborne cameras. *Photogrammetrie – Fernerkundung – Geoinformation (PFG)*, 2010(2): 131-139.

Slater, P.N., Biggar S.F., Thome, K.J., Gellman, D.I., Spyak, P.R., 1996. Vicarious Radiometric Calibration of EOS Sensors. *Journal of Atmospheric and Oceanic Technology,* 13 (2): 349-359.

SMEAR, 2013. SMEAR research stations. http://www.atm.helsinki.fi/SMEAR/ (accessed 10 June, 2013)

Smith, G. M., Milton, E. J., 1999. The use of the empirical line method to calibrate remotely sensed data to reflectance. *International Journal of Remote Sensing*, 20(13): 2653–2662.

Song, C., Woodcock, C.E., Seto, K.C., Lenney, M.P., Macomber, S.A., 2001. Classification and change detection using Landsat TM data: when and how to correct atmospheric effects? *Remote Sensing of Environment,* 75(2): 230–244.

Souchon, J-P., Thom, C., Meynard, C., Martin, O., Pierrot-Deseilligny, M., 2010. The IGN CAMv2 system. *The Photogrammetric Record*, 25(132): 402-421.

Spreckels, V., Syrek, L., Schlienkamp, A., 2010. DGPF Project: Evaluation of digital photogrammetric camera systems – stereoplotting. *Photogrammetrie – Fernerkundung – Geoinformation (PFG)*, 2010(2): 117-130.

Stensaas, G., Lee, G., 2008. Driving toward a worldwide acceptance procedure for digital airborne sensors. *International Archives of the Photogrammetry, Remote Sensing and Spatial Information Sciences,* 38(1B): 561-566.

Suomalainen, J., Hakala, T., Peltoniemi, J., Puttonen, E., 2009. Polarised multiangular reflectance measurements using the Finnish geodetic institute field goniospectrometer. *Sensors*, 9(5): 3891-3907.

Tuominen, S., Pekkarinen, A., 2004. Local radiometric correction of digital aerial photographs for multi source forest inventory. *Remote Sensing of Environment*, 89(2004): 72-82.

UltraMap, 2013. UltraMap 3.0 workflow software system. http://www.microsoft.com/ultracam/en-us/UltraMapModules.aspx (accessed 10 June, 2013)

USGS, 2013. Digital Aerial Quality Assurance. http://calval.cr.usgs.gov/past-activities/digaerial/digital_qa/ (accessed 10 June, 2013)

Vermote, E.F., Tanré, D., Deuzé, J.L., Herman, M., Morcrette, J.J., 1997. Second simulation of the satellite signal in the solar spectrum, 6S: an overview. *IEEE Transactions on Geoscience and Remote Sensing*, 35(3): 675-686.

Wanner, W., Li, X., Strahler, A.H., 1995. On the derivation of kernels for kernel driven models of bidirectional reflectance. *Journal of Geophysical Research,* 100(D10): 21 077–21 089.

Wagner, R., 2011. Leica ADS80 and Leica XPro: a total solution for photogrammetric mapping. *Photogrammetric Week 2011*, (Fritsch, D., Ed.), Wichmann Verlag, Heidelberg, Germany, pp. 79-87.

Waser, L.T., Klonus, S., Ehlers, M., Khler, M., Jung, A., 2010. Potential of digital sensors for land cover and tree species classifications - a case study in the framework of the DGPF-project. *Photogrammetrie – Fernerkundung – Geoinformation (PFG)*, 2010(2): 141-156.

Wiechert, A., Gruber, M., 2011. UltraCam and UltraMap – towards all in one solution by photogrammetry. *Photogrammetric Week 2011*, (Fritsch, D., Ed.), Wichmann Verlag, Heidelberg, Germany, pp. 33-38.

Wu, X., 2006. Radiometric calibration of aerial digital imagery. I*n the proceedings of the 13th Australasian remote sensing and photogrammetry conference*, 20-24 November 2006, Canberra, Australia, unpaginated CDROM, 6p.

Wulder, M.A., White, J.C., Coggins, S., Ortlepp, S.M., Coops, N.C., Heath, J., Mora, B., 2012. Digital high spatial resolution aerial imagery to support forest health monitoring: the mountain pin beetle context. *Journal of Applied Remote Sensing*, 6(1): 10p.

Zebedin, L., Klaus, A., Gruber-Geymayer, B., Karner, K., 2006. Towards 3D map generation from digital aerial images. *ISPRS Journal of Photogrammetry and Remote Sensing*, 60(2006): 413-427.

Suomen Geodeettisen laitoksen julkaisut:
Veröffentlichungen des Finnischen Geodätischen Institutes:
Publications of the Finnish Geodetic Institute:

1. Y. VÄISÄLÄ: Tafeln für geodätische Berechnungen nach den Erddimensionen von Hayford. Helsinki 1923. 30 S.
2. Y. VÄISÄLÄ: Die Anwendung der Lichtinterferenz zu Längenmessungen auf grösseren Distanzen. Helsinki 1923. 22 S.
3. ILMARI BONSDORFF, Y. LEINBERG, W. HEISKANEN: Die Beobachtungsergebnisse der südfinnischen Triangulation in den Jahren 1920-1923. Helsinki 1924. 235 S.
4. W. HEISKANEN: Untersuchungen über Schwerkraft und Isostasie. Helsinki 1924. 96 S. 1 Karte.
5. W. HEISKANEN: Schwerkraft und isostatische Kompensation in Norwegen. Helsinki 1926. 33 S. 1 Karte.
6. W. HEISKANEN: Die Erddimensionen nach den europäischen Gradmessungen. Helsinki 1926. 26 S.
7. ILMARI BONSDORFF, V.R. ÖLANDER, Y. LEINBERG: Die Beobachtungsergebnisse der südfinnischen Triangulation in den Jahren 1924-1926. Helsinki 1927. 164 S. 1 Karte.
8. V.R. ÖLANDER: Ausgleichung einer Dreieckskette mit Laplaceschen Punkten. Helsinki 1927. 49 S. 1 Karte.
9. U. PESONEN: Relative Bestimmungen der Schwerkraft auf den Dreieckspunkten der südfinnischen Triangulation in den Jahren 1924-1925. Helsinki 1927. 129 S.
10. ILMARI BONSDORFF: Das Theorem von Clairaut und die Massenverteilung im Erdinnern. Helsinki 1929. 10 S.
11. ILMARI BONSDORFF, V.R. ÖLANDER, W. HEISKANEN, U. PESONEN: Die Beobachtungsergebnisse der Triangulationen in den Jahren 1926-1928. Helsinki 1929. 139 S. 1 Karte.
12. W. HEISKANEN: Über die Elliptizität des Erdäquators. Helsinki 1929. 18 S.
13. U. PESONEN: Relative Bestimmungen der Schwerkraft in Finnland in den Jahren 1926-1929. Helsinki 1930. 168 S. 1 Karte.
14. Y. VÄISÄLÄ: Anwendung der Lichtinterferenz bei Basismessungen. Helsinki 1930. 47 S.
15. M. FRANSSILA: Der Einfluss der den Pendel umgebenden Luft auf die Schwingungszeit beim v. Sterneckschen Pendelapparat. Helsinki 1931. 23 S.
16. Y. LEINBERG: Ergebnisse der astronomischen Ortsbestimmungen auf den finnischen Dreieckspunkten. Helsinki 1931. 162 S.
17. V.R. ÖLANDER: Über die Beziehung zwischen Lotabweichungen und Schwereanomalien sowie über das Lotabweichungssystem in Süd-Finnland. Helsinki 1931. 23 S.
18. PENTTI KALAJA, UUNO PESONEN, V.R. ÖLANDER, Y. LEINBERG: Beobachtungsergebnisse. Helsinki 1933. 240 S. 1 Karte.
19. R.A. HIRVONEN: The continental undulations of the geoid. Helsinki 1934. 89 pages. 1 map.
20. ILMARI BONSDORFF: Die Länge der Versuchsbasis von Helsinki und Längenveränderungen der Invardrähte 634-637. Helsinki 1934. 41 S.
21. V.R. ÖLANDER: Zwei Ausgleichungen des grossen südfinnischen Dreieckskranzes. Helsinki 1935. 66 S. 1 Karte.
22. U. PESONEN, V.R. ÖLANDER: Beobachtungsergebnisse. Winkelmessungen in den Jahren 1932-1935. Helsinki 1936. 148 S. 1 Karte.
23. R.A. HIRVONEN: Relative Bestimmungen der Schwerkraft in Finnland in den Jahren 1931, 1933 und 1935. Helsinki 1937. 151 S.
24. R.A. HIRVONEN: Bestimmung des Schwereunterschiedes Helsinki-Potsdam im Jahre 1935 und Katalog der finnischen Schwerestationen. Helsinki 1937. 36 S. 1 Karte.
25. T.J. KUKKAMÄKI: Über die nivellitische Refraktion. Helsinki 1938. 48 S.
26. Finnisches Geodätisches Institut 1918-1938. Helsinki 1939. 126 S. 2 Karten.
27. T.J. KUKKAMÄKI: Formeln und Tabellen zur Berechnung der nivellitischen Refraktion. Helsinki 1939. 18 S.
28. T.J. KUKKAMÄKI: Verbesserung der horizontalen Winkelmessungen wegen der Seitenrefraktion. Helsinki 1939. 18 S.
29. ILMARI BONSDORFF: Ergebnisse der astronomischen Ortsbestimmungen im Jahre 1933. Helsinki 1939. 47 S.
30. T. HONKASALO: Relative Bestimmungen der Schwerkraft in Finnland im Jahre 1937. Helsinki 1941. 78 S.
31. PENTTI KALAJA: Die Grundlinienmessungen des Geodätischen Institutes in den Jahren 1933-1939 nebst Untersuchungen über die Verwendung der Invardrähte. Helsinki 1942. 149 S.
32. U. PESONEN, V.R. ÖLANDER: Beobachtungsergebnisse. Winkelmessungen in den Jahren 1936-1940. Helsinki 1942. 165 S. 1 Karte.
33. PENTTI KALAJA: Astronomische Ortsbestimmungen in den Jahren 1935-1938. Helsinki 1944. 142 S.
34. V.R. ÖLANDER: Astronomische Azimutbestimmungen auf den Dreieckspunkten in den Jahren 1932-1938; Lotabweichungen und Geoidhöhen. Helsinki 1944. 107 S. 1 Karte.
35. U. PESONEN: Beobachtungsergebnisse. Winkelmessungen in den Jahren 1940-1947. Helsinki 1948. 165 S. 1 Karte.
36. Professori Ilmari Bonsdorffille hänen 70-vuotispäivänään omistettu juhlajulkaisu. Publication dedicated to Ilmari Bonsdorff on the occasion of his 70th anniversary. Helsinki 1949. 262 pages. 13 maps.
37. TAUNO HONKASALO: Measuring of the 864 m-long Nummela standard base line with the Väisälä light interference comparator and some investigations into invar wires. Helsinki 1950. 88 pages.
38. V.R. ÖLANDER: On the geoid in the Baltic area and the orientation of the Baltic Ring. Helsinki 1950. 26 pages.
39. W. HEISKANEN: On the world geodetic system. Helsinki 1951. 25 pages.
40. R.A. HIRVONEN: The motions of Moon and Sun at the solar eclipse of 1947 May 20th. Helsinki 1951. 36 pages.

41. PENTTI KALAJA: Catalogue of star pairs for northern latitudes from 55° to 70°for astronomic determination of latitudes by the Horrebow-Talcott method. Helsinki 1952. 191 pages.
42. ERKKI KÄÄRIÄINEN: On the recent uplift of the Earth's crust in Finland. Helsinki 1953. 106 pages. 1 map.
43. PENTTI KALAJA: Astronomische Ortsbestimmungen in den Jahren 1946-1948. Helsinki 1953. 146 S.
44. T.J. KUKKAMÄKI, R.A. HIRVONEN: The Finnish solar eclipse expeditions to the Gold Coast and Brazil 1947. Helsinki 1954. 71 pages.
45. JORMA KORHONEN: Einige Untersuchungen über die Einwirkung der Abrundungsfehler bei Gross-Ausgleichungen. Neu-Ausgleichung des südfinnischen Dreieckskranzes. Helsinki 1954. 138 S. 3 Karten.
46. Professori Weikko A. Heiskaselle hänen 60-vuotispäivänään omistettu juhlajulkaisu. Publication dedicated to Weikko A. Heiskanen on the occasion of his 60th anniversary. Helsinki 1955. 214 pages.
47. Y. VÄISÄLÄ: Bemerkungen zur Methode der Basismessung mit Hilfe der Lichtinterferenz. Helsinki 1955. 12 S.
48. U. PESONEN, TAUNO HONKASALO: Beobachtungsergebnisse der finnischen Triangulationen in den Jahren 1947-1952. Helsinki 1957. 91 S.
49. PENTTI KALAJA: Die Zeiten von Sonnenschein, Dämmerung und Dunkelheit in verschiedenen Breiten. Helsinki 1958. 63 S.
50. V.R. ÖLANDER: Astronomische Azimutbestimmungen auf den Dreieckspunkten in den Jahren 1938-1952. Helsinki 1958. 90 S. 1 Karte.
51. JORMA KORHONEN, V.R. ÖLANDER, ERKKI HYTÖNEN: The results of the base extension nets of the Finnish primary triangulation. Helsinki 1959. 57 pages. 5 appendices. 1 map.
52. V.R. ÖLANDER: Vergleichende Azimutbeobachtungen mit vier Instrumenten. Helsinki 1960. 48 pages.
53. Y. VÄISÄLÄ, L. OTERMA: Anwendung der astronomischen Triangulationsmethode. Helsinki 1960. 18 S.
54. V.R. ÖLANDER: Astronomical azimuth determinations on trigonometrical stations in the years 1955-1959. Helsinki 1961. 15 pages.
55. TAUNO HONKASALO: Gravity survey of Finland in years 1945-1960. Helsinki 1962. 35 pages. 3 maps.
56. ERKKI HYTÖNEN: Beobachtungsergebnisse der finnischen Triangulationen in den Jahren 1953-1962. Helsinki 1963. 59 S.
57. ERKKI KÄÄRIÄINEN: Suomen toisen tarkkavaaituksen kiintopisteluettelo I. Bench mark list I of the Second Levelling of Finland. Helsinki 1963. 164 pages. 2 maps.
58. ERKKI HYTÖNEN: Beobachtungsergebnisse der finnischen Triangulationen in den Jahren 1961-1962. Helsinki 1963. 32 S.
59. AIMO KIVINIEMI: The first order gravity net of Finland. Helsinki 1964. 45 pages.
60. V.R. ÖLANDER: General list of astronomical azimuths observed in 1920-1959 in the primary triangulation net. Helsinki 1965. 47 pages. 1 map.
61. ERKKI KÄÄRIÄINEN: The second levelling of Finland in 1935-1955. Helsinki 1966. 313 pages. 1 map.
62. JORMA KORHONEN: Horizontal angles in the first order triangulation of Finland in 1920-1962. Helsinki 1966. 112 pages. 1 map.
63. ERKKI HYTÖNEN: Measuring of the refraction in the Second Levelling of Finland. Helsinki 1967. 18 pages.
64. JORMA KORHONEN: Coordinates of the stations in the first order triangulation of Finland. Helsinki 1967. 42 pages. 1 map.
65. Geodeettinen laitos - The Finnish Geodetic Institute 1918-1968. Helsinki 1969. 147 pages. 4 maps.
66. JUHANI KAKKURI: Errors in the reduction of photographic plates for the stellar triangulation. Helsinki 1969. 14 pages.
67. PENTTI KALAJA, V.R. ÖLANDER: Astronomical determinations of latitude and longitude in 1949-1958. Helsinki 1970. 242 pages. 1 map.
68. ERKKI KÄÄRIÄINEN: Astronomical determinations of latitude and longitude in 1954-1960. Helsinki 1970. 95 pages. 1 map.
69. AIMO KIVINIEMI: Niinisalo calibration base line. Helsinki 1970. 36 pages. 1 sketch appendix.
70. TEUVO PARM: Zero-corrections for tellurometers of the Finnish Geodetic Institute. Helsinki 1970. 18 pages.
71. ERKKI KÄÄRIÄINEN: Astronomical determinations of latitude and longitude in 1961-1966. Helsinki 1971. 102 pages. 1 map.
72. JUHANI KAKKURI: Plate reduction for the stellar triangulation. Helsinki 1971. 38 pages.
73. V.R. ÖLANDER: Reduction of astronomical latitudes and longitudes 1922-1948 into FK4 and CIO systems. Helsinki 1972. 40 pages.
74. JUHANI KAKKURI AND KALEVI KALLIOMÄKI: Photoelectric time micrometer. Helsinki 1972. 53 pages.
75. ERKKI HYTÖNEN: Absolute gravity measurement with long wire pendulum. Helsinki 1972. 142 pages.
76. JUHANI KAKKURI: Stellar triangulation with balloon-borne beacons. Helsinki 1973. 48 pages.
77. JUSSI KÄÄRIÄINEN: Beobachtungsergebnisse der finnischen Winkelmessungen in den Jahren 1969-70. Helsinki 1974. 40 S.
78. AIMO KIVINIEMI: High precision measurements for studying the secular variation in gravity in Finland. Helsinki 1974. 64 pages.
79. TEUVO PARM: High precision traverse of Finland. Helsinki 1976. 64 pages.

80. R.A. HIRVONEN: Precise computation of the precession. Helsinki 1976. 25 pages.

81. MATTI OLLIKAINEN: Astronomical determinations of latitude and longitude in 1972-1975. Helsinki 1977. 90 pages. 1 map.

82. JUHANI KAKKURI AND JUSSI KÄÄRIÄINEN: The Second Levelling of Finland for the Aland archipelago. Helsinki 1977. 55 pages.

83. MIKKO TAKALO: Suomen Toisen tarkkavaaituksen kiintopisteluettelo II. Bench mark list II of the Second Levelling of Finland. Helsinki 1977. 150 sivua.

84. MATTI OLLIKAINEN: Astronomical azimuth determinations on triangulation stations in 1962-1970. Helsinki 1977. 47 pages. 1 map.

85. MARKKU HEIKKINEN: On the tide-generating forces. Helsinki 1978. 150 pages.

86. PEKKA LEHMUSKOSKI AND JAAKKO MÄKINEN: Gravity measurements on the ice of Bothnian Bay. Helsinki 1978. 27 pages.

87. T.J. KUKKAMÄKI: Väisälä interference comparator. Helsinki 1978. 49 pages.

88. JUSSI KÄÄRIÄINEN: Observing the Earth Tides with a long water-tube tiltmeter. Helsinki 1979. 74 pages.

89. Publication dedicated to T.J. Kukkamäki on the occasion of his 70th anniversary. Helsinki 1979. 184 pages.

90. B. DUCARME AND J. KÄÄRIÄINEN: The Finnish Tidal Gravity Registrations in Fennoscandia. Helsinki 1980. 43 pages.

91. AIMO KIVINIEMI: Gravity measurements in 1961-1978 and the results of the gravity survey of Finland in 1945-1978. Helsinki 1980. 18 pages. 3 maps.

92. LIISI OTERMA: Programme de latitude du tube zénithal visuel de l'observatoire Turku-Tuorla systéme amélioré de 1976. Helsinki 1981. 18 pages.

93. JUHANI KAKKURI, AIMO KIVINIEMI AND RAIMO KONTTINEN: Contributions from the Finnish Geodetic Institute to the Tectonic Plate Motion Studies in the Area between the Pamirs and Tien-Shan Mountains. Helsinki 1981. 34 pages.

94. JUSSI KÄÄRIÄINEN: Measurement of the Ekeberg baseline with invar wires. Helsinki 1981. 17 pages.

95. MATTI OLLIKAINEN: Astronomical determinations of latitude and longitude in 1976-1980. Helsinki 1982. 90 pages. 1 map.

96. RAIMO KONTTINEN: Observation results. Angle measurements in 1977-1978. Helsinki 1982. 29 pages.

97. G.P. ARNAUTOV, YE N. KALISH, A. KIVINIEMI, YU F. STUS, V.G. TARASIUK, S.N. SCHEGLOV: Determination of absolute gravity values in Finland using laser ballistic gravimeter. Helsinki 1982. 18 pages.

98. LEENA MIKKOLA (EDITOR): Mean height map of Finland. Helsinki 1983. 3 pages. 1 map.

99. MIKKO TAKALO AND JAAKKO MÄKINEN: The Second Levelling of Finland for Lapland. Helsinki 1983. 144 pages.

100. JUSSI KÄÄRIÄINEN: Baseline Measurements with invar wires in Finland 1958-1970. Helsinki 1984. 78 pages.

101. RAIMO KONTTINEN: Plate motion studies in Central Asia. Helsinki 1985. 31 pages.

102. RAIMO KONTTINEN: Observation results. Angle measurements in 1979-1983. Helsinki 1985. 30 pages.

103. J. KAKKURI, T.J. KUKKAMÄKI, J.-J. LEVALLOIS ET H. MORITZ: Le 250^e anniversaire de la mesure de l'arc du meridien en Laponie. Helsinki 1986. 60 pages.

104. G. ASCH, T. JAHR, G. JENTZSCH, A. KIVINIEMI AND J. KÄÄRIÄINEN: Measurements of Gravity Tides along the "Blue Road Geotraverse" in Fennoscandia. Helsinki 1987. 57 pages.

105. JUSSI KÄÄRIÄINEN, RAIMO KONTTINEN, LU QIANKUN AND DU ZONG YU: The Chang Yang Standard Baseline. Helsinki 1986. 36 pages.

106. E.W. GRAFAREND, H. KREMERS, J. KAKKURI AND M. VERMEER: Adjusting the SW Finland Triangular Network with the TAGNET 3-D operational geodesy software. Helsinki 1987. 60 pages.

107. MATTI OLLIKAINEN: Astronomical determinations of latitude and longitude in 1981-1983. Helsinki 1988. 37 pages.

108. MARKKU POUTANEN: Observation results. Angle measurements in 1967-1973. Helsinki 1988. 35 pages.

109. JUSSI KÄÄRIÄINEN, RAIMO KONTTINEN AND ZSUZSANNA NÉMETH: The Gödöllö Standard Baseline. Helsinki 1988. 66 pages.

110. JUSSI KÄÄRIÄINEN AND HANNU RUOTSALAINEN: Tilt measurements in the underground laboratory Lohja 2, Finland, in 1977-1987. Helsinki 1989. 37 pages.

111. MIKKO TAKALO: Lisäyksiä ja korjauksia Suomen tarkkavaaitusten linjastoon 1977-1989. Helsinki 1991. 98 sivua.

112. RAIMO KONTTINEN: Observation results. Angle measurements in the Pudasjärvi loop in 1973-1976. Helsinki 1991. 42 pages.

113. RAIMO KONTTINEN, JORMA JOKELA AND LI QUAN: The remeasurement of the Chang Yang Standard Baseline. Helsinki 1991. 40 pages.

114. JUSSI KÄÄRIÄINEN, RAIMO KONTTINEN AND MARKKU POUTANEN: Interference measurements of the Nummela Standard Baseline in 1977, 1983, 1984 and 1991. Helsinki 1992. 78 pages.

115. JUHANI KAKKURI (editor): Geodesy and geophysics. Helsinki 1993. 200 pages.

116. JAAKKO MÄKINEN, HEIKKI VIRTANEN, QIU QI-XIAN AND GU LIANG-RONG: The Sino-Finnish absolute gravity campaign in 1990. Helsinki 1993. 49 pages.

117. RAIMO KONTTINEN: Observation results. Geodimeter observations in 1971-72, 1974-80 and 1984-85. Helsinki 1994. 58 pages.

118. RAIMO KONTTINEN: Observation results. Angle measurements in 1964-65, 1971, 1984 and 1986-87. Helsinki 1994. 67 pages.

119. Jorma Jokela: The 1993 adjustment of the Finnish First-Order Terrestrial Triangulation. Helsinki 1994. 137 pages.

120. Markku Poutanen (editor): Interference measurements of the Taoyuan Standard Baseline. Helsinki 1995. 35 pages.

121. Jorma Jokela: Interference measurements of the Chang Yang Standard Baseline in 1994. Kirkkonummi 1996. 32 pages.

122. Olli Jaakkola: Quality and automatic generalization of land cover data. Kirkkonummi 1996. 39 pages.

123. Matti Ollikainen: Determination of orthometric heights using GPS levelling. Kirkkonummi 1997. 143 pages.

124. Tiina Kilpeläinen: Multiple Representation and Generalization of Geo-Databases for Topographic Maps. Kirkkonummi 1997. 229 pages.

125. Jussi Kääriäinen and Jaakko Mäkinen: The 1979-1996 gravity survey and the results of the gravity survey of Finland 1945-1996. Kirkkonummi 1997. 24 pages. 1 map.

126. Zhitong Wang: Geoid and crustal structure in Fennoscandia. Kirkkonummi 1998. 118 pages.

127. Jorma Jokela and Markku Poutanen: The Väisälä baselines in Finland. Kirkkonummi 1998. 61 pages.

128. Markku Poutanen: Sea surface topography and vertical datums using space geodetic techniques. Kirkkonummi 2000. 158 pages

129. Matti Ollikainen, Hannu Koivula and Markku Poutanen: The Densification of the EUREF Network in Finland. Kirkkonummi 2000. 61 pages.

130. Jorma Jokela, Markku Poutanen, Zhao Jingzhan, Pei Weili, Hu Zhenyuan and Zhang Shengshu: The Chengdu Standard Baseline. Kirkkonummi 2000. 46 pages.

131. Jorma Jokela, Markku Poutanen, Zsuzsanna Németh and Gábor Virág: Remeasurement of the Gödöllö Standard Baseline. Kirkkonummi 2001. 37 pages.

132. Andres Rüdja: Geodetic Datums, Reference Systems and Geodetic Networks in Estonia. Kirkkonummi 2004. 311 pages.

133. Heikki Virtanen: Studies of Earth Dynamics with the Superconducting Gravimeter. Kirkkonummi 2006. 130 pages.

134. Juha Oksanen: Digital elevation model error in terrain analysis. Kirkkonummi 2006. 142 pages. 2 maps.

135. Matti Ollikainen: The EUVN-DA GPS campaign in Finland. Kirkkonummi 2006. 42 pages.

136. Annu-Maaria Nivala: Usability perspectives for the design of interactive maps. Kirkkonummi 2007. 157 pages.

137. Xiaowei Yu: Methods and techniques for forest change detection and growth estimation using airborne laser scanning data. Kirkkonummi 2007. 132 pages.

138. Lassi Lehto: Real-time content transformations in a WEB service-based delivery architecture for geographic information. Kirkkonummi 2007. 150 pages.

139. Pekka Lehmuskoski, Veikko Saaranen, Mikko Takalo and Paavo Rouhiainen: Suomen Kolmannen tarkkavaaituksen kiintopisteluettelo. Bench Mark List of the Third Levelling of Finland. Kirkkonummi 2008. 220 pages.

140. Eija Honkavaara: Calibrating digital photogrammetric airborne imaging systems using a test field. Kirkkonummi 2008. 139 pages.

141. Markku Poutanen, Eero Ahokas, Yuwei Chen, Juha Oksanen, Marita Portin, Sari Ruuhela, Heli Suurmäki (editors): Geodeettinen laitos – Geodetiska Institutet – Finnish Geodetic Institute 1918–2008. Kirkkonummi 2008. 173 pages.

142. Mika Karjalainen: Multidimensional SAR Satellite Images – a Mapping Perspective. Kirkkonummi 2010. 132 pages.

143. Maaria Nordman: Improving GPS time series for geodynamic studies. Kirkkonummi 2010. 116 pages.

144. Jorma Jokela and Pasi Häkli: Interference measurements of the Nummela Standard Baseline in 2005 and 2007. Kirkkonummi 2010. 85 pages.

145. Eetu Puttonen: Tree Species Classification with Multiple Source Remote Sensing Data. Kirkkonummi 2012. 162 pages.

146. Juha Suomalainen: Empirical Studies on Multiangular, Hyperspectral, and Polarimetric Reflectance of Natural Surfaces. Kirkkonummi 2012. 144 pages.

147. Leena Matikainen: Object-based interpretation methods for mapping built-up areas. Kirkkonummi 2012. 210 pages.

148. Lauri Markelin: Radiometric calibration, validation and correction of multispectral photogrammetric imagery. Kirkkonummi 2013. 160 pages.